Sum frequency generation vibrational spectroscopy of steroidal structure side chains of polyimide surfaces

Nguyen Thi Trinh

Japan Advanced Institute of Science and Technology

Doctoral Dissertation

Sum frequency generation vibrational spectroscopy of steroidal structure side chains of polyimide surfaces

Nguyen Thi Trinh

Supervisor: Prof. Goro Mizutani

Graduate School of Advanced Science and Technology
Japan Advanced Institute of Science and Technology
Materials Science
September 2021

Abstract

Polyimide (PI) films coated on glass substrate are commonly used to align the liquid crystal (LC) molecules in liquid crystal display (LCD) devices. Among them, PI containing steroidal side chains is expected to be helpful because it provides a wide range of pretilt angles according to its diamine ratio. Unfortunately, the orientation and conformation of molecules at the PI surface after rubbing have not been fully known yet so far. To the best of my knowledge, there is no study investigating the molecular orientation and conformation of the steroidal structure and the alkyl side chain at the rubbed PI film surface like the one in this study.

Ullah *et al.* reported the second harmonic generation (SHG) intensity of rubbed PI-30 film shows anisotropic SHG intensity patterns as a function of the angle of the sample rotation angle. To analyze the experimental result, they assumed that only the steroidal side chains of PI containing steroidal structure side chains have microscopic optical nonlinearity. However, Ullah *et al.* have not checked the validity of the assumption yet. In this study, I observed SHG response from unrubbed PI film surfaces at several different molar fractions of side-chain diamine in PI containing steroidal side chains to examine whether or not this assumption was correct. I found that both the PI main chains and PI side chains contribute similarly to the SHG intensity. The SHG intensity in S_{in}/P_{out} normalized by P_{in}/P_{out} was the smallest for the unrubbed PI film without steroidal side chains (PI-0). This fact indicates that the microscopic nonlinear dipoles are standing nearly upright at the surface of the unrubbed PI-0 film. In contrast, their orientational spread is wider when the side chains are involved.

Several analytical techniques are used to study polymer films, such as infrared spectroscopy, atomic force microscopy, and near-edge X-ray absorption fine structure spectroscopy. However, they are not appropriate for analyzing the steroidal structure and the alkyl chain parts. On the other hand, sum frequency generation (SFG) vibrational spectroscopy has been demonstrated as a helpful surface analytical technique. Because this technique is sensitive to non-centrosymmetric parts of materials, it is commonly applied to determine vibrational resonances of molecules adsorbed at surfaces and interfaces. In this study, the molecular orientation of steroidal side chains at the rubbed PI surfaces was investigated by SFG vibrational spectroscopy to establish a correlation between the molecular structure and LC alignment on it.

In SFG measurements, I have investigated three types of PI films with units possessing a 30% fraction of steroidal side chains (PI-30), including unrubbed PI-30 film, rubbed PI-30 film, and rubbed PI-30 film with a poly (methyl methacrylate) (PMMA) overlayer. Before analyzing the details of the SFG spectra of the PI-30 film, I first examine whether or not the SFG response originates from the PI-30 film surface. For this purpose, I measured the SFG spectra of the rubbed PI-30 films with and without a PMMA layer for PPP and SSP polarization combinations. The thickness of the PMMA layer was ~ 5 nm. The SFG intensity decreased dramatically after the sample was covered with the very thin PMMA layer for the PPP polarization combination. Furthermore, the peaks in the spectra changed drastically after PMMA deposition for the SSP polarization combination. These results indicate that the SFG of the rubbed PI-30 film mainly originates from the PI film surface, and the SFG contribution from the PI/glass substrate interface and the bulk PI can be ignored.

Based on the SFG spectrum of the rubbed PI-30 film in the CH stretching region from 2800 to 3000 cm^{-1} at an azimuthal angle of $\gamma = 0^o$ and for a PPP polarization combination, I found that the frequencies of the symmetric and antisymmetric stretches of the CH_3 groups at the end of the alkyl chain are different from those of the two CH_3 groups on the steroidal structure and the adjacent CH_3 group.

To consider the effect of the rubbing process on the orientation of the CH_3 groups at the PI side chain, I focus on the CH_3 symmetric stretching modes in 2850-2890 cm^{-1} region. The SFG spectra of the rubbed PI-30 film at azimuthal-angle intervals of 45° for a PPP polarization combination were observed. The spectra showed that the isopropyl group is pointing toward the air side from the PI surface, but their average orientation is not affected by rubbing because the length of the alkyl chain in this PI is short. However, a slight anisotropy of the symmetric stretching mode of the CH_3 group next

to the steroidal structure was observed after rubbing in the SFG spectra, and its average tilt angle was estimated as $\theta_0 = 40^o \pm 10^o$ in the rubbing direction. These results indicate that the rubbing appears to cause conformational changes of the CH_3 group near the steroidal structure, but the rubbing does not significantly affect the orientation of the isopropyl group at the end of the PI side chain.

The molecular interaction between an alignment layer and LC molecules is the most crucial factor in LC alignment. Therefore, the ultimate goal of my study was to establish which structural factor of rubbed PI films with steroidal side chains is most strongly correlated with LC alignment. There are three possible structural factors were considered, including (1) the phenyl rings, (2) the steroidal structure and the adjacent CH_3 group, and (3) the isopropyl group and the neighboring methylene group in the PI side chain. Among them, factor (3) can be excluded because it does not show any anisotropy after rubbing. Consequently, only two factors (1) and (2) are possibly correlated with LC alignment. Unfortunately, I cannot determine which of them is mainly related to LC alignment so far, and further study is necessary for resolving this issue.

Keywords: polyimide, sum frequency generation vibrational spectroscopy, molecular orientation, alignment layer, and steroidal structure.

Acknowledgments

First of all, I would like to express my heartfelt gratitude to my supervisor, Professor Goro Mizutani, for his excellent guidance, support, and encouragement. He spent many hours fixing the problems of our experimental system with me, explaining the theory behind the technique, connecting me with the resources that I need, and teaching me how to become an independent researcher. In addition, I learned the way to balance my personal life and my research career from him. He is not only my supervisor but also my counselor, friend, and role model. Working under his supervision has been extremely enjoyable and effective.

Next, I would like to express my sincere thanks to Dr. Khuat Thi Thu Hien for her initial help in operating the SFG experimental system. I learned a lot about the SFG technique and problem-solving skills from her. In addition, she is always a great source of advice, support, and encouragement in all situations.

Additionally, I would like to express my sincere thanks to Dr. Yoshitaka Murakami and Dr. Takashi Okada from JSR Corporation for sending me the polyimide films and giving me many valuable comments on this work.

I would also like to thank Prof. Haruyuki Sano from Ishikawa College for his valuable advice for solving technical problems in our SFG system.

I would like to express my special gratitude to Assoc. Prof. Yuki Nagao for his excellent guidance in my minor research project and for his valuable suggestions to improve my doctoral dissertation.

I would like to thank Sakura Science Exchange Program for giving me a chance to come to JAIST in 2015. My life has changed after that trip. Further, I gratefully acknowledge the financial support from the Ministry of Education, Culture, Sports, Science, and Technology (MEXT, Japan) for providing the scholarship for my doctoral program.

Many thanks to all members of Mizutani lab for their kind help at the beginning I came here and for the wonderful moments we shared in lab excursions. In addition, I thank all of the Vietnamese students in JAIST; I had a memorable time working and play with you. All of you made my doctoral life is more colorful, joyful, and meaningful.

Finally, I would like to express my deepest gratitude and sincere thanks to my family for their love, care, and encouragement. I especially thank my parents for the support, love, and education they have given to me that built the foundation for my accomplishments.

Table of Contents

CHAPTER 1. INTRODUCTION

This chapter introduces the topic of my dissertation. I first present a brief overview of polyimide and the previous studies about the orientation and conformation of molecules at polyimide surfaces. I then explain the objective of this study and show the dissertation outline.

1.1 Background

Polyimide (PI) is a polymer that consists of imide monomers. An imide is a functional group in a molecule that has a general structure similar to that depicted below

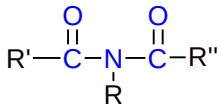

Although PI was first synthesized in 1908 by Bogert and Renshaw,[1] it was not developed as material until 1955. Kapton was the first commercial PI in the early 1960s. After the success of Kapton, PIs have been synthesized and investigated extensively. According to the monomers, PIs can be widely classified as fully aromatic PIs, semi-aromatic PIs, and fully aliphatic PIs.[2] At present, PIs are a class of high-performance polymers with numerous superior properties because of strong intermolecular forces between the polymer chains.[2–4] These properties include high glass transition temperature (T_g), excellent mechanical properties with tensile strength over 100 MPa, high thermal stability, high chemical resistance, good electrical insulation with volume resistivity at 10^{16}-10^{17} Ω.cm and surface resistivity at 10^{15}-10^{16} Ω.cm, and superior dielectric properties.

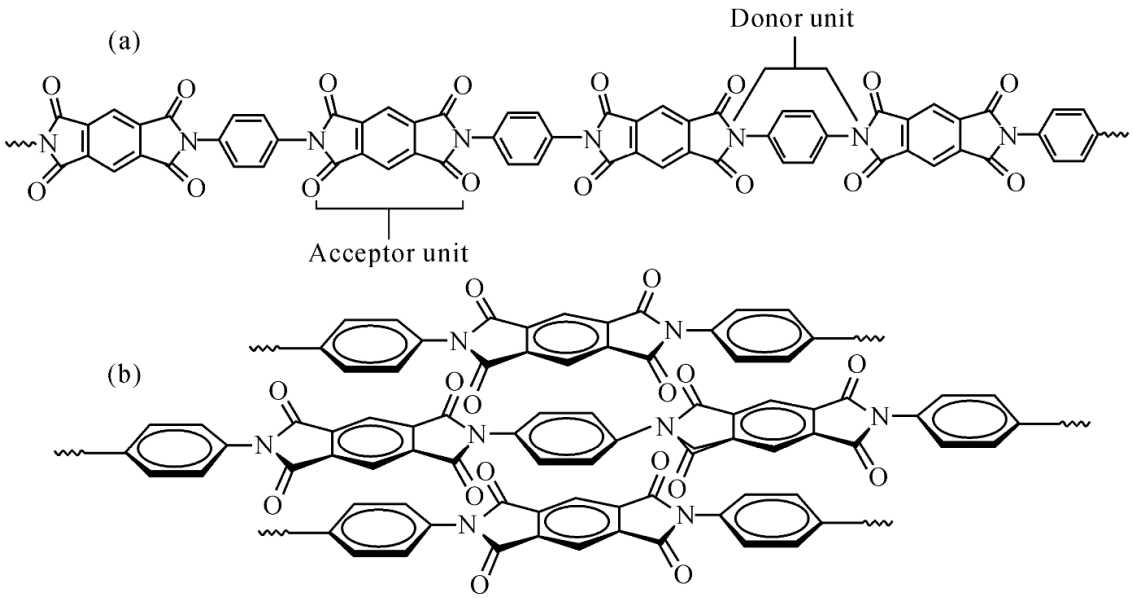

Figure 1.1 Charge transfer complexes in PIs (a) Intramolecular structure (b) Intermolecular structure.[2]

PI includes a charge transfer complex consisting of two different types of monomers called a donor, and an acceptor, as shown in Fig. 1.1.[2] Nitrogen atoms (donors) have a higher electron density than the carbonyl groups (acceptors), so the donors lend some of their electrons to the acceptors to keep them tight. The charge transfer complex works between adjacent units in the PI chain and between chains. As a result, the PI chains will pile up like paper strips, with paired donors and acceptors pulling the chains closer together, as shown in Fig. 1.1 (b). This charge transfer complex holds the PI chains tightly and makes them impossible to move around. It is the reason why PIs are so strong.

PI is used in various applications such as aerospace, electrical, electronics, and photonics applications because of its outstanding properties.[5] The electrical properties are highly stable over a large temperature range,[3], so PI is ideally suited for electrical and electronics applications. Although PI was widely used in electrical industries in the 1960s, the history of PI for electronics just really began in the early 1970s as highly purified, and high-heat-resistant PI was first fabricated for microelectronics.[6] After that, the PI application of microelectronics expanded rapidly. At the end of the 1970s, with the expansion of semiconductor integration, PI has been transferred from electrical insulation materials to electronic materials. One of the essential electronics applications of PI is an alignment layer for Liquid crystal (LC) molecules in LC flat-panel display devices.[7–12] Moreover, PI films have also been applied for microelectrodes,[13] solar cells,[14] and sensors.[15] Recently, PIs with high optical transparency and low dielectric constants such as colorless PIs have been used for optoelectronic and flexible display applications as shown in Fig. 1.2.[16–18]

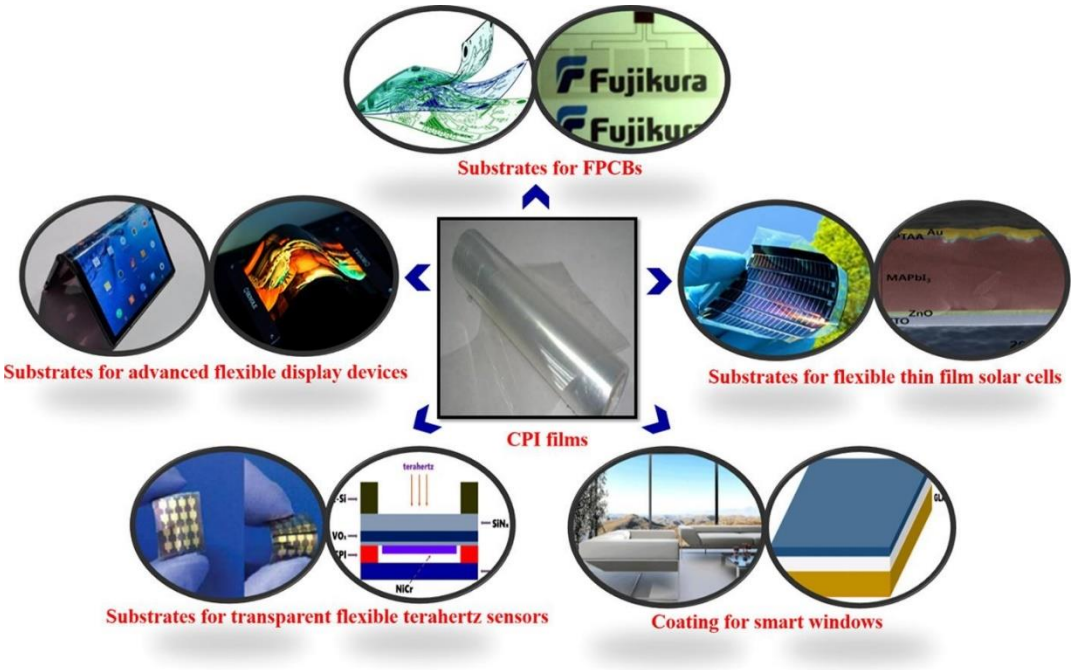

Figure 1.2 The latest applications of colorless PI films in optoelectrical devices.[16]

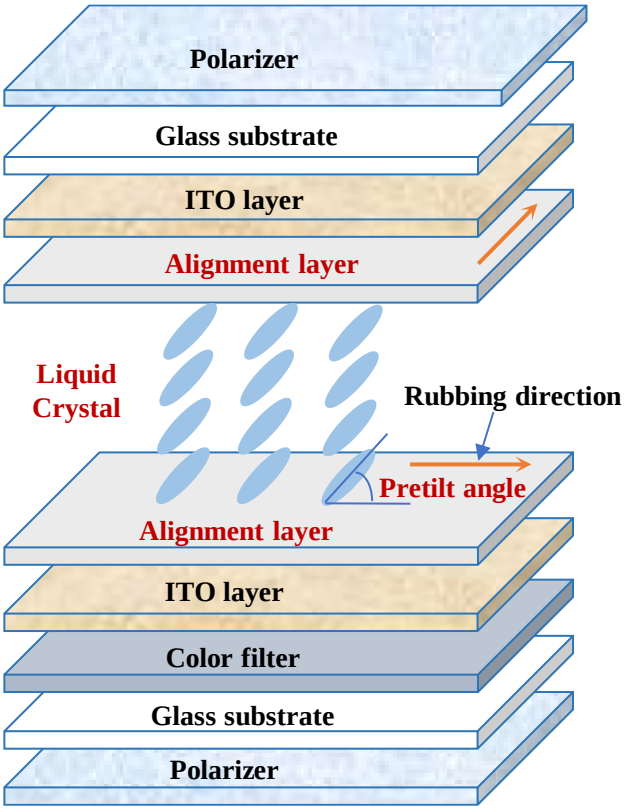

Figure 1.3 The typical structure of the LCD device.

Liquid crystal display (LCD) industry started in the early 1970s with small segment-type displays for calculators and watches. After much development, LCD has become an essential component for smartphones, large screen televisions, and laptops. As shown in Fig. 1.3, LC materials are usually sandwiched between two glass substrates carrying an alignment layer. The following two steps allow us to understand the LC alignment mechanism.[19] First, the LC molecules of the first LC monolayer are aligned via a short-range interaction between the LC molecules and the alignment layer. The alignment of the LC molecules of the first monolayer then propagates to the bulk via a long-range interaction among the LC molecules.

The pretilt angle is defined as an angle between the plane of the alignment layer and the axis of the LC molecule, as illustrated in Fig.1.3. This angle plays a crucial role in determining both the optical and electrical performance of LCD devices. Namely, the LC orientation is not uniform and results in an ununiformed image as the pretilt angle is not constant throughout the panel.[20] In addition, the requirement of the pretilt angle differs depending on the display operating mode, as shown in Fig.1.4.[11] Twisted nematic TN mode (displays for laptops) requests 3-6 degrees; optically-compensated bend OCB mode (LCDs with fast response time and wide viewing angle) requests 6-10 degrees; bi-stable bend-splay mode (LCDs requiring memory effect, such as e-books) requests ~ 50 degrees; and vertical alignment VA mode (LCDs for TVs) requests nearly 90 degrees.[8,11,21] As a result, the control of the pretilt angle is critical.

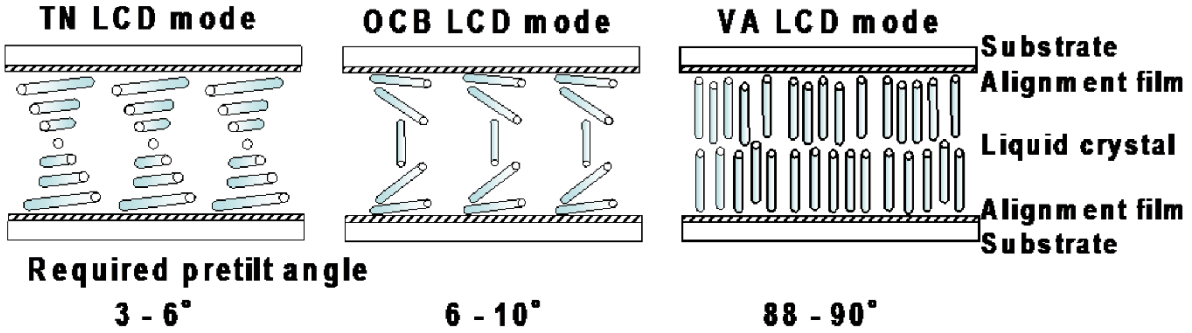

Figure 1.4 Schematic cross-sectional views of the several LCD modes.[11]

A variety of factors affect the pretilt angle, i.e., LC material, LC alignment layer material and its side chain structure, the conditions of film preparation, and alignment process (rubbing process or photoalignment).[8] It is known that the pretilt angle strongly depends on LC alignment layer materials and its side chain structure. Consequently, correctly choosing LC alignment layer materials is essential for controlling pretilt angles. At present, PI is one of the best candidates for the LC alignment layer because of its excellent properties. It is known that pretilt angle is strongly dependent on the polarity of the PI surface.[18] Namely, the pretilt angle increases by introducing long alkyl side chains or other nonpolar groups (fluorine group) into PIs because the PI surface polarity decreases.

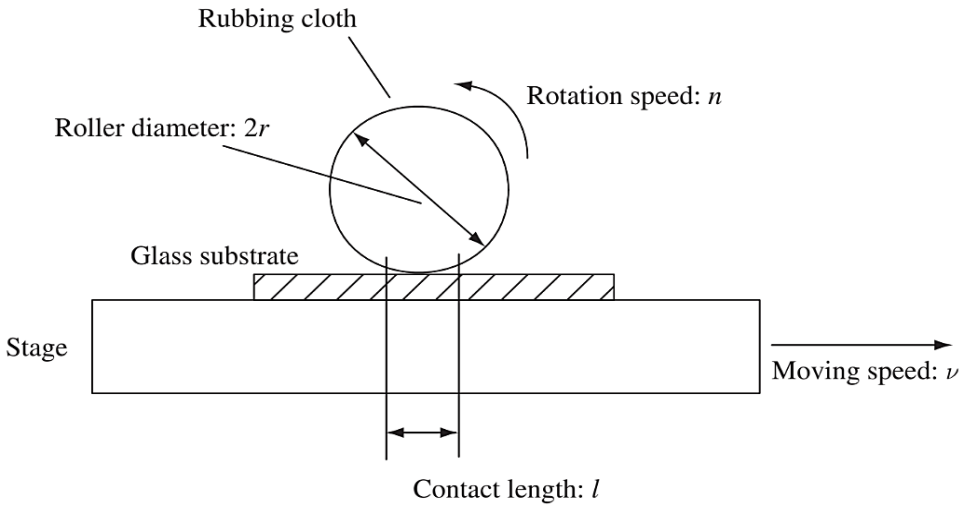

Figure 1.5 Illustration of the rubbing process.[22]

PI surface must be treated to make a uniform alignment of the LC molecules with a specific pretilt angle. The rubbing process is a major method adopted in the mass-production of flat-panel LCD devices because it is a simple process and can be applied to a large area at a low cost. A PI-coated glass substrate is commonly rubbed once by a rotation drum-covered cloth with short fibers, as shown in Fig. 1.5.[22] There are many types of rubbing cloths with different fiber shapes,[8] such as rayon, cotton, and nylon. The standard demands for rubbing cloth are high LC alignment performance, appropriate pretilt angle, appropriate surface anchoring

strength, abrasion resistance, no damage to voltage holding characteristics, no rubbing cords, no dust, and low charging ability. In addition, the material quality, i.e., the diameter of filament, the density of filament, pile length, and coefficient of friction, needs to be controlled.

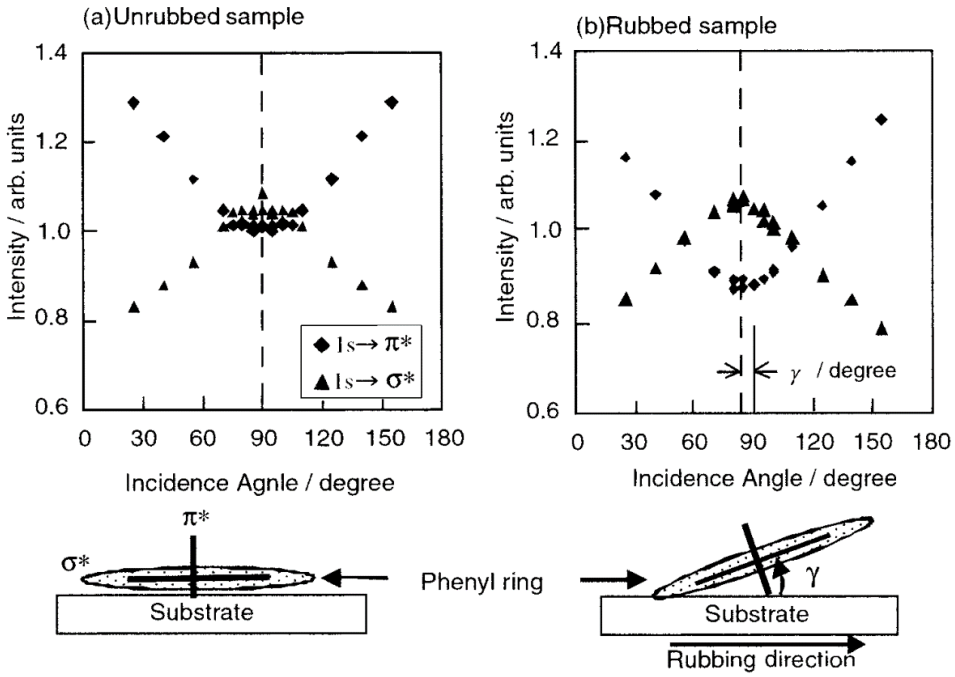

Figure 1.6 Angular dependence of the resonance intensities for unrubbed (a) and rubbed (b) CP7CC3 samples.[23]

In general, the experimental results indicate that PI main chains are aligned by rubbing. Sakamoto *et al.*[24] studied the molecular orientation of a polyimide without a sidechain (PMDA-ODA PI) before and after rubbing by IR absorption spectroscopy. They reported that the molecules in the unrubbed PI film are oriented parallel to the substrate surface with a standard deviation of 6.5°. On the other hand, the PI chains are oriented in the rubbing direction and are tilted up on average by 8.5° from the surface plane in the rubbed PI film. Sung *et al.*[25] used sum frequency generation (SFG) vibrational spectroscopy to investigate PMDA-ODA PI films made by spin-coating and ionized cluster beam deposition (ICBD) methods. They reported that SFG spectra of the PI films made in different ways were different in the CO stretching region. These SFG spectra revealed that the PI main chains lie mainly along the surface for spin-coated films, while they are generally upright in the surface for ICBD films. Sakai *et al.*[23] used surface-sensitive near-edge X-ray absorption fine structure spectroscopy (NEXAFS) to investigate the surface orientation of a PI film with a side chain. They found that the rubbing process caused the surface tilt angle between the axis of the PI main chain and the rubbing direction (γ) as shown in Fig.1.6. In other words, the phenyl ring of the PI main chain is oriented parallel to the PI surface on average for the unrubbed PI film while the symmetry axis shifts from 90 degrees to (90 degrees - γ) for the rubbed PI film. In addition, the angle γ is strongly related to the LC pretilt angle.

The effect of the rubbing process on PI side chains at surfaces has been intensively investigated. The studies indicate that it depends on the length, component, and configuration of PI side chains. Shirota *et al.*[26] investigated the effect of the rubbing process on the distributions of trifluoromethyl side chains by optical second harmonic generation (SHG) in PI surfaces. They reported that the symmetry of the PI side chain changes from $C_{\infty v}$ to C_s by rubbing, and an asymmetry of the polar angle is induced in the rubbing direction. Sakai *et al.*[27] observed an in-plane anisotropy in the SHG signal profile of cyanobiphenyl side chains at a rubbed PI surface. The result means the rubbing process transforms the side-chain orientation at the PI surface. Oh-e *et al.*[28] investigated PIs with short alkyl side chains (1–7 carbon atoms) and pointed out that the orientation of the alkyl side chains is hardly affected by rubbing.

On the other hand, a significant azimuthal anisotropy induced by rubbing was observed by Jayathilake *et al.* in the study of the PI film with the long alkyl side chains (18 carbon atoms).[29] The results can be explained by the molecular organization of the side chain. It is known that the alkyl side chain length is a crucial parameter to determine the molecular organization and order at surfaces or interfaces.[29] For example, long alkyl chains with more than 10 carbon atoms have better molecular organization and order at surfaces.

Despite widely using in the LCD industry, the rubbing process has some problems producing thin-film transistor LCDs because it generates dust and has electrostatic issues.[18] Therefore, alternative methods have been developed to solve the problems of the rubbing process. These alternative methods are divided into two categories.[30] In the first category, the LC molecules are aligned by an electric or magnetic field coming from outside the LC cell. The substrate surface is correlated to the aligned LC molecules. The aligned LC molecules on the surface align the LC molecules in bulk after the electric or magnetic field is removed, such as photoalignment. The other category uses surface alignment induced by the surface anisotropy such as microgroove surfaces and Langmuir-Blodgett films. Among alternative methods, photoalignment is a promising method which can substitute rubbing method in the future.

Photoalignment is a non-contact alignment technology in which the alignment film surface is treated by irradiating the polymer with polarized light to induce an anisotropic distribution of molecules of the alignment film.[18] The anisotropic generation by polarized light is called the Weigert effect. This effect was discovered in 1920 and can be understood as: the molecule strongly absorbs light, and a photochemical reaction then occurs when the electric vector of the photons matches the molecule transition moment. However, the photoalignment mechanisms in some materials are not yet understood because the photochemical reactions are different in each material. Among the photoalignment methods being used, the photoisomerization method used PI containing azobenzene in the main chain (Azo-PIs) is the most attractive.[21,31]

1.2 Objective

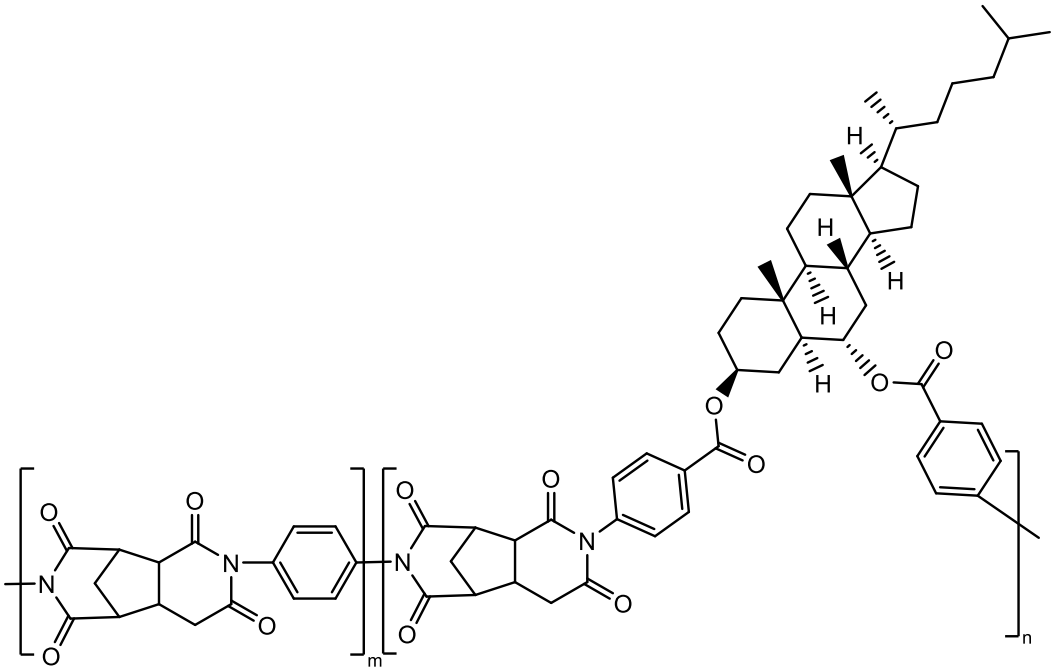

Figure 1.7 Chemical structure of PI containing steroidal side chains used in this study.

PI containing steroidal side chains has been synthesized by Nishikawa in JSR Corp. since 2011.[11] This PI has a side chain structure like a typical LC molecule. Namely, it consists of two benzoate groups, a steroidal structure as a rigid part and an alkyl side chain as a flexible part, as shown in Fig.1.7. Furthermore, it is known that by changing the fraction of units with a steroidal structure side chain, any required pretilt angle from 3º to 90º can be achieved. Hence, PI containing steroidal side chains is very useful for different LCD applications.

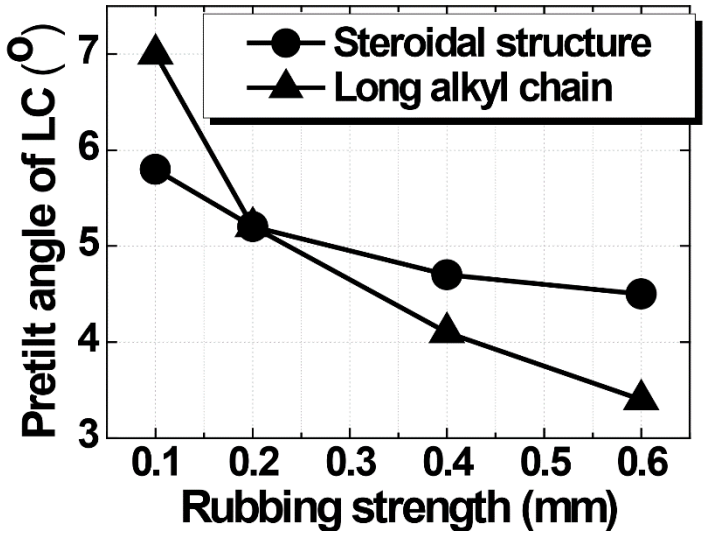

Figure 1.8 Relationship between rubbing strength and LC pretilt angle.[11]

Figure 1.8 shows the relationship between the rubbing strength and the LC pretilt angle.[11] The LC pretilt angle gradually decreases as the rubbing strength increases in the PI with a long alkyl chain. On the other hand, the LC pretilt angle does not change too much in the case of the PI with a steroidal structure. It suggests that the pretilt angle of the LC molecules on the PI with a steroidal structure is more stable than that on the PI with a long alkyl side chain. In addition, PI with steroidal side chains shows good electrical properties than PI with long alkyl side chains, and PI with fluorine atoms as shown in Fig.1.9.[11] Voltage holding ratio (VHR) is defined as the capacity to keep the charged voltage in the LCD. It is demonstrated that higher VHR gives good electrical properties. The PI with steroidal structure has the highest VHR because of the low polarization side-chain structure.

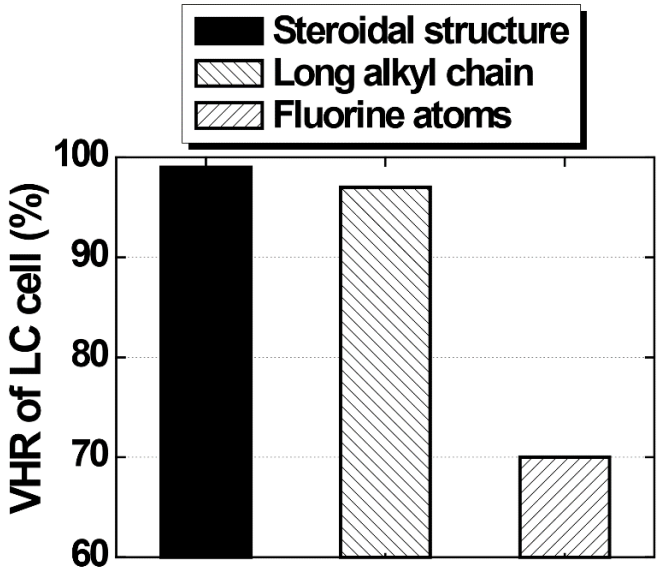

Figure 1.9 Voltage holding ratios of LC cells using three types of PI.[11]

Although PI containing steroidal side chains possesses outstanding properties[11], and it promises to become an excellent alignment layer for various LCD applications, the orientation and conformation of molecules at the PI surface after rubbing have not been fully known yet. For example, Ullah *et al.* assumed that only the steroidal parts have microscopic optical nonlinearity when investigating a PI film containing a 30% fraction of steroidal side chains.[32] They reported that the phenyl rings are aligned in the rubbing direction. However, the assumption of Ullah *et al.* has not been checked the validity yet. Moreover, to the best of my knowledge, there is no study investigating the molecular orientation and conformation of the steroidal structure and the alkyl side chain at the rubbed PI film surface like the one in this study. Hence, it is unknown yet which part of the rubbed PI film containing steroidal side chains is most strongly correlated with LC alignment.

The correlation between the molecular orientation at the surface of the PI containing steroidal side chains and the alignment of LC molecules on this rubbed PI film is not only

interesting from a scientific perspective. However, it is also desirable from an industrial perspective. Because it helps to understand the mechanism of LC alignment on the rubbed polymer surface and provides a reference for the design of new PI containing steroidal side chains for future commercial research in the display industry. However, it requests strong industry-university cooperation to accomplish this work.

1.3 Outline of dissertation

The dissertation has been organized in the following way:

Chapter 1 briefly introduces PI and the previous studies about the molecular orientation and conformation at PI surfaces. Then, this chapter will explain the objective of the research and provide the dissertation outline.

Chapter 2 introduces the theory of SFG and SHG, the origin of molecular vibrations, and the classification of SFG vibrational spectroscopy. Moreover, this chapter will describe how I can derive molecular orientation information from SFG vibrational spectra and SHG data.

Chapter 3 presents the definition of steroids and structures of several types of steroids. In addition, this chapter will explain the steroidal structure of the PI side chain used in this study.

Chapter 4 describes the sample preparation, SFG, and SHG experimental setups. In addition, this chapter will introduce the new sample rotation stage designed for this study.

Chapter 5 examines the assumption of Ullah *et al.* by analyzing SHG signals of unrubbed PI films with different side-chain diamine ratios.

Chapter 6 investigates the effect of the experimental conditions on the SFG spectrum and the quality of the PI sample in use and storage. In addition, proof of SFG from the PI film surface will be shown in this chapter.

Chapter 7 analyzes the molecular orientation and conformation of rubbed PI film surfaces. First, molecular vibrational modes of the rubbed PI film in an SFG spectrum will be assigned. Polarization dependence and azimuthal angle dependence of SFG spectroscopy will be then investigated to find out the quantitative information about the orientation of molecules at rubbed PI surfaces. Finally, the correlation between the PI surface orientation and LC alignment will be discussed.

Chapter 8 presents some conclusions drawn in this study.

References

[1] M. Taylor Bogert and R. Rex Renshaw, J. Am. Chem. Soc. **30**, 1135 (2002).

[2] A.S. Mathews, I. Kim, and C.S. Ha, Macromol. Res. **15**, 114 (2007).

[3] M. Fahim, J. Bijwe, and H.S. Nalwa, *Polyimides for Microelectronics and Tribology Applications* (2001).

[4] T. Matsumoto, High Perform. Polym. **13**, (2001).

[5] K.L.M. Malay K. Ghosh, *Polyimides: Fundamentals and Applications* (1996).

[6] T.O. and K.M. K. Sato, S. Harada, A. Saiki, T. Kimura, IEEE Trans. Parts, Hybrids, Packag. **9**, 176 (1973).

[7] Z. Liu, F. Yu, Q. Zhang, Y. Zeng, and Y. Wang, Eur. Polym. J. **44**, 2718 (2008).

[8] S. Ishihara and M. Mizusaki, J. Soc. Inf. Disp. **28**, 44 (2020).

[9] R. Arafune, K. Sakamoto, S. Ushioda, S. Tanioka, and S. Murata, Phys. Rev. E - Stat. Physics, Plasmas, Fluids, Relat. Interdiscip. Top. **58**, 5914 (1998).

[10] J. Stöhr and M.G. Samant, J. Electron Spectros. Relat. Phenomena **98**–**99**, 189 (1999).

[11] M. Nishikawa, J. Photopolym. Sci. Technol. **24**, 317 (2011).

[12] Q.H. Lu, X.M. Lu, J. Yin, Z.K. Zhu, Z.G. Wang, and H. Hiraoka, Japanese J. Appl. Physics, Part 1 Regul. Pap. Short Notes Rev. Pap. **41**, 4635 (2002).

[13] M. Vomero, P. van Niekerk, V. Nguyen, N. Gong, M. Hirabayashi, A. Cinopri, K. Logan, A. Moghadasi, P. Varma, and S. Kassegne, J. Micromechanics Microengineering **26**, 025018 (2016).

[14] X. Mathew, J.P. Enriquez, A. Romeo, and A.N. Tiwari, Sol. Energy **77**, 831 (2004).

[15] S. Wang, R. Li, C. Zheng, C. Cheng, Y. Yu, S. Bai, G. Feng, and A. Hu, J. Laser Micro Nanoeng. **11**, 285 (2016).

[16] C. Yi, W. Li, S. Shi, K. He, P. Ma, M. Chen, and C. Yang, Sol. Energy **195**, 340 (2020).

[17] P.K. Tapaswi and C.S. Ha, Macromol. Chem. Phys. **220**, 1 (2019).

[18] Q.H. Lu and F. Zheng, *Polyimides for Electronic Applications* (Elsevier Inc., 2018).

[19] K. Usami, K. Sakamoto, Y. Uehara, and S. Ushioda, Appl. Phys. Lett. **86**, 1 (2005).

[20] B. Chae, S. Bin Kim, S. Woo Lee, S. Il Kim, W. Choi, B. Lee, M. Ree, K. Hoon Lee, and J. Chul Jung, Macromolecules **35**, 10119 (2002).

[21] K. Usami and K. Sakamoto, J. Appl. Phys. **110**, (2011).

[22] T. Uchida, M. Hirano, and H. Sakai, Liq. Cryst. **5**, 1127 (1989).

[23] T. Sakai, K. Ishikawa, H. Takezoe, N. Matsuie, Y. Yamamoto, H. Ishii, Y. Ouchi, H. Oji, and K. Seki, J. Phys. Chem. B **105**, 9191 (2001).

[24] K. Sakamoto, R. Arafune, N. Ito, S. Ushioda, Y. Suzuki, and S. Morokawa, J. Appl. Phys. **80**, 431

(1996).

[25] J. Sung, D. Kim, C.N. Whang, M. Oh-E, and H. Yokoyama, J. Phys. Chem. B **108**, 10991 (2004).

[26] K. Shirota, K. Ishikawa, H. Takezoe, A. Fukuda, and T. Shiibashi, Jpn. J. Appl. Phys. **34**, L316 (1995).

[27] T. Sakai, J.G. Yoo, Y. Kinoshita, K. Ishikawa, H. Takezoe, A. Fukuda, T. Nihira, and H. Endo, Appl. Phys. Lett. **71**, 2274 (1997).

[28] M. Oh-e, A.I. Lvovsky, X. Wei, and Y.R. Shen, J. Chem. Phys. **113**, 8827 (2000).

[29] H.D. Jayathilake, M.H. Zhu, C. Rosenblatt, A.N. Bordenyuk, C. Weeraman, and A. V. Benderskii, J. Chem. Phys. **125**, (2006).

[30] M.H. Kohki Takatoh, N.I. Mitsuhiro Koden, R.H. And, and M. Sakamoto, *Alignment Technology and Applications of Liquid Crystal Devices* (CRC Press, 2005).

[31] K. Sakamoto, K. Usami, and K. Miki, Mol. Cryst. Liq. Cryst. **611**, 153 (2015).

[32] M.S. Ullah, S. Asai, Y. Inomata, K.T.T. Hien, G. Mizutani, Y. Murakami, and T. Okada, E-Journal Surf. Sci. Nanotechnol. **15**, 7 (2017).

CHAPTER 2. METHODOLOGY

This chapter provides a general description of the SFG process and how I can derive molecular orientation information from SFG spectra and SHG data.

2.1 SFG theory

SFG is a second-order nonlinear optical process occurring when two input beams at frequencies ω_1 and ω_2 overlap in a nonlinear optical medium and generate a sum frequency output at $\omega_{SFG} = \omega_1 + \omega_2$.[1–6] Surface SFG spectra were first observed by Shen *et al.* in 1987, at the University of California, Berkeley (USA). SHG is a particular case of SFG where $\omega_1 = \omega_2$. Generally, SHG process occurs when an input beam at frequency ω irradiates a nonlinear optical medium and generates a second harmonic output at frequency $\omega_{SHG} = 2\omega$.[7,8]

To comprehend the SFG process, it is helpful to begin with linear optics that nearly govern all the optical phenomena we see in our daily lives. Considering a molecule consists of two or more atoms, it is known that each atom is composed of a positively charged nucleus and one or more negatively charged electrons bound to the nucleus. The charge separation allows each atom in the molecule to form an electric dipole. This dipole starts to oscillate when the molecule is located in an electrical field. In line with classical laws of electromagnetism, the dipoles themselves act as electromagnetic radiation sources. The induced electric dipole μ is proportional to the electrical field strength by

$$\boldsymbol{\mu} = \boldsymbol{\mu}_0 + \alpha \boldsymbol{E}, \qquad (2.1)$$

where μ_0 is the static dipole of the material, and α is the polarizability of the molecular electrons.

It is more beneficial to consider the dipole moment per unit volume in condensed phases, commonly named polarization (P). In an electric field

$$\boldsymbol{P} = \boldsymbol{P^{(0)}} + \varepsilon_0 \chi^{(1)} \boldsymbol{E}, \qquad (2.2)$$

where $P^{(0)}$ is the static polarization, and $\chi^{(1)}$ is the macroscopic average of α which is commonly called the linear (first-order) susceptibility, ε_0 is the permittivity in a vacuum. The induced dipole oscillates at the same frequency as the electric field and emits light at the incident frequency. For a simple molecular material, the susceptibility is a function of the number of molecules per unit volume N multiplied by the molecular polarizability averaged over all the orientations of the molecules in the material,

$$\chi^{(1)} = N < \alpha > /\varepsilon_0. \qquad (2.3)$$

As the electric field E is strong enough, the response of the electrons to the field is no longer linear. Hence, higher-order terms in E need to be added in the dipole moment expression

$$\boldsymbol{\mu} = \boldsymbol{\mu}_0 + \alpha \boldsymbol{E} + \beta : \boldsymbol{EE} + \gamma \vdots \boldsymbol{EEE} + \cdots, \qquad (2.4)$$

where β and γ are the first- and second-order hyperpolarizabilities, respectively. The notation $\beta : \boldsymbol{EE}$ denotes $\sum_{j,k} \beta_{ijk} \boldsymbol{E}_j \boldsymbol{E}_k$. Assuming zero-static polarization, the polarization for bulk material becomes

$$\boldsymbol{P} = \varepsilon_0 \left(\chi^{(1)} \boldsymbol{E} + \chi^{(2)} : \boldsymbol{EE} + \chi^{(3)} \vdots \boldsymbol{EEE} + \cdots \right) = \boldsymbol{P}^{(1)} + \boldsymbol{P}^{(2)} + \boldsymbol{P}^{(3)} + \cdots, \qquad (2.5)$$

where $\chi^{(2)}$ and $\chi^{(3)}$ are the second-and third-order nonlinear susceptibilities, respectively. They are generally smaller than $\chi^{(1)}$ and only become considerable when the electromagnetic field is strong such as in pulsed lasers.

SFG arises from the second term $\boldsymbol{P}^{(2)} = \varepsilon_0 \chi^{(2)} : \boldsymbol{EE}$ in Eq. (2.5). It includes two different incident electric fields. The incident electric fields can be written as:

$$\boldsymbol{E} = \boldsymbol{E_1} e^{-i\omega_1 t} + \boldsymbol{E_2} e^{-i\omega_2 t} + c.c. \qquad (2.6)$$

Here $\boldsymbol{E_1}$, $\boldsymbol{E_2}$ and ω_1, ω_2 are the strengths and frequencies of the two incident electric fields, respectively; c.c. is complex conjugate. In this case, the second-order term of the polarization $\boldsymbol{P}^{(2)}$ of Eq. (2.5) becomes

$$\boldsymbol{P}^{(2)} = \varepsilon_0 \chi^{(2)} \left(\boldsymbol{E}_1^2 e^{-2i\omega_1 t} + \boldsymbol{E}_2^2 e^{-2i\omega_2 t} + 2\boldsymbol{E_1 E_2} e^{-i(\omega_1+\omega_2)t} + 2\boldsymbol{E_1 E}_2^* e^{-i(\omega_1-\omega_2)t} + c.c. \right) + 2\varepsilon_0 \chi^{(2)} (|\boldsymbol{E}_1|^2 + |\boldsymbol{E}_2|^2). \qquad (2.7)$$

Among the terms on the right-hand side of Eq. (2.7), $2\boldsymbol{E_1 E_2} e^{-i(\omega_1+\omega_2)t}$ has the frequency that equals the sum of the frequencies of the two input beams. If I define $\boldsymbol{P}_{SFG}^{(2)} = \mathbf{P}(\omega_1 + \omega_2) e^{-i(\omega_1+\omega_2)t}$, then I have

$$\mathbf{P}(\omega_1 + \omega_2) = 2\varepsilon_0 \chi^{(2)} \boldsymbol{E_1 E_2}. \qquad (2.8)$$

This equation shows that the induced nonlinear response from the material works as a new source to generate the SFG signal at a sum frequency $\omega_{SFG} = \omega_1 + \omega_2$.

Now, I start from Maxwell's equations to deduce the wave equation describing the evolution of the SFG field as below

$$\nabla . \boldsymbol{D} = \rho,$$

$$\nabla . \boldsymbol{B} = 0,$$

$$\nabla \times \boldsymbol{E} = -\frac{\partial \boldsymbol{B}}{\partial t},$$

$$\nabla \times \boldsymbol{H} = \frac{\partial \boldsymbol{D}}{\partial t} + \boldsymbol{J}. \qquad (2.9)$$

Here **J** is the electric current density, ρ is the electric charge density, and **D** is the electric displacement field. **H** and **B** are the forms of the magnetic field

$$\boldsymbol{B} = \mu_0 \boldsymbol{H}. \qquad (2.10)$$

$$\boldsymbol{D} = \varepsilon_0 \boldsymbol{E} + \boldsymbol{P}. \qquad (2.11)$$

I assume that the nonlinear effect happens in an environment with no free charge and no free current. Taking $\nabla \times$ on both sides of the third Maxwell's equation, I have

$$\nabla \times (\nabla \times \boldsymbol{E}) = -\nabla \times \frac{\partial \boldsymbol{B}}{\partial t} = -\mu_0 \nabla \times \frac{\partial \boldsymbol{H}}{\partial t} = -\mu_0 \frac{\partial^2 \boldsymbol{D}}{\partial t^2}. \qquad (2.12)$$

As shown in Eq. (2.5), the polarization consists of linear and nonlinear parts. It can be rewritten as $\boldsymbol{P} = \boldsymbol{P}^{(1)} + \boldsymbol{P}^{NL}$. Therefore, $\boldsymbol{D} = \boldsymbol{D}^{(1)} + \boldsymbol{P}^{NL}$, where $\boldsymbol{D}^{(1)} = \varepsilon_0 \boldsymbol{E} + \boldsymbol{P}^{(1)}$. In a lossless and dispersionless environment $\boldsymbol{D}^{(1)} = \varepsilon_0 \varepsilon^{(1)} \boldsymbol{E}$. Equation (2.12) can be written as

$$\nabla \times (\nabla \times \boldsymbol{E}) + \mu_0 \varepsilon_0 \varepsilon^{(1)} \frac{\partial^2 \boldsymbol{E}}{\partial t^2} = -\mu_0 \frac{\partial^2 \boldsymbol{P}^{NL}}{\partial t^2}. \qquad (2.13)$$

I note that $c = \frac{1}{\sqrt{\varepsilon_0 \mu_0}}$ is the speed of light, so Eq. (2.13) can be converted to

$$\nabla \times (\nabla \times \boldsymbol{E}) + \frac{\varepsilon^{(1)}}{c^2} \frac{\partial^2 \boldsymbol{E}}{\partial t^2} = -\frac{1}{\varepsilon_0 c^2} \frac{\partial^2 \boldsymbol{P}^{NL}}{\partial t^2}. \qquad (2.14)$$

To simplify the equation, I use $\nabla \times (\nabla \times \boldsymbol{E}) = \nabla(\nabla . \boldsymbol{E}) - \nabla^2 \boldsymbol{E}$. Generally, the value of the term $\nabla(\nabla . \boldsymbol{E})$ is small and can be ignored for the slowly varying field used in SFG. As a result, the wave equation can be simplified to

$$\nabla^2 \boldsymbol{E} - \frac{\varepsilon^{(1)}}{c^2} \frac{\partial^2 \boldsymbol{E}}{\partial t^2} = \frac{1}{\varepsilon_0 c^2} \frac{\partial^2 \boldsymbol{P}^{NL}}{\partial t^2}. \qquad (2.15)$$

This equation indicates that the nonlinear polarization of an environment acts as a source term for the electric field evolution.

2.2 SFG vibrational spectroscopy theory

In most SFG vibrational spectroscopy, one incident beam is in the visible range. The other incident beam is frequency-tunable in the mid-IR range because it is typically used to investigate vibrational resonances of molecules adsorbed at surfaces or interfaces.[5] A general geometry for the experimental SFG setup is shown in Fig. 2.1, in which the projections of the **k** vector of the visible and IR beams on the surface have the same direction.

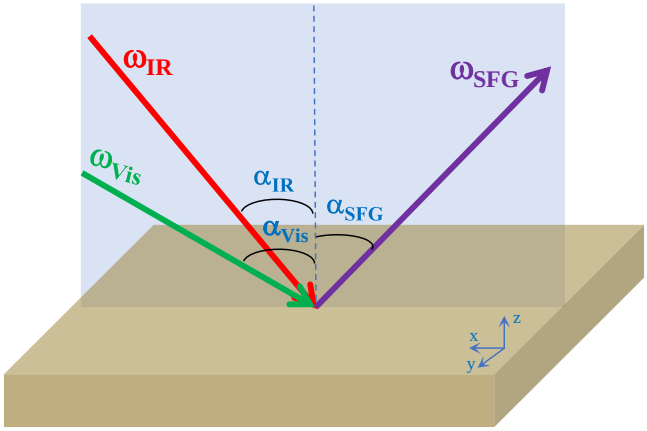

Figure 2.1. Schematic illustration of SFG process at a surface.

SFG has a strong signal in one direction determined by phase-matching conditions. For efficient energy transfer from ω_{Vis} and ω_{IR} to ω_{SFG} both energy and momentum conservation must be satisfied as below

$$\omega_{SFG} = \omega_1 + \omega_2, \qquad (2.16)$$

$$\boldsymbol{k}_{SFG_{//}} = \boldsymbol{k}_{Vis_{//}} + \boldsymbol{k}_{IR_{//}}. \qquad (2.17)$$

Here $\boldsymbol{k}_{SFG}$, $\boldsymbol{k}_{Vis}$, and $\boldsymbol{k}_{IR}$ are the wave vectors of sum frequency, visible and infrared beams, respectively. Equation (2.17) is commonly known as the phase-matching condition for SFG reflection geometry (Fig. 2.1) given by the parallel component of the **k** vectors of the involved light beams. In scalar form, it can be rewritten as:

$$k_{SFG} \sin \alpha_{SFG} = k_{Vis} \sin \alpha_{Vis} + k_{IR} \sin \alpha_{IR}, \qquad (2.18)$$

where α_{SFG}, α_{Vis}, and α_{IR} are the angles to the surface normal of SFG, visible, and IR beams, respectively. Equation (2.18) is called a surface phase-matching condition.

It is known that $\chi^{(2)}$ is the macroscopic average of the molecular hyperpolarizabilities β of the molecules adsorbed at the surface/interface

$$\chi^{(2)}_{ijk} = \frac{N}{\varepsilon_0} \sum_{lmn} \langle R(\psi) R(\theta) R(\varphi) \beta^{(2)}_{lmn} \rangle, \qquad (2.19)$$

where $R(\psi)R(\theta)R(\varphi)$ is the product of three rotation matrices using all three Euler angles to convert from the molecular coordinate system to the surface coordinate system. The <> bracket

indicates the orientational average, and N is the number of molecules per unit volume. Using perturbation theory, $\beta_{lmn}^{(2)}$ maybe deduced

$$\beta_{lmn}^{(2)} = \frac{1}{2\hbar}\frac{M_{lm}A_n}{\omega_q - \omega_{IR} - i\Gamma}, \tag{2.20}$$

where M_{lm}, A_n are the Raman and IR transition moments, respectively, ω_q is the vibrational resonance frequency, and Γ^{-1} is the relaxation time of the excited vibrational state. This equation explains why to be SFG active, both Raman and IR must be active. M_{lm}, A_n are defined as the following

$$M_{lm} = \sum_s \left[\frac{\langle g|\mu_l|s\rangle\langle s|\mu_m|v\rangle}{\hbar(\omega_{SFG} - \omega_{sg})} - \frac{\langle g|\mu_m|s\rangle\langle s|\mu_l|v\rangle}{\hbar(\omega_{Vis} + \omega_{sg})}\right],$$

$$A_n = \langle v|\mu_n|g\rangle, \tag{2.21}$$

where μ is the electric dipole operator, $|g\rangle$ is the ground state, $|v\rangle$ is the excited vibrational state, and $|s\rangle$ is any other state. Substituting the frequency-dependent term of $\beta_{lmn}^{(2)}$ in Eq. (2.20) into $\chi_{ijk}^{(2)}$ in Eq. (2.19), I have

$$\chi_{ijk}^{(2)} = \frac{N}{2\hbar\varepsilon_0}\sum_{lmn}\frac{\langle R(\psi)R(\theta)R(\varphi)M_{lm}A_n\rangle}{\omega_q - \omega_{IR} - i\Gamma}. \tag{2.22}$$

This equation shows that when the IR frequency matches the frequency of a molecular vibrational mode, $\omega_q - \omega_{IR}$ goes to zero, and the magnitude of $\chi_{ijk}^{(2)}$ increases. In other words, the SFG process is resonantly enhanced, as depicted in Fig. 2.2.[5] Therefore, a vibrational spectrum of the adsorbed molecules is obtained by detecting the SFG response as a function of IR frequency.

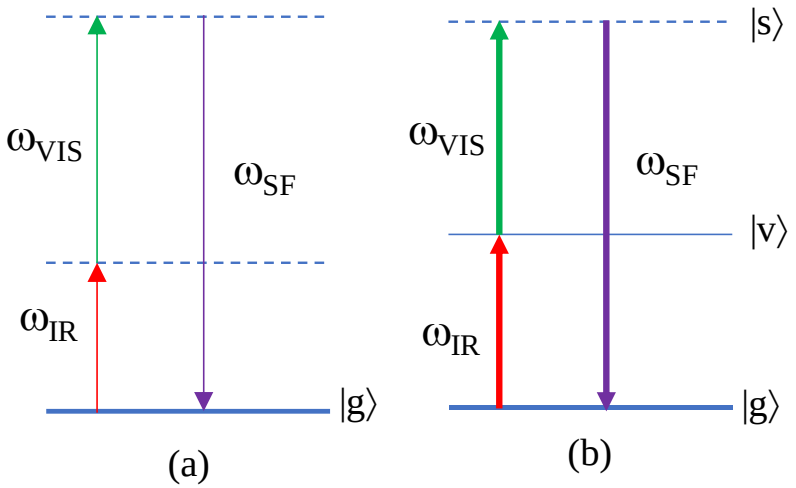

Figure 2.2 Schematic energy-level diagram for SFG process. (a) off resonance, (b) on resonance.[5]

$\chi_{ijk}^{(2)}$ is a third rank tensor which changes sign under inversion $\chi_{ijk}^{(2)} = -\chi_{-i-j-k}^{(2)}$. However, all directions are equivalent in centrosymmetric media $\chi_{ijk}^{(2)} = \chi_{-i-j-k}^{(2)}$. It can only be true under the condition that $\chi_{ijk}^{(2)}$=0. It is a reason why SFG does not occur in centrosymmetric media. It only occurs in asymmetric media such as surfaces or interfaces. At present, SFG is one of the most effective techniques for the investigation of surfaces and interfaces.

It is noted that when describing an electromagnetic wave coming on a planar surface, it is possible to resolve its associated **E** field into two components. One is polarized parallel (p) to the plane of incidence. The other is polarized perpendicular (s) to the plane of incidence, as shown in Fig.2.3.[5] Generally, electromagnetic equations consider the s and p polarizations separately because they behave differently at the surface/interface.

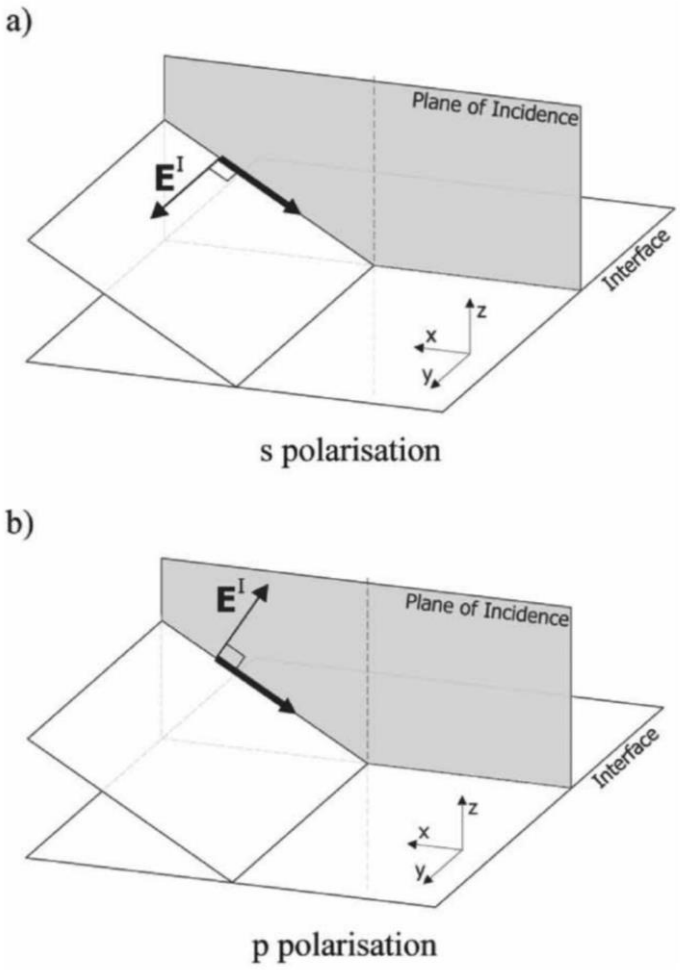

Figure 2.3 s- and p- polarized incident **E** fields.[5]

2.3 SFG quantitative analysis

Figure 2.4 shows how I can derive molecular orientation information from SFG data. In general, the effective second-order nonlinear susceptibility $\chi_{\text{eff}}^{(2)}$ can be directly obtained from the SFG signal and the incident laser beams.[9] Then, the macroscopic SFG susceptibility tensor elements $\chi_{ijk}^{(2)}$ can be deduced according to the quantitative correction of the Fresnel factors and local field factors. $\beta_{lmn}^{(2)}$ can be estimated from Raman and IR spectroscopy. It is known that the $\chi_{ijk}^{(2)}$ elements are directly related to the molecular hyperpolarizability $\beta_{lmn}^{(2)}$ through a transformation of the Euler angle. This relation is commonly mathematical and can be straightforwardly calculated. To extract quantitative molecular orientation information, a model for the orientational distribution is assumed and then finds values of $\theta, \psi,$ and φ by fitting the observed data. The SFG intensity in the reflection direction is given by

$$I(\omega_{SFG}) \propto \left|\chi_{eff}^{(2)}\right|^2 I(\omega_{vis}) I(\omega_{IR}), \qquad (2.23)$$

where $I(\omega_{vis})$ and $I(\omega_{IR})$ are the intensities of the visible and IR beams, respectively. $\chi_{\text{eff}}^{(2)}$ is the effective second-order nonlinear susceptibility tensor. $\chi_{\text{eff}}^{(2)}$ is defined using the experimental geometry and input/output polarization combinations.

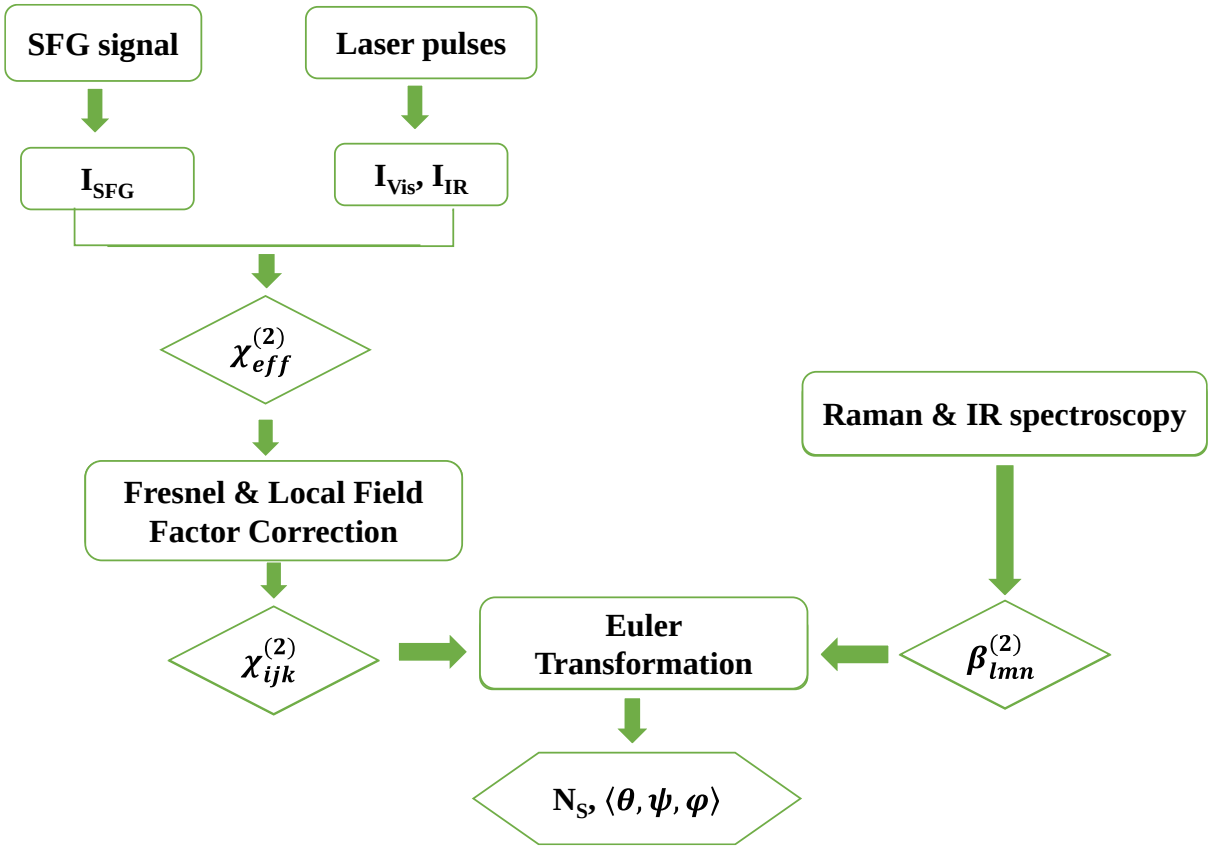

Figure 2.4 Schematic illustration of the quantitative analysis of the SFG data.

The azimuthal angle γ is defined as the angle between the rubbing direction and the plane of incidence, as shown in Fig. 2.5. Analysis of the azimuthal angle dependence of the SFG spectra gives information of the molecular orientation at the surface or interface.[10] For PPP polarization combination, there are eight elements of second-order nonlinear susceptibility $\chi^{(2)}_{ijk}$ contributing to the SFG signal

$$\begin{aligned}\chi^{(2)}_{\mathrm{eff,PPP}}(\gamma) = &-L_x(\omega_{SFG})L_x(\omega_{vis})L_x(\omega_{IR})\cos\alpha_{SFG}\cos\alpha_{vis}\cos\alpha_{IR}\,\chi^{(2)}_{xxx} - \\ &L_x(\omega_{SFG})L_x(\omega_{vis})L_z(\omega_{IR})\cos\alpha_{SFG}\cos\alpha_{vis}\sin\alpha_{IR}\,\chi^{(2)}_{xxz} - \\ &L_x(\omega_{SFG})L_z(\omega_{vis})L_z(\omega_{IR})\cos\alpha_{SFG}\sin\alpha_{vis}\sin\alpha_{IR}\,\chi^{(2)}_{xzz} - \\ &L_x(\omega_{SFG})L_z(\omega_{vis})L_x(\omega_{IR})\cos\alpha_{SFG}\sin\alpha_{vis}\cos\alpha_{IR}\,\chi^{(2)}_{xzx} + \\ &L_z(\omega_{SFG})L_x(\omega_{vis})L_x(\omega_{IR})\sin\alpha_{SFG}\cos\alpha_{vis}\cos\alpha_{IR}\,\chi^{(2)}_{zxx} + \\ &L_z(\omega_{SFG})L_z(\omega_{vis})L_x(\omega_{IR})\sin\alpha_{SFG}\sin\alpha_{vis}\cos\alpha_{IR}\,\chi^{(2)}_{zzx} + \\ &L_z(\omega_{SFG})L_x(\omega_{vis})L_z(\omega_{IR})\sin\alpha_{SFG}\cos\alpha_{vis}\sin\alpha_{IR}\,\chi^{(2)}_{zxz} + \\ &L_z(\omega_{SFG})L_z(\omega_{vis})L_z(\omega_{IR})\sin\alpha_{SFG}\sin\alpha_{vis}\sin\alpha_{IR}\,\chi^{(2)}_{zzz}, \end{aligned} \qquad (2.24)$$

where the coordinates x, y, and z are defined in Fig. 2.5. α_{SFG}, α_{vis}, and α_{IR} are the angles of incidence of the SFG, visible, and IR beams relative to the surface normal, respectively. $L_i(\omega)$ $(i = x, y, z)$ is the Fresnel factor, representing local field of incident and output radiations at the surface at frequency $\omega = \omega_{SFG}, \omega_{vis}, or\ \omega_{IR}$, given by[10]

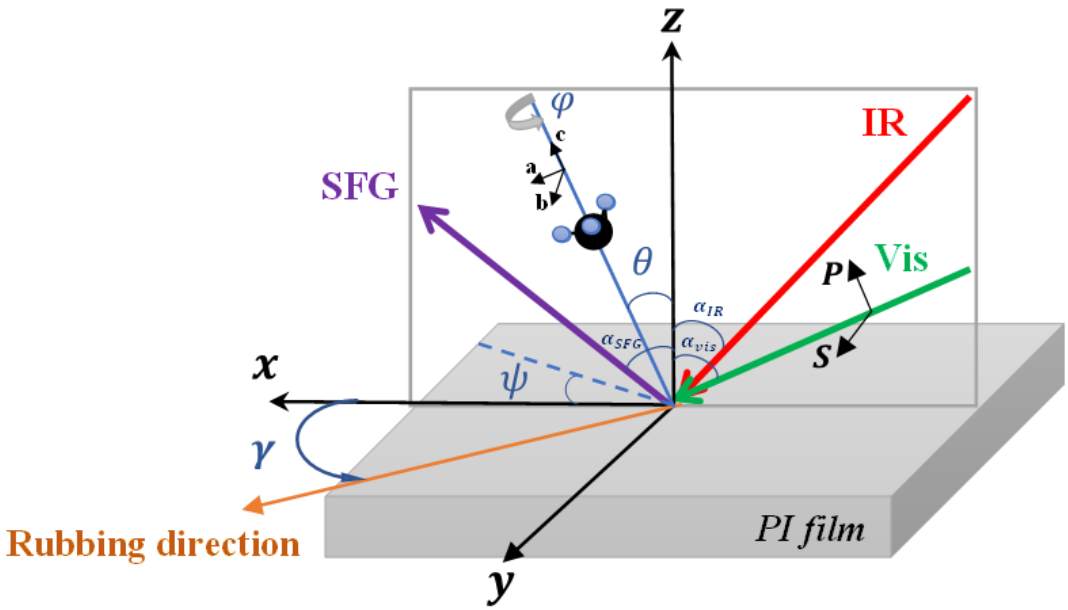

Figure 2.5 Experimental geometry and surface coordinate system.

$$L_x(\omega) = 1 - \frac{R_{p12} + R_{p23}e^{2i\beta}}{1 + R_{p12}R_{p23}e^{2i\beta}},$$

$$L_y(\omega) = 1 + \frac{R_{s12} + R_{s23}e^{2i\beta}}{1 + R_{s12}R_{s23}e^{2i\beta}},$$

$$L_z(\omega) = \left(1 + \frac{R_{p12} + R_{p23}e^{2i\beta}}{1 + R_{p12}R_{p23}e^{2i\beta}}\right)\left(\frac{n_1}{n'}\right)^2, \quad (2.25)$$

where $R_{p,s12}$ and $R_{p,s23}$ are the reflection Fresnel factors for s or p polarized beams at the air/PI and the PI/glass substrate interfaces. For example

$$R_{p12} = \frac{n_2 \cos\alpha_1 - n_1 \cos\alpha_2}{n_2 \cos\alpha_1 + n_1 \cos\alpha_2},$$

$$R_{s12} = \frac{n_1 \cos\alpha_1 - n_2 \cos\alpha_2}{n_1 \cos\alpha_1 + n_2 \cos\alpha_2} n_1, \quad (2.26)$$

where α_1 is the angle of incidence in the air, α_2 is the angle of refraction in the PI, and α_3 is the angle of refraction in the glass substrate, as shown in Fig.2.6. The refractive indices n_1, n_2, n_3, and n' are wavelength-dependent, so the Fresnel factors have to be calculated for each frequency ω. The factor $\beta = 2\pi \frac{n_2 h \cos\alpha_2}{\lambda_0}$ is the phase for the interference at the air/PI interface between the incident beam and reflection from the PI/glass substrate interface. h is the thickness of PI film, λ_0 is wavelength in a vacuum. The refractive index of the interfacial layer n' can be estimated using the slab model with a hemispherical cavity[11]

$$\left(\frac{1}{n'}\right)^2 = \frac{4n_2^2 + 2}{n_2^2(n_2^2 + 5)}. \quad (2.27)$$

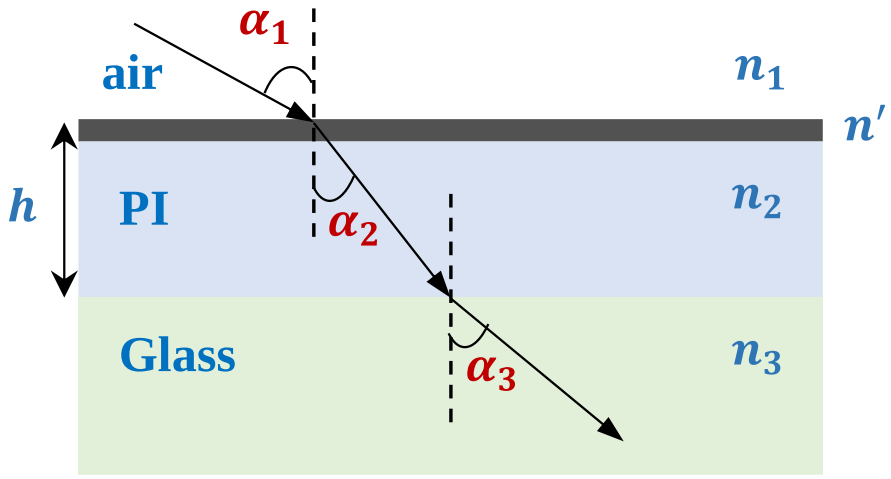

Figure 2.6. The 4-layer model was used to calculate the Fresnel factors.

The second-order nonlinear hyperpolarizability $\beta^{(2)}_{lmn}$ of a molecule is generally defined in the molecular coordinates (a, b, c), shown in Fig.2.5. It has 27 elements in total, but the number of non-zero elements is less due to molecular symmetry. I assume that the CH_3 group has C_{3v} symmetry. In this case, there are only three nonvanishing independent elements β_{ccc} and $\beta_{aac} = \beta_{bbc} = r\beta_{ccc}$. The value of r ranges from 1.66 to 3.5.[11–13] However, I will find that this variation of the parameter r does not significantly affect my discussion in Chapter VI. The orientation of a methyl group is given by the Euler angles (θ, ψ, φ), as described in Fig. 2.5. The transformation of $\beta^{(2)}_{lmn}$ to the molecular surface susceptibility of the methyl group $\beta^{(2)}_{ijk}$ is expressed as:

$$\beta^{(2)}_{ijk}(\theta, \psi, \varphi) = \sum_{lmn} U_{ijk,lmn}(\theta, \psi, \varphi)\beta^{(2)}_{lmn}, \qquad (2.28).$$

where $U_{ijk,lmn}(\theta, \psi, \varphi)$ is a product of three Euler matrices (Appendix C).[14] To determine the macroscopic surface susceptibility tensor of the methyl group, I average over the orientational distribution $f(\theta, \psi, \varphi)$

$$\chi^{(2)}_{ijk}(\gamma) = N \iiint d\theta d\psi d\varphi f(\theta, \psi, \varphi)\beta^{(2)}_{ijk}(\theta, \psi, \varphi). \qquad (2.29).$$

Equations (2.28) and (2.29) mean that the second-order nonlinear susceptibility of the surface depends on the molecular number density N, molecular orientation, and the hyperpolarizability of the methyl group. If I know its hyperpolarizability, the methyl group's orientation can be determined by measuring the SFG spectra of the corresponding CH_3 vibration at different azimuthal angles. I assume that each methyl group can freely rotate around the c-axis, so the rotation angle φ can be integrated from 0 to 2π to average over all possible orientations measured in the experiment.[4,10] Consequently, $f(\theta, \psi, \varphi)$ becomes a function of the tilt angle θ and the azimuthal angle ψ of the methyl group :

$$f(\theta, \psi, \varphi) = \frac{1}{4\pi^2\sigma_\theta\sigma_\psi} exp\left(-\frac{(\theta - \theta_0)^2}{2\sigma_\theta^2} - \frac{(\psi - \gamma)^2}{2\sigma_\psi^2}\right). \qquad (2.30).$$

Here, θ_0 is the average tilt angle, σ_θ is the tilt angle distribution width, and σ_ψ is the azimuthal angle distribution width around the rubbing direction.

In SFG vibrational spectroscopy, if the IR frequency is near vibrational resonance, $\chi^{(2)}_{eff}$ can be written as:

$$\chi^{(2)}_{eff} \propto A^{(2)}_{NR}e^{i\phi} + \sum_q \frac{A_q\Gamma_q}{\omega_{IR} - \omega_q + i\Gamma_q}, \qquad (2.31)$$

where $A_{NR}^{(2)}$ and ϕ are the amplitude and phase of the non-resonant part of the SFG response, ω_{IR} is the frequency of the IR light, and A_q, ω_q, and Γ_q are the amplitude, resonant frequency, and the line width of the q^{th} vibrational mode, respectively. From Eqs. (2.23) and (2.31), I have:

$$I(\omega_{SFG}) \propto \left| A_{NR}^{(2)} e^{i\phi} + \sum_q \frac{A_q \Gamma_q}{\omega_{IR} - \omega_q + i\Gamma_q} \right|^2 . \quad (2.32)$$

Equation (2.32) is usually used to fit measured SFG spectra.

According to theory for analyzing SFG spectra, Jayathilake *et al.* have developed a MATLAB program to calculate the effective second-order nonlinear susceptibility of the CH_3 symmetric stretching mode[15]. Therefore, I adopted their model to analyze the obtained azimuthal angle dependence of the SFG spectra in this study, as shown in Appendix D.

SFG vibrational spectroscopy has also been adopted to investigate structures of ***chiral molecules***.[16–18] At present, chiral molecules play an essential role in chemistry, biology, and medicine. A chiral molecule is a molecule that is not superimposable on its mirror image, as shown in Fig. 2.7.[19] On the other hand, a molecule that is superimposable on its mirror image is called an achiral molecule. Generally, all chiral molecules contain an atom that is connected to four *different* substituent groups.

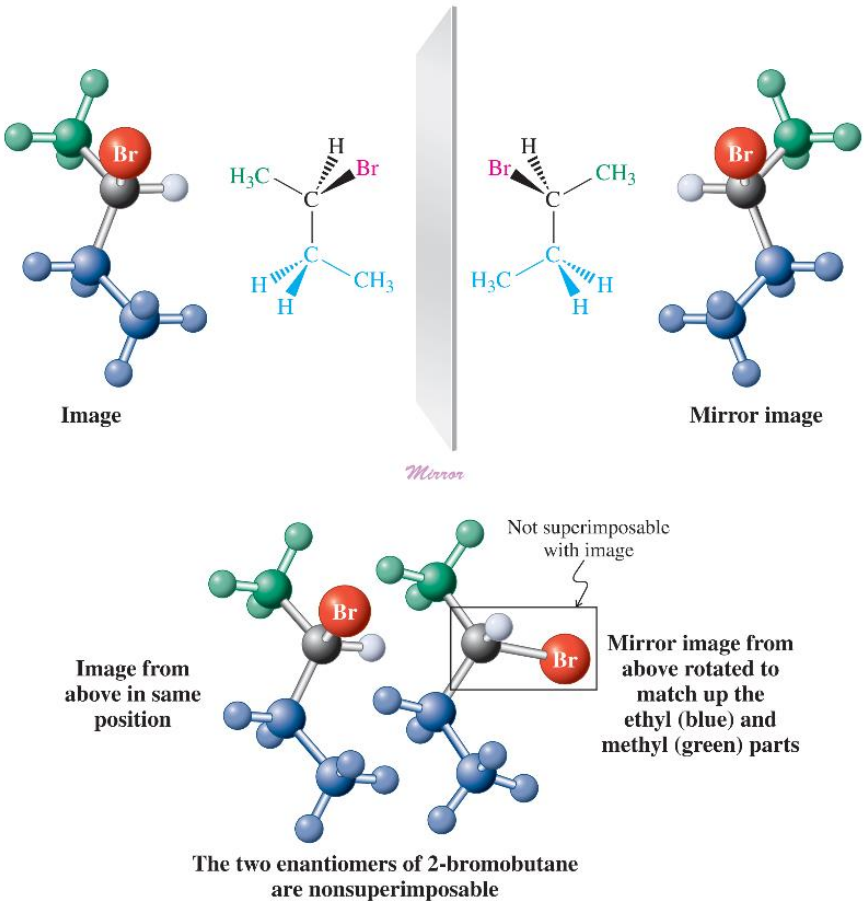

Figure 2.7 An example of a chiral molecule: 2-bromobutane.[19]

Practically, there are only seven nonzero $\chi_{ijk}^{(2)}$ elements: $\chi_{xxz}^{(2)} = \chi_{yyz}^{(2)}$, $\chi_{xzx}^{(2)} = \chi_{yzy}^{(2)}$, $\chi_{zxx}^{(2)} = \chi_{zyy}^{(2)}$ and $\chi_{zzz}^{(2)}$, for an isotropic achiral surface with the $C_{\infty v}$ symmetry.[11,18] These seven elements can be deduced by measuring SFG with SSP, SPS, PSS, and PPP polarization combinations. However, there are six additional nonzero $\chi_{ijk}^{(2)}$ elements: $\chi_{xyz}^{(2)}$, $\chi_{yxz}^{(2)}$, $\chi_{zxy}^{(2)}$, $\chi_{zyx}^{(2)}$, $\chi_{xzy}^{(2)}$ and $\chi_{yzx}^{(2)}$, for a chiral surface with the C_{∞} symmetry.[18] These orthogonal elements $\chi_{ijk}^{(2)}$ $(i \neq j \neq k)$ can be probed by measuring SFG with PSP, SPP, and PPS polarization combinations.

2.4 Classification of SFG vibrational spectroscopy

Based on the laser and detector systems, SFG vibrational spectroscopy can usually be classified into two types: narrowband (scanning) and broadband vibrational spectroscopy.[4,6] As shown in Fig. 2.8(a),[20] a picosecond (ps) pulsed laser such as a mode-locked Nd^{3+}: YAG laser is generally utilized to pump an optical parametric generator/amplifier (OPG/OPA) system and generate coherent tunable IR light. The tunable IR light and the frequency-doubled light (532nm) from the laser then overlap on the sample to generate SFG light in the reflection direction. Finally, by a photomultiplier (PMT) and gated integrator system, the SFG signal is detected and recorded. The narrowband SFG vibrational spectroscopy has high spectral resolution (below 5 cm^{-1}). However, it takes time to obtain a spectrum because only one wavenumber in the SFG spectrum can be recorded at each tuning step.

Figure 2.8(b)[21] shows a typical experimental setup for the broadband SFG vibrational spectroscopy. In this system, a femtosecond (fs) laser such as a mode-locked Ti: sapphire laser is usually utilized to generate high-energy broadband mid-IR pulses are generated by pumping OPA system. The visible beam is usually a narrowband pulse also achieved from the laser source. The narrowband visible beam and the broadband mid-IR beam overlap on a sample to excite multiple vibrational bands. The broadband SFG spectrum is then collected and recorded by a spectrometer coupling with a charge-coupled device (CCD) array. Although a broadband SFG vibrational spectroscopy has a higher speed of spectral collection than a narrow SFG vibrational spectroscopy, its spectral resolution is usually lower than a narrow SFG vibrational spectroscopy because of the relatively broader bandwidth of the visible beam.

(a)

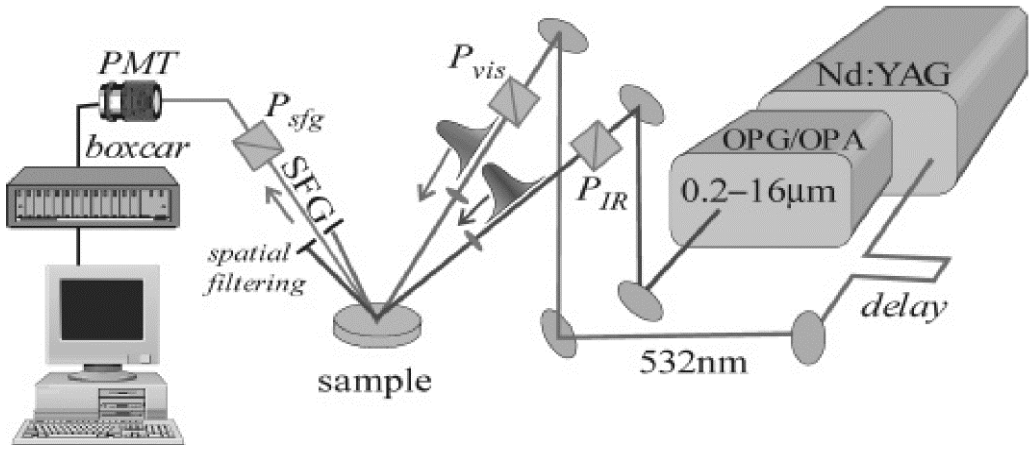

(b)

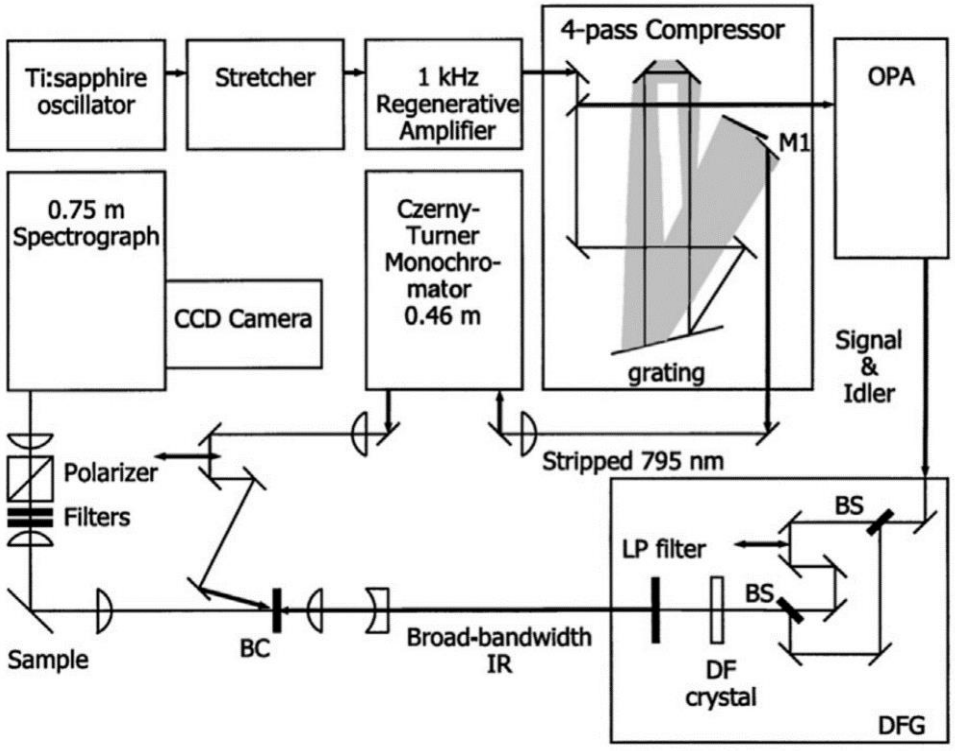

Figure 2.8 A typical experimental setup for (a) the narrowband[20] and (b) the broadband[21] SFG vibrational spectroscopy

2.5 SHG quantitative analysis

SHG is a useful technique to measure the molecular orientation distribution of polymer surfaces and interfaces.[7,11,22–24] For molecules with a dominant hyperpolarizability element $\beta_{ccc}^{(2)}$ along the long molecular axis c, the macroscopic nonlinear susceptibility responsible for the SHG is given by

$$\chi_{ijk}^{(2)} = N_s\langle(\hat{\boldsymbol{\imath}}\cdot\hat{\boldsymbol{c}})(\hat{\boldsymbol{\jmath}}\cdot\hat{\boldsymbol{c}})(\hat{\boldsymbol{k}}\cdot\hat{\boldsymbol{c}})\rangle\beta_{ccc}^{(2)}, \qquad (2.33)$$

where N_s is the surface molecular density, *i*, *j*, and *k* refer to the laboratory coordinates x, y, or z, and the brackets mean an average over the molecular orientations. In unrubbed polymer films, the molecular distribution is polar regarding the normal surface direction and isotropic in the surface x-y plane. Thus, there are only two independent nonvanishing elements of $\chi_{ijk}^{(2)}$ related to the molecular orientation as:

$$\chi_{zzz}^{(2)} = N_s\langle cos^3\theta\rangle\beta_{ccc}^{(2)},$$
$$\chi_{zii}^{(2)} = \chi_{izi}^{(2)} = \chi_{iiz}^{(2)} = \tfrac{1}{2}N_s\langle sin^2\theta cos\theta\rangle\beta_{ccc}^{(2)}, \quad (2.34)$$

where *i*, *j* = x, y, and θ is the tilt angle between $\hat{\boldsymbol{c}}$ and $\hat{\boldsymbol{z}}$. Here $\hat{\boldsymbol{z}}$ is along the normal to the film surface.

If I further assume that I have two kinds of polar molecules on the surface, Eq (2.34) will then become,

$$\chi_{zzz}^{(2)} = N_M\langle cos^3\theta_M\rangle\beta_{Mccc}^{(2)} + N_{X2}\langle cos^3\theta_{X2}\rangle\beta_{X2ccc}^{(2)}, \quad (2.35)$$

$$\chi_{zxx}^{(2)} = \chi_{zyy}^{(2)} = \tfrac{1}{2}N_M\langle cos\theta_M - cos^3\theta_M\rangle\beta_{Mccc}^{(2)} + \tfrac{1}{2}N_{X2}\langle cos\theta_{X2} - cos^3\theta_{X2}\rangle\beta_{X2ccc}^{(2)}. \quad (2.36)$$

The hyperpolarizabilities $\beta_{Mccc}^{(2)}$ and $\beta_{X2ccc}^{(2)}$ are those of units without and with the steroidal side chains, respectively. The above nonvanishing elements of $\chi^{(2)}$ can be measured by SHG. The SHG intensity is given by[2]

$$I(2\omega) \propto \left|\chi_{eff}^{(2)}\right|^2 I^2(\omega). \qquad (2.37)$$

Here $I(\omega)$ is the intensity of the incident laser beam and $\chi_{eff}^{(2)}$ is the effective nonlinear susceptibility. $\chi_{eff}^{(2)}$ is defined by[23]

$$\boldsymbol{\chi}_{eff}^{(2)} = [\hat{\boldsymbol{e}}(2\omega)\cdot\boldsymbol{L}(2\omega)]\boldsymbol{\chi}^{(2)} : [\boldsymbol{L}(\omega)\cdot\hat{\boldsymbol{e}}(\omega)][\boldsymbol{L}(\omega)\cdot\hat{\boldsymbol{e}}(\omega)]. \qquad (2.38)$$

Here $\hat{\boldsymbol{e}}$ are unit polarization vectors for input beam at ω and output beam at 2ω, and $\boldsymbol{L}$'s are the local-field factor or Fresnel factor tensors for SHG field and fundamental beam, respectively. Using $\chi_{eff}^{(2)}$ determined by SHG measurements and $\boldsymbol{L}$, the nonzero $\chi^{(2)}$ elements can be deduced.

References

[1] Y.R. Shen, C.K. Chen, and A.R.B. de Castro, Springer Ser. Opt. Sci. **26**, 77 (1981).

[2] Y.R. Shen, Nature **337**, 519 (1989).

[3] Y.R. Shen, J. Phys. Chem. C **116**, 15505 (2012).

[4] C. Zhang, Appl. Spectrosc. **71**, 1717 (2017).

[5] A.G. Lambert, P.B. Davies, and D.J. Neivandt, Appl. Spectrosc. Rev. **40**, 103 (2005).

[6] C.S. Tian and Y.R. Shen, Surf. Sci. Rep. **69**, 105 (2014).

[7] Y.R. Shen, Annu. Rev. Phys. Chem. **40**, 327 (1989).

[8] S.C. Hong, M. Oh-E, X. Zhuang, Q. Shen, J.J. Ge, B.W. Harris, and S.Z.D. Cheng, Phys. Rev. E - Stat. Nonlinear, Soft Matter Phys. **63**, 517061 (2001).

[9] C.D. Bain, J. Chem. Soc., Faraday Trans. **91**, 1281 (1995).

[10] H.D. Jayathilake, M.H. Zhu, C. Rosenblatt, A.N. Bordenyuk, C. Weeraman, and A. V. Benderskii, J. Chem. Phys. **125**, (2006).

[11] X. Zhuang, P.B. Miranda, D. Kim, and Y.R. Shen, Phys. Rev. B - Condens. Matter Mater. Phys. **59**, 12632 (1999).

[12] K. Wolfrum and A. Laubereau, Chem. Phys. Lett. **228**, 83 (1994).

[13] G.R. Bell, C.D. Bain, and R.N. Ward, J. Chem. Soc., Faraday Trans. **92**, 515 (1996).

[14] C. Hirose, N. Akamatsu, and K. Domen, Appl. Spectrosc. **46**, 1051 (1992).

[15] H.D. Jayathilake, in (VDM Verlag Dr. Mueller, 2010).

[16] M.A. Belkin, T.A. Kulakov, K.-H. Ernst, L. Yan, and Y.R. Shen, Phys. Rev. Lett. **85**, 4474 (2000).

[17] L. Fu, J. Liu, and E. C. Y. Yan, J. Am. Chem. Soc. **133**, 8094 (2011).

[18] L. Fu, Z. Wang, and E.C.Y. Yan, Int. J. Mol. Sci. **12**, 9404 (2011).

[19] K.P.C. Vollhardt and N.E. Schore, *Organic Chemistry: Structure and Function*, 6th ed. (W. H. Freeman, 2010).

[20] D. Kim and Y.R. Shen, Appl. Phys. Lett. **74**, 3314 (1999).

[21] L.J. Richter, T.P. Petralli-Mallow, and J.C. Stephenson, Opt. Lett. **23**, 1594 (1998).

[22] K. Shirota, K. Ishikawa, H. Takezoe, A. Fukuda, and T. Shiibashi, Jpn. J. Appl. Phys. **34**, L316 (1995).

[23] M.B. Feller, W. Chen, and Y.R. Shen, Phys. Rev. A **43**, 6778 (1991).

[24] X. Wei, S.C. Hong, X. Zhuang, T. Goto, and Y.R. Shen, Phys. Rev. E - Stat. Physics, Plasmas, Fluids, Relat. Interdiscip. Top. **62**, 5160 (2000).

CHAPTER 3. STEROIDAL STRUCTURE

This chapter presents the definition of steroids and the structures of several types of steroids. Additionally, the steroidal structure of the PI side chain used in this study will also be described.

3.1 Structure of steroids

3.1.1 Parent hydrocarbons

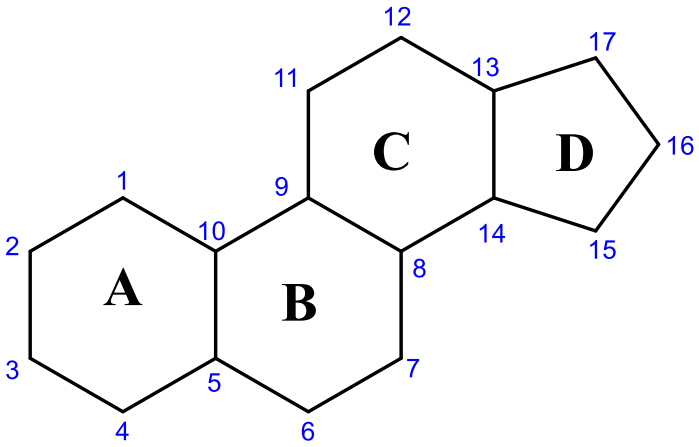

Figure 3.1. Steroid skeleton.

Steroids possess the skeleton of perhydrocyclopentanophenanthrene with a four alicyclic ring system as shown in Fig. 3.1.[1,2] Three rings are six-membered, and the fourth ring is five-membered. These rings are fused and have 17 carbon atoms. These carbon atoms are numbered, and the rings are lettered to identify easily. Because of substituents at other locations of the alicyclic ring system, the variation of the side chains attached to C-17, and the different configurations of the steroid skeleton, there are many steroids.[3] Some of the essential steroids are cholesterol and related compounds, bile salts, and certain hormones such as cortisone and sex hormones.

The steroid skeleton appears planar, and substituents on the alicyclic rings can be located either above or below the ring plane as it is drawn in two-dimensional (2D) shape, as shown in Fig. 3.2.[4] Substituents located below the ring plane are illustrated with dashed lines or with broken lines ( ). Hence, they are referred to as α-configuration. On the other hand, substituents located above the ring plane are drawn with solid lines or with dark wedges ( ). Hence, they are referred to as β-configuration. Conventionally, the angular methyl groups numbered 18, 19 attached to C-13 and C-10, respectively, and the side chains attached to C-17 have the β-configuration.

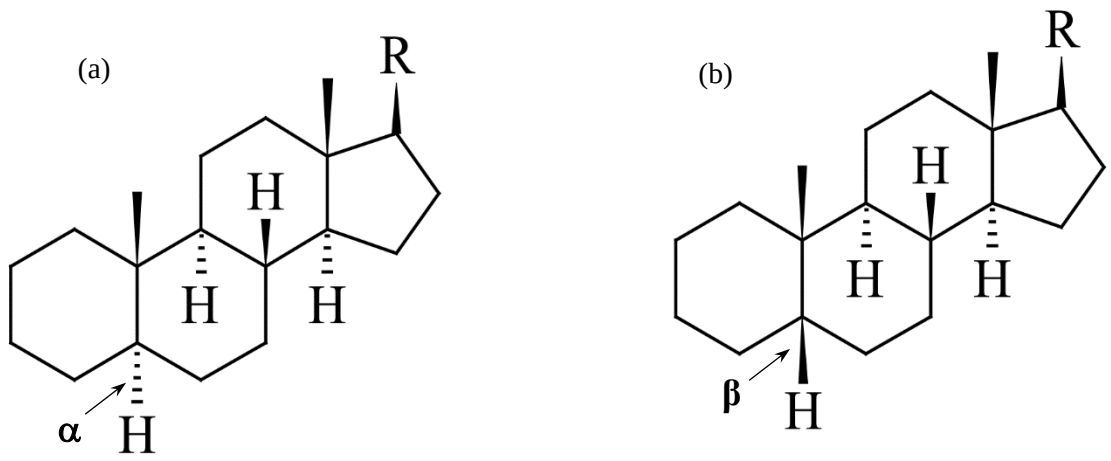

Figure 3.2 (a) 5α-Configuration, (b) 5β-Configuration.[4]

There are six types of skeletal steroids mainly concerned.[1] In general, all except one of these have the four alicyclic systems, the exception being compounds of the vitamin D group where ring B has been opened as follows

(1) Estrane *(or* oestrane*)* is the simplest steroidal structure consisting of the four alicyclic ring systems and a methyl group at C-13, but it lacks a methyl group at C-10 and a side chain C-17, as shown in Fig. 3.3(a).

(2) The hydrocarbon consists of the four alicyclic ring systems and methyl groups at C-10 and C-13 but lacks a side chain at C-17, as shown in Fig. 3.3(b) is named androstane.

(3) There are two additional carbon atoms at C-17 of the *androstane* structure that gives the hydrocarbon named pregnane, as shown in Fig. 3.3(c).

(4) The C_{24} structure with a short alkyl side chain is called cholane, as shown in Fig. 3.3(d).

(5) Cholestane is a hydrocarbon possessing a branched chain with eight carbon atoms attached to C-17, as shown in Fig. 3.3(e).

(6) *Vitamin D and its derivatives* are derived from steroidal structures by opening ring B, as shown in Fig. 3.3(f).

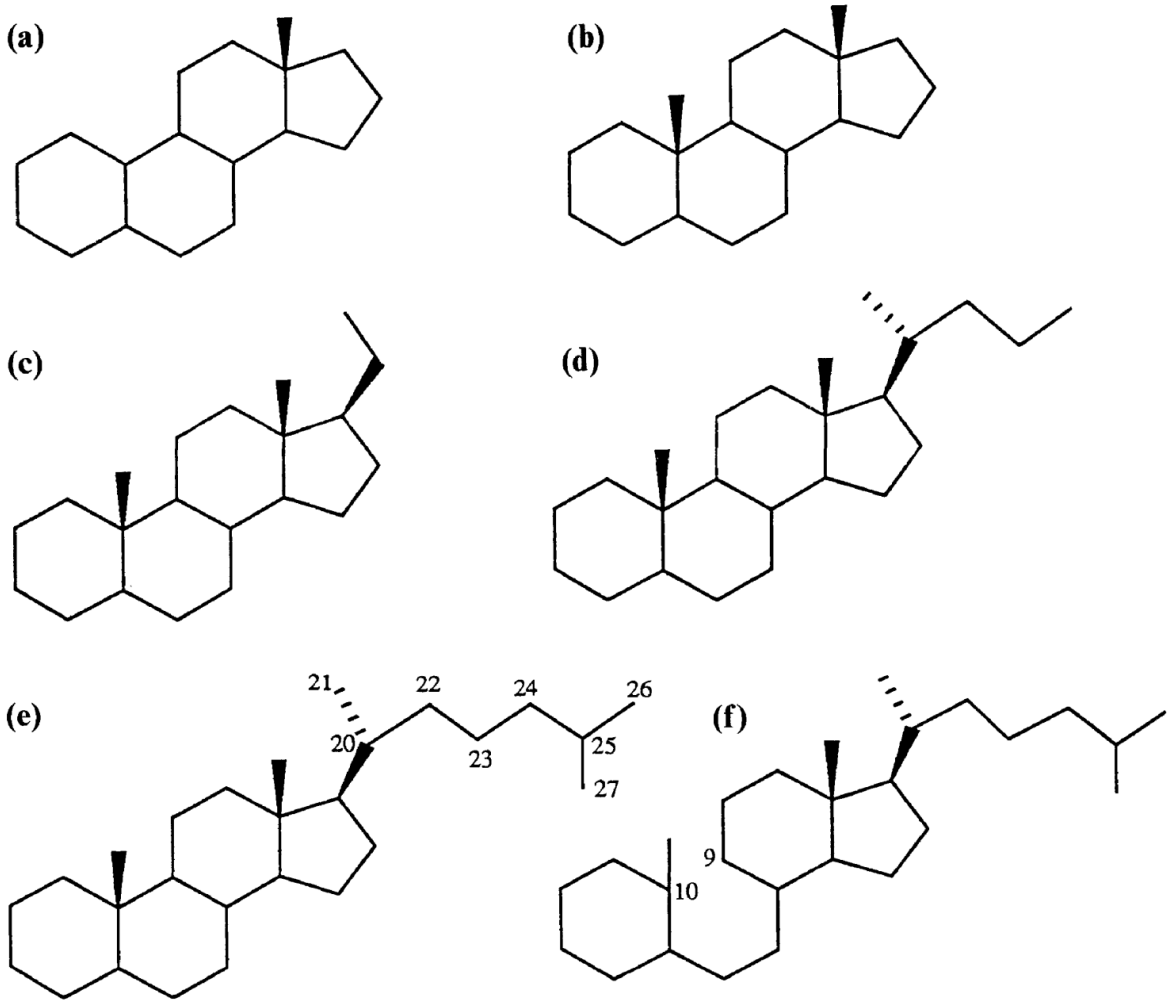

Figure 3.3 Six types of skeletal steroids. (a) Estrane; (b) androstane; (c) pregnane; (d) cholane; (e) cholestane; and (f) 9,10-secocholestane.[1]

3.1.2 Conformation

The three-dimensional (3D) shape of the alicyclic rings in the steroid skeleton is determined by cyclohexane. It is known that a planar structure for cyclohexane is impossible. In practice, the cyclohexane ring (A/B/C) commonly has the flip conformation, and ring D exists in a half-chair conformation.[4] As a result, the steroid ring system is not planar in the 3D shape, and substituents on the cyclohexane rings can be located at the *axial* or the *equatorial* positions, as shown in Fig. 3.4. The *axial* positions point perpendicular to the ring plane, while the *equatorial* positions only make a slight angle compared to the ring plane.

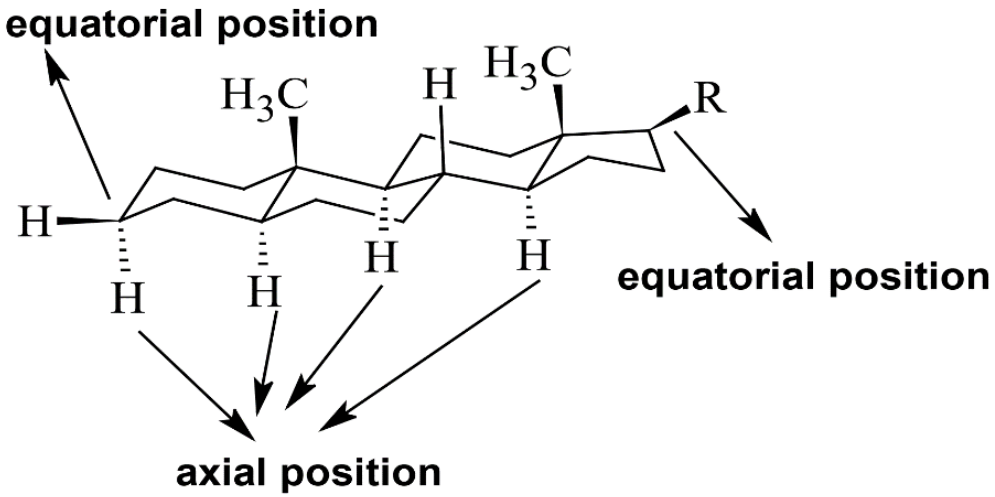

Figure 3.4 *Axial* and the *equatorial* positions in the steroid skeleton.[4]

There are three fusions in a steroid skeleton because it consists of four alicyclic rings. Each ring fusion can occur either in a *cis*- or *trans*-ring fusion. The ring fusion is called *cis* as these bonds lie on the same side of the ring system, or *trans* as they are opposite sides, as shown in Fig. 3.5. Generally, the A/B ring fusion has the *trans* configuration in some steroids and has a *cis* configuration in others, while both the B/C and C/D ring fusions mostly have the *trans* configuration in natural steroids.[4] Figure 3.6 shows the 3D structures of three kinds of natural steroids: *trans-trans-trans* (cholestanol), cis-*trans-trans* (cholic acid), and *cis-trans-cis* (digitoxigenin). Due to their stability, most natural steroids have a *trans* configuration at all three fusions.[3] This is the reason that the steroids are rigid and semi-flat in structures.

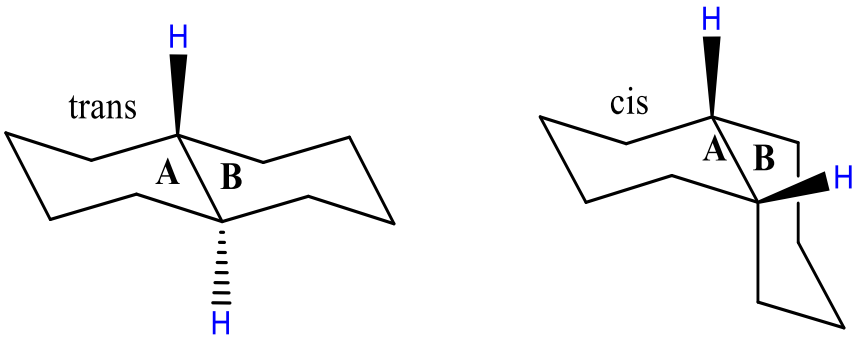

Figure 3.5 *cis*- and *trans*-ring fusions.

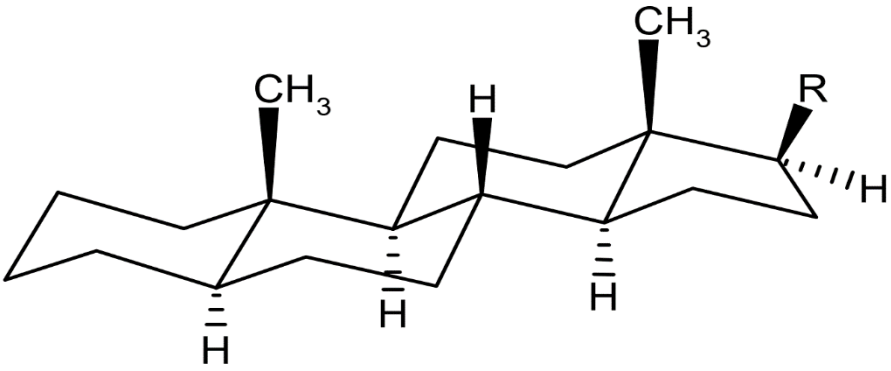

trans-trans-trans

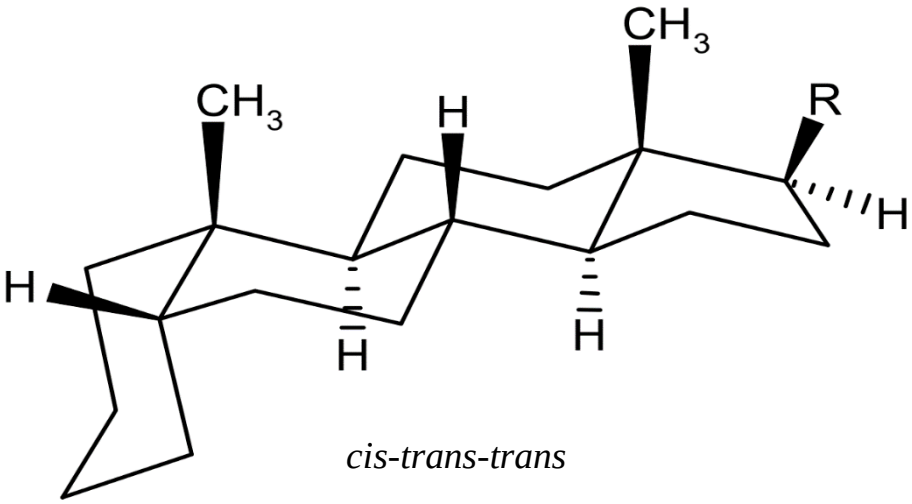

cis-trans-trans

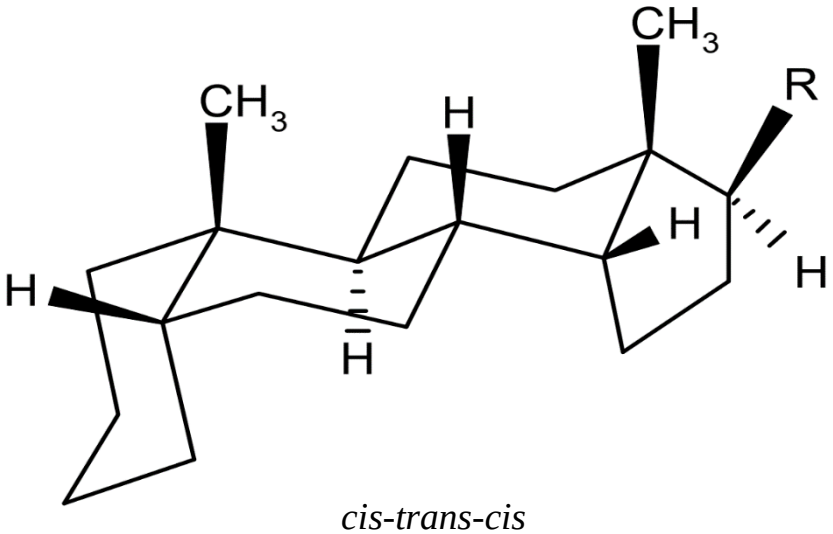

cis-trans-cis

Figure 3.6 3D structures of three kinds of natural steroids.[4]

3.2 Side chain structure of the polyimide used in this study

Figure 3.7 shows the chemical structure of the side chain of the PI used in this study. It consists of the four alicyclic ring systems with two methyl groups at C-10 and C-13 like a steroid molecule, two benzoate groups at C-3 and C-6, and an alkyl chain named 6-methylheptan-2-yl group at C-17. This PI side chain can also be divided into two parts. One is a rigid part containing two benzoate groups and the steroidal structure. The other is a flexible part containing a 6-methylheptan-2-yl group. On the other hand, a steroidal structure and alkyl chain are also the main components of a cholestanol molecule (Fig. 3.8), and their SFG response was studied by Kett et al.[5]

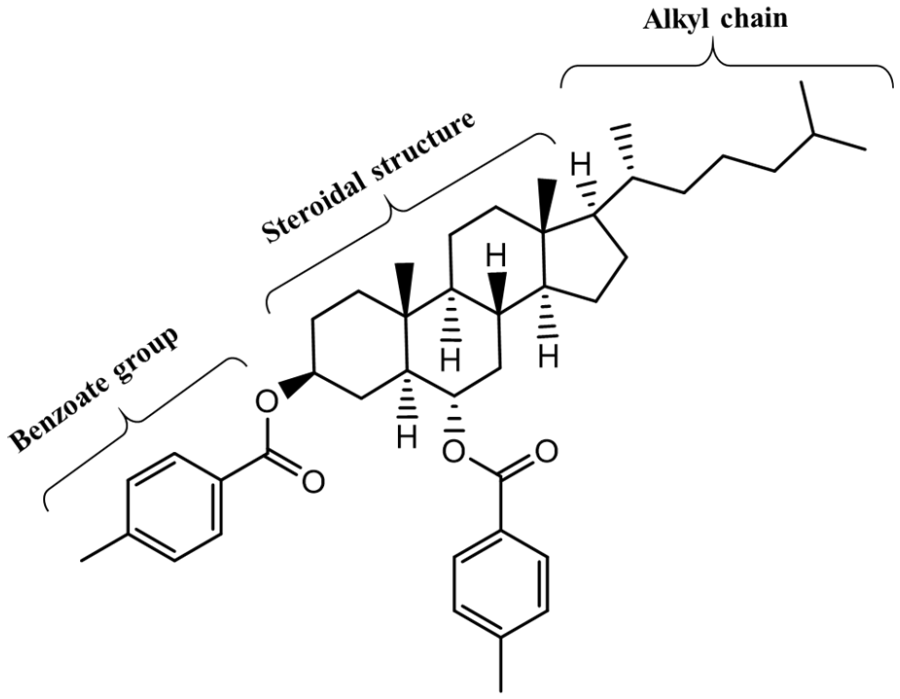

Figure 3.7 Structure of the steroidal structure side chain used in this study.

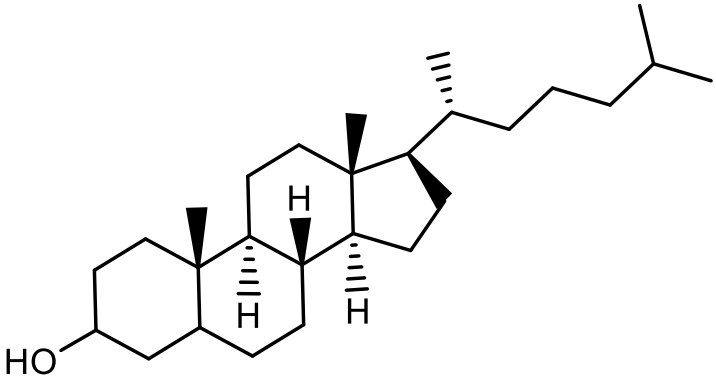

Figure 3.8 Cholestanol.

The PI side chain of the PI used in this study has a chemical structure similar to the most common LC molecule called a rod-shaped molecule. Generally, a rod-shaped molecule is composed of two moieties, including a rigid core and a flexible chain.[6] The rigid core usually contains one or two phenyl rings. The flexible chain usually contains an alkyl chain, as shown in Fig. 3.9.[7] It is known that the phenyl rings of LC molecules might interact with the phenyl rings of the PI side chain through π-π interactions. In contrast, the alkyl chains of LC molecules might interact with the side chains of the PI through van der Waals interactions.[8] Because of the similar molecular structure of the PI side chains used in this study and LC molecules, the orientation direction of the rubbed PI side chains might efficiently be transmitted to the LC molecules.

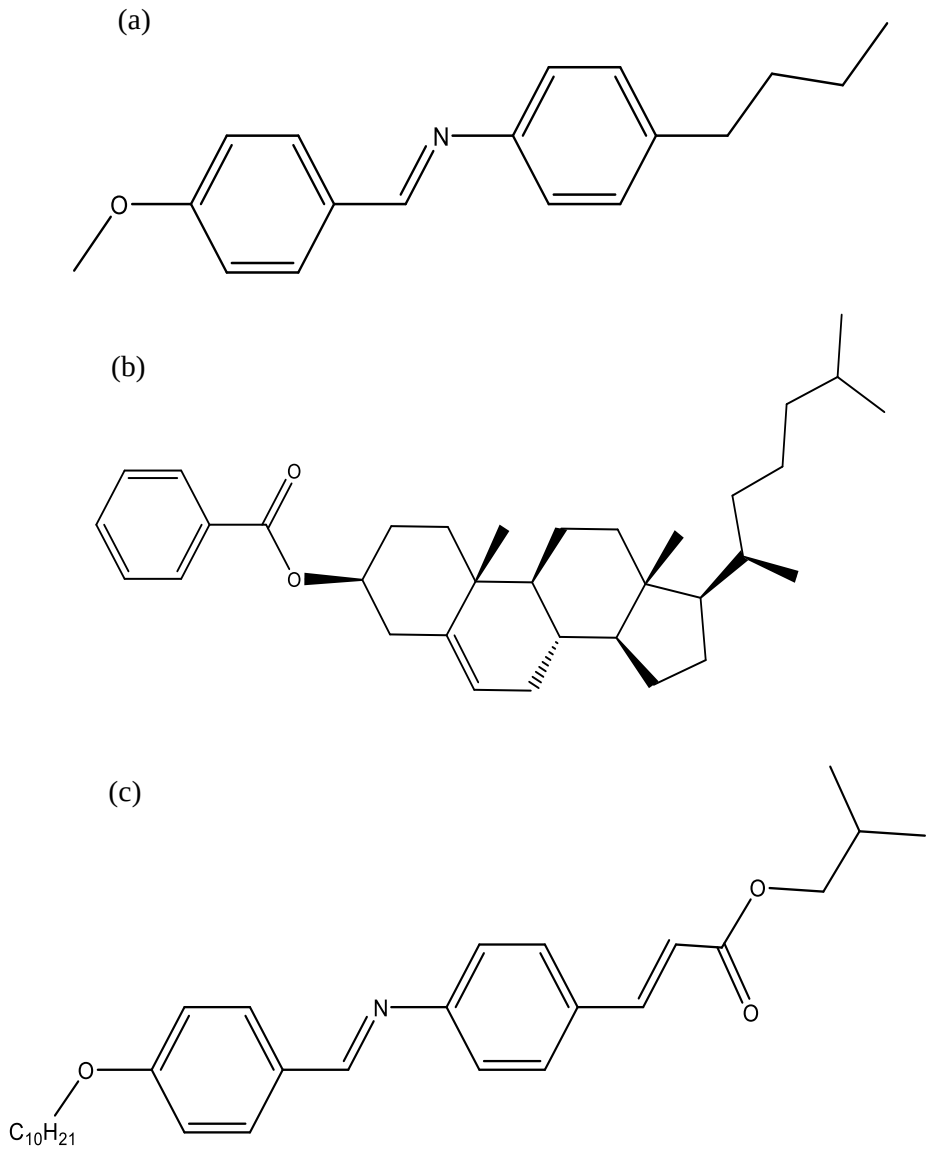

Figure 3.9 Molecular structures of the typical LC molecules forming liquid crystalline mesophases: a) N-(p-methoxybenzylidene)-p-butylaniline (MBBA), b) 5-cholesten-3-yl benzoate (cholesteryl benzoate), and c) D-2-methylbutyl 4–[4-n-decyloxybenzylideneamino]- cinnamate (DOBAMBC).[7]

References

[1] D.N. Kirk and B.A. Marples, Steroid Anal. **1**, 1 (1995).

[2] G.P. Moss, Pure Appl. Chem. **61**, 1783 (1989).

[3] K. Tantuco, E. Deretey, and I.G. Csizmadia, J. Mol. Struct. THEOCHEM **503**, 97 (2000).

[4] D. Kumar, V. Kumar, and P. Jalwal, ~ 124 ~ Int. J. Chem. Stud. **4**, 124 (2016).

[5] P.J.N. Kett, M.T.L. Casford, and P.B. Davies, J. Phys. Chem. B **117**, 6455 (2013).

[6] P.J. Collings and J.W. Goodby, *Introduction to Liquid Crystals* (CRC Press, Second Edition, 2019).

[7] C. Esteves, E. Ramou, A.R.P. Porteira, A.J. Moura Barbosa, and A.C.A. Roque, Adv. Opt. Mater. **8**, (2020).

[8] S. W. Lee, S. J. Lee, S. G. Hahm, T. J. Lee, B. Lee, B. Chae, S. B. Kim, J. C. Jung, W. C. Zin, B. H. Sohn, and M. Ree, Macromolecules **38**, 4331 (2005).

CHAPTER 4. EXPERIMENTAL PROCEDURE

This chapter gives a description of the sample preparation process and the SFG/SHG optical setup. Details of how the SFG/SHG signal is collected are also described.

4.1 Sample preparation

The chemical structure of the polyimide containing steroidal side chains used in this study is shown in Fig. 1.7. I used unrubbed PI films with five different molar fractions of the steroidal part, PI-0, PI-30, PI-60, PI-90, and PI-100, for SHG measurement. Here the molar fraction in molar% is represented by the number after "PI-". Three types of PI-30 films, including unrubbed PI-30, rubbed PI-30, and rubbed PI film with a PMMA layer, were used for SFG measurement. These PI films were provided by JSR Corp. They were put in plastic boxes after preparation for transport and stored in a dry box in the experimental room. The room temperature was always kept at ~ 22^{o}C.

The reaction scheme of the PI film synthesis is shown in Fig. 4.1. First, (polyamic) acid (PAA) solution was synthesized from 2,3,5-tricarboxy-cyclopentyl acetic dianhydride (TCA-AH), 1,4-phenylenediamine, steroidal structure diamine is different to obtain the PI samples with varying fractions of a molar of the steroidal side chain. For example, the molar ratio of TCA-AH: phenylenediamine: steroidal side chain diamine is fixed at 10:7:3 to synthesize the PI-30 film, while this molar ratio is fixed at 10:4:6 to synthesis the PI-60 film. The PAA films were then prepared by spin-coating on non-alkali glass plates. The coated films were dried for 2 min at 80^{0}C to evaporate the solvent and 30 min at 230^{0}C under a nitrogen atmosphere to induce the imidization. The thickness of the PI film was about 80 nm. The spinning rate controlled the PI film thickness. After drying, the unrubbed PI plates were cut into 20×15 mm^2 pieces.

To obtain the rubbed PI-30 samples, a rubbing machine with a roller covered with nylon cloth was used. The PI-30 films were rubbed once under the following conditions: the rotational speed of the roller was 400 rpm, the translational speed of the sample was 30 mm/sec, and the pile impression depth indicating the rubbing strength was 0.4 mm. It should be emphasized here that the rubbing strength was weak enough to affect the molecular orientation at the PI side chain only. After the rubbing process, the glass plates were cut into 20×15 mm^2 pieces for SFG measurements. Fig. 4.2 shows the rubbed and unrubbed PI-30 films after preparation. These PI films were colorless and transparent.

The rubbed PI-30 film with a poly (methyl methacrylate) (PMMA) overlayer was prepared to prove that the observed SFG spectra in this study mainly originate from the PI surface, and the contribution from the PI/glass substrate interface and the bulk PI is not significant. Figure 4.3 shows the chemical structure of PMMA. The thickness of the PMMA layer was ~5 nm.

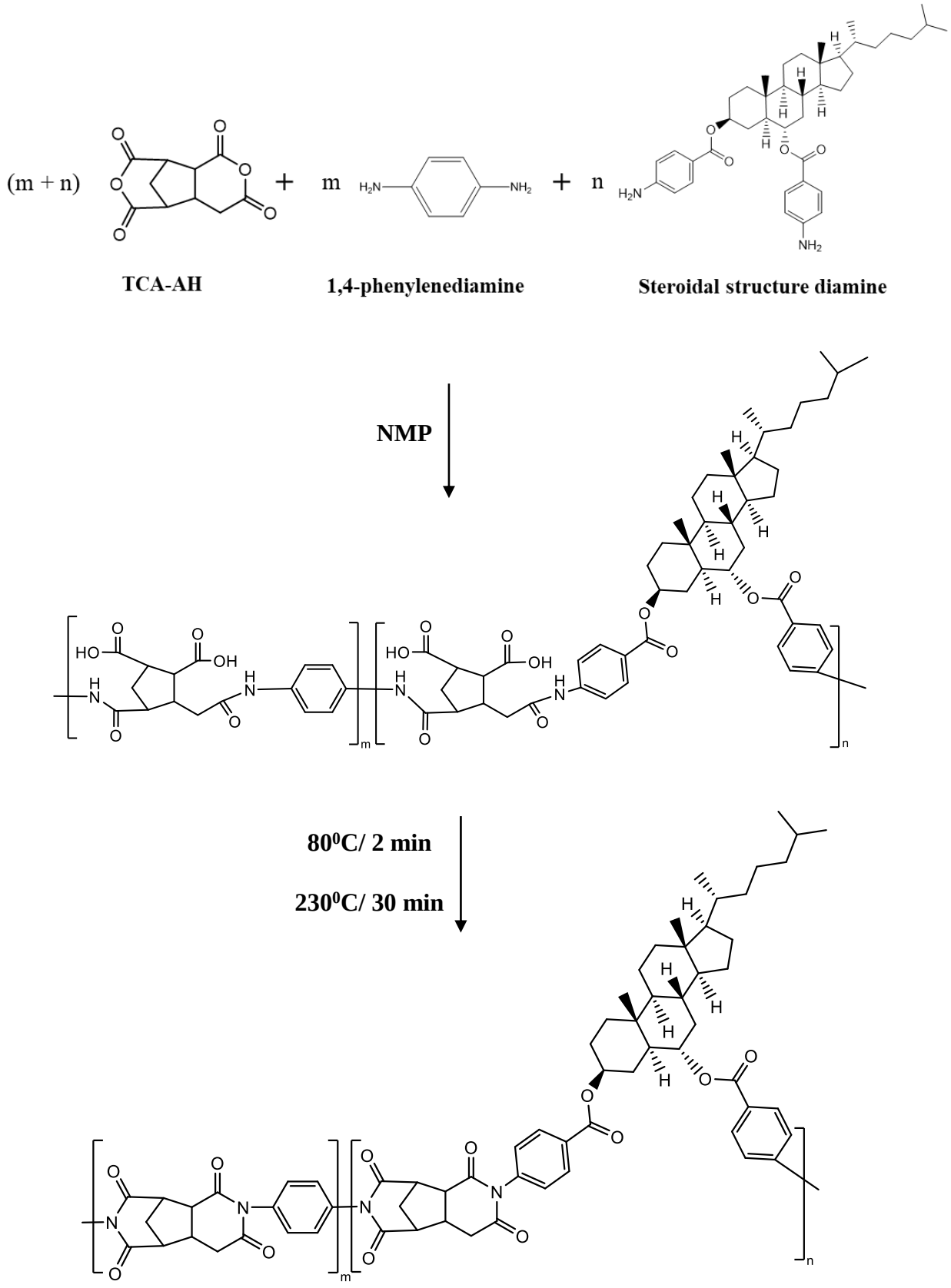

Figure 4.1 Synthesis of the PAA and the PI films.

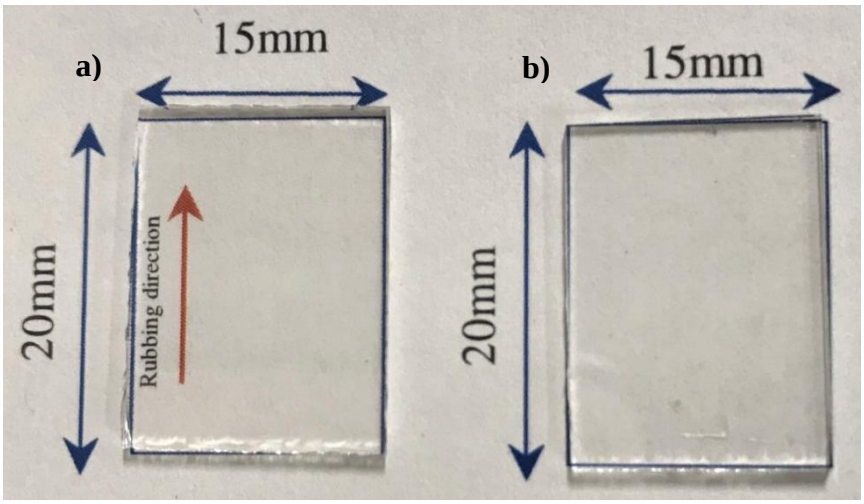

Figure 4.2. PI-30 films after preparation: a) rubbed sample, b) unrubbed sample.

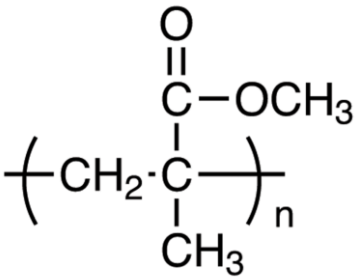

Figure 4.3 Chemical structure of PMMA

4.2 SFG measurement

4.2.1 SFG experimental setup

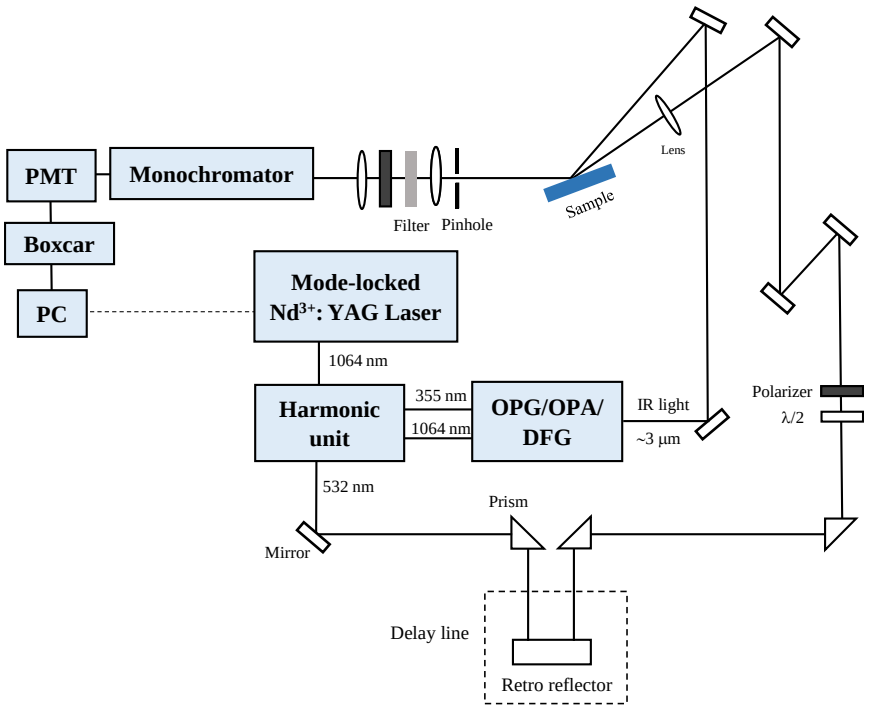

Figure 4.4 SFG optical setup

Figure 4.4 shows the experimental configuration for SFG measurement. A picosecond pulsed, mode-locked Nd^{+3}: YAG laser (PL2143B, EKSPLA) was used at the fundamental wavelength 1064 nm. The repetition rate was 10 Hz, with a pulse duration of 30ps. The fundamental beam was then separated into two parts in a harmonics unit, as shown in Fig. 4.5. A part of the 1064 nm beam passes through a $K^{*}DP$ nonlinear crystal (SHG) to generate a second harmonic beam at 532 nm. A part of the 532 nm beam is directly used as the visible beam for the SFG vibrational spectroscopy. The other part of 532 nm beam passes through another $K^{*}DP$ nonlinear crystal (THG) to generate a third harmonic beam at 355 nm. The third harmonic beam and a part of the 1064 nm beam are then utilized to pump optical parametric generation/optical parametric amplification/ difference frequency generation OPG/OPA/DFG system (PG401/DFG2-18P, EKSPLA) to produce the tunable IR beam for the SFG vibrational spectroscopy as shown in Fig. 4.6.

The first part of the 355nm beam (15%) reflected by mirrors M1 and M8 enters the LBO crystal and generates a diverging broadband parametric super fluorescence signal determined by the phase-matching condition. Mirror M9 then reflects both parametric and pumping signals to the LBO crystal. Mirrors M8 separates parametric and pumping signals. The parametric signal then passes a telescope (L5 and L6) and a diffraction grating DG (echelle grating) by mirror M11. The mirror M12 reflects the signal from the DG to the LBO crystal, where it coincides with the second part of the 355nm beam (85%). Therefore, the parametric signal is

amplified. After the filters F1-F3, the parametric signal can be separated into two parts by mirror M19. One directs to the output S4, and the other enters the difference frequency generator (DFG). In DFG, the 1064 nm pulse and the parametric pulse are mixed in the $AgGaS_2$ crystal to generate the tuned IR beam in 2-8μm. Here the frequency of the IR output is controlled by adjusting the angle of the DG.

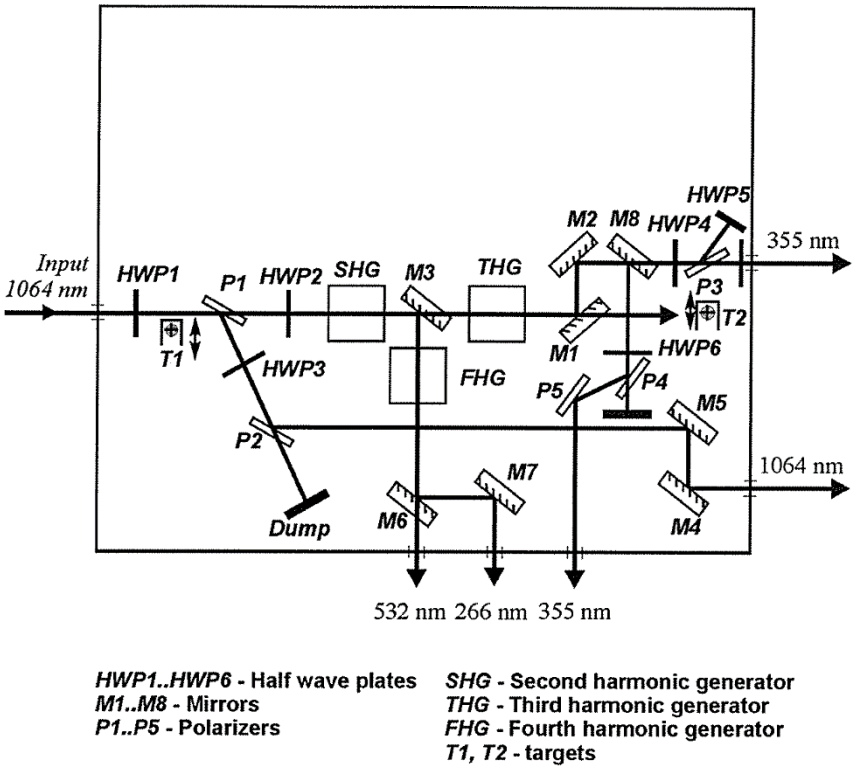

Figure 4.5 Optical setup of Harmonic unit.

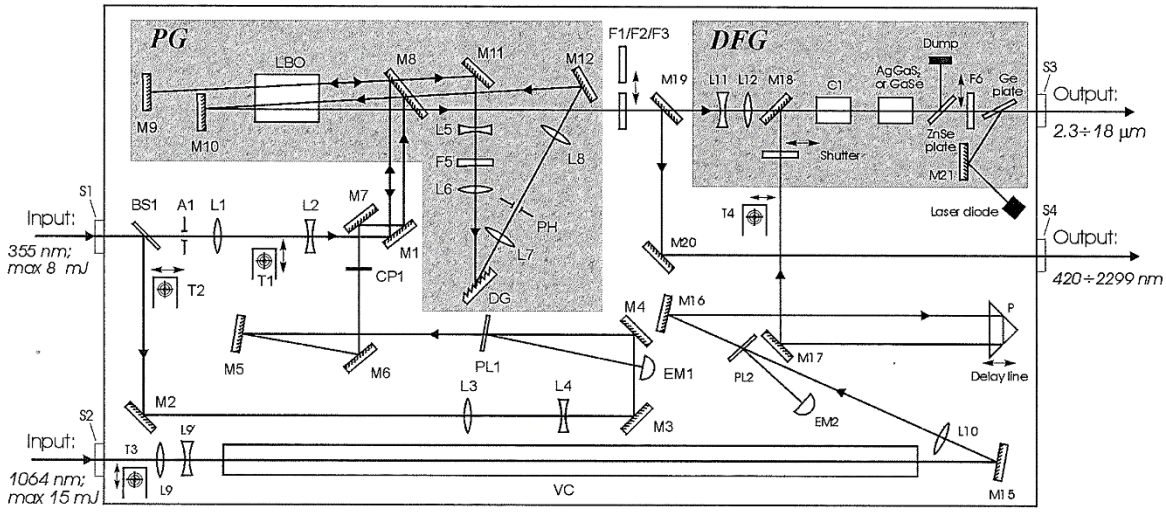

Figure 4.6 Optical setup of PG401/DFG2-18P.

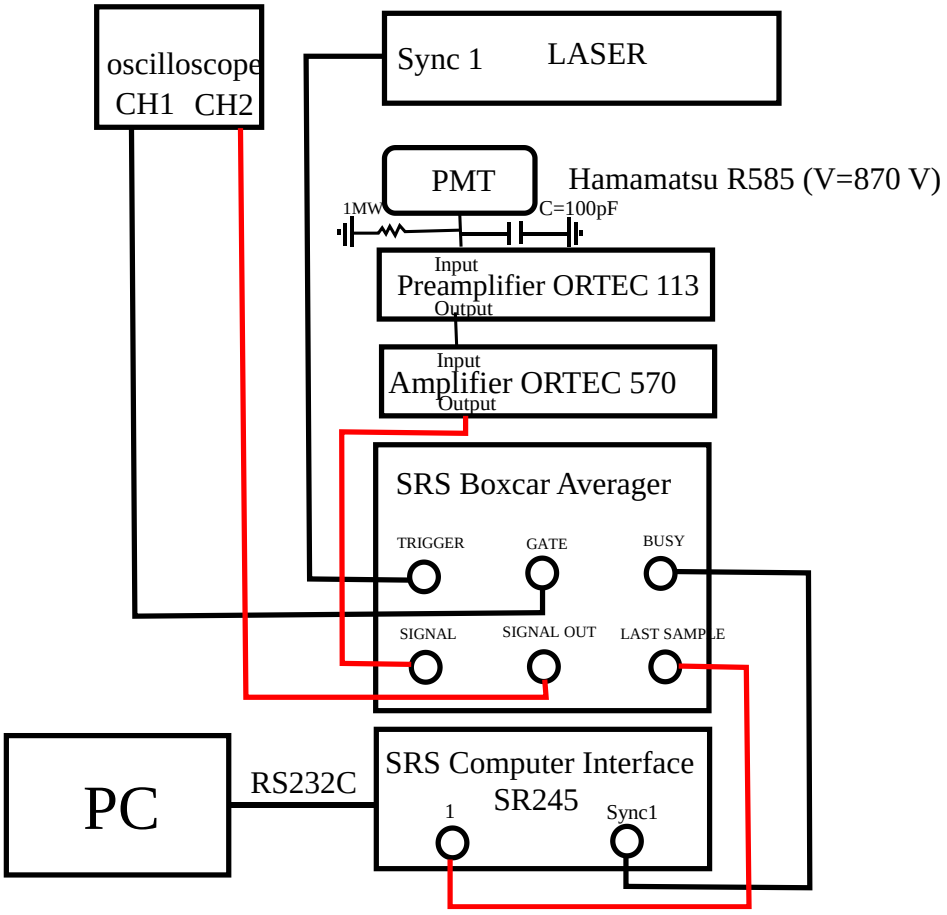

Figure 4.7 Electric setup of the SFG system.

To generate an SFG signal in this study, the visible beam at 532 nm and the tunable IR beam from 3.3 to 3.6 μm were spatially and temporally overlapped at the PI surface with incidence angles 80° and 45°, respectively. The temporal overlap of the IR and the visible beams can be adjusted by using a delay line made of a retroreflector mounted on a translation stage, and the spatial overlap of the IR and the visible beams can be attained by adjusting the IR beam position. In addition, a half-waveplate followed by a polarizer is commonly used to change the visible beam power. In this study, the laser power is approximately 250μJ/pulse for the IR beam and about 80 μJ/pulse for the visible beam.

The SFG output was detected in the reflection direction. To separate the residual 532nm signal and IR signal from the SFG signal, three band-pass filters (SV0490, Asahi) were used. In addition, a focusing lens (f=150mm) is inserted to collect the SFG signal and direct it into a grating monochromator (SG-100, Nihon Koken Kogyo). The monochromator is an optical device used to separate the demanded wavelength. Slits were placed in the entrance and the exit of the monochromator to control the bandpass of light. After the SFG signal passed the monochromator, it was directed to the photomultiplier tube PMT (R-585, Hamamatsu). Based on a photoelectric effect, the PMT converts the SFG light to an electric signal. To recover fast analog signals from the noisy background, the signal from the PMT went through a gated integrator and boxcar averager, as shown in Fig. 4.7. The gated integrator amplifies and

integrates the signal present during the time the gate is open, ignoring noise and interference that may be present at other times. The boxcar averager refers to averaging the output of the gated integrator over many shots of the experiment to increase the signal-to-noise ratio. A computer interface transfers the signal to the computer in which the data is collected and stored.

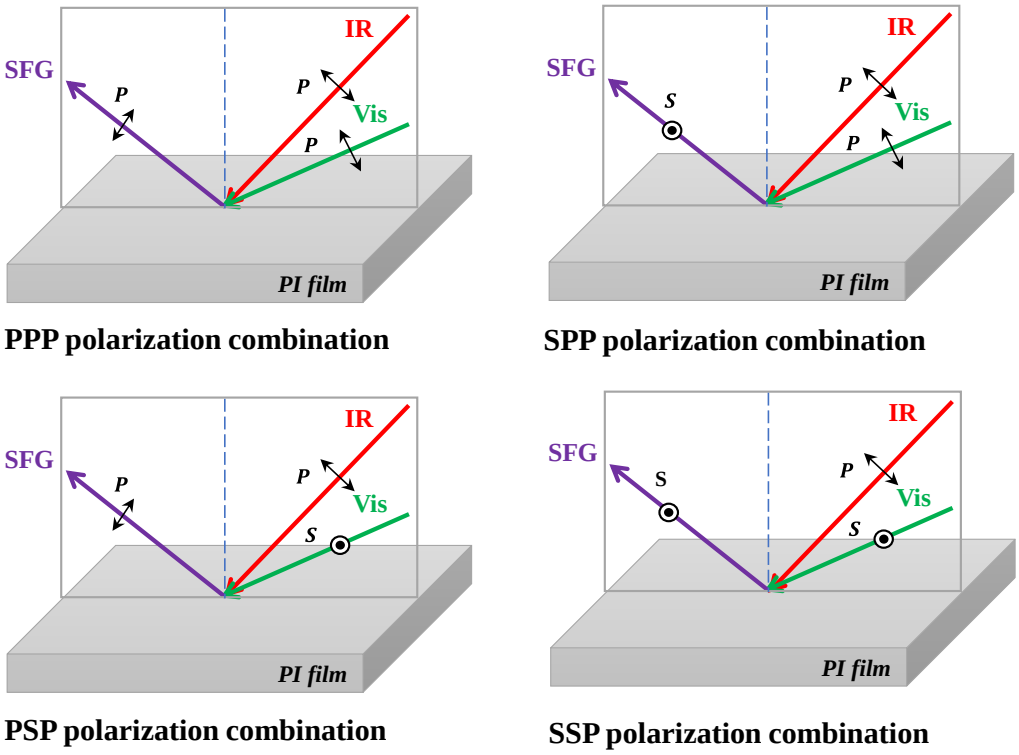

Figure 4.8 Schematic illustration of PPP, SPP, PSP, and SSP polarization combinations in SFG measurements.

In this study, the PI film was mounted on a 360° rotation stage. The SFG spectra were measured with different input/output polarization combinations (PPP, PSP, SSP, and SPP) as shown in Fig. 4.8d the various values of the azimuthal angle γ. Signals of 600 pulses were accumulated at each step in an SFG spectrum. All SFG spectra were observed at least twice to ensure reproducibility. For analysis, SFG data were fitted by Eq. (2.32) in Chapter 2 using Curve Fitting Tool in MATLAB. A MATLAB program was created to extract the data within Curve Fitting Tool to plot a fitting curve, as shown in Appendix E.

Table 4.1 shows the refractive indices used for the SFG orientational analysis. The refractive indices of the rubbed PI-30 film interfaces were measured using spectroscopic ellipsometry and provided by JSR Corp. The refractive index of the polyimide/air interface was estimated using the slab model to calculate local-field correction at the interface, as mentioned in Chapter 2. I adopted the refractive index of glass measured by Filmetrics, Inc. (KLA Corp.).

Table 4.1. Indices of refraction of the rubbed PI-30 films

Beam	Refractive index		
	Polyimide	Glass substrate	Polyimide/air
IR (2149 nm)	1.546	1.436	1.236
Visible (532 nm)	1.590	1.461	1.254
SFG (462 nm)	1.606	1.465	1.260

4.2.2 Original sample holder equipped with rotation mechanism

To investigate the SFG spectra of the rubbed PI-30 as a function of the azimuthal angle, a 360^{o} rotation stage (Sigma Koki KSP-256) was used. It was mounted on a new sample holder designed specifically for this measurement, as shown in Fig. 4.9. The outline drawing of the new sample holder is shown in Appendix F.

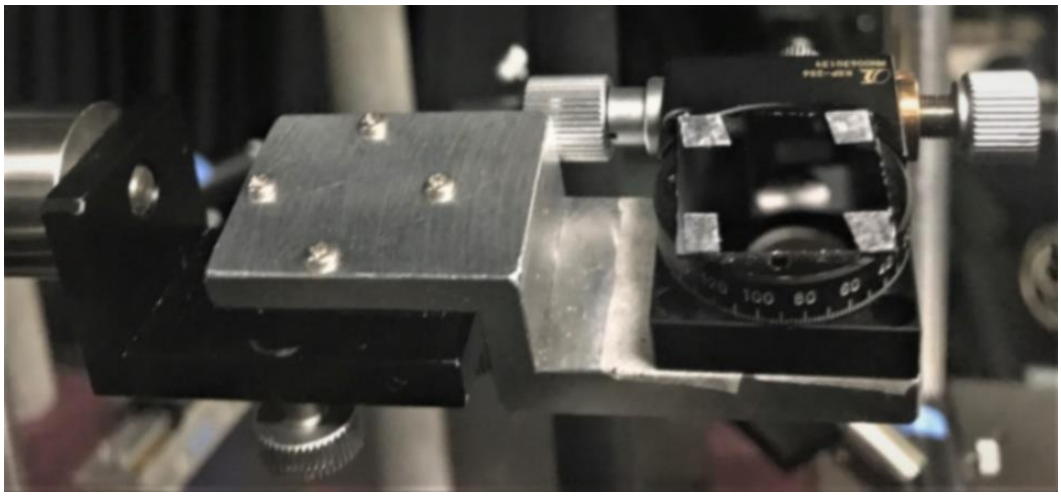

Figure 4.9. The 360^{o} rotation stage was used in this study.

4.3 SHG measurement

Figure 4.10 shows the experimental configuration for SHG measurement. A picosecond Nd^{3+}: YAG laser (PL2143B, EKSPLA) operating at 10 Hz was used in conjunction with a harmonic unit to generate a visible beam at 532 nm. The visible beam irradiated an unrubbed sample mounted on a sample stage with pulse energy of ~ 20μJ/pulse. The SHG output was recorded in the same way as the SFG measurement.

In this study, I collected SHG data for two input/output polarization combinations, S_{in}/P_{out} (S-polarized fundamental beam and P-polarized SHG) and P_{in}/P_{out}. For each data point, signal accumulation was done for 15000 laser shots. The sample holder held two samples simultaneously, and their absolute SHG intensity was compared using a sliding mechanism. At each time, I measured the SHG signal of a PI-60 film and then one of the PI films with different molar fractions of side-chain diamine (PI-0, PI-30, PI-60, PI-90, and PI-100). The SHG signal of the PI-60 film was used to normalize the SHG signal of the other samples. I used two samples for each molar fraction of side-chain diamine and measured their SHG response to ensure reproducibility.

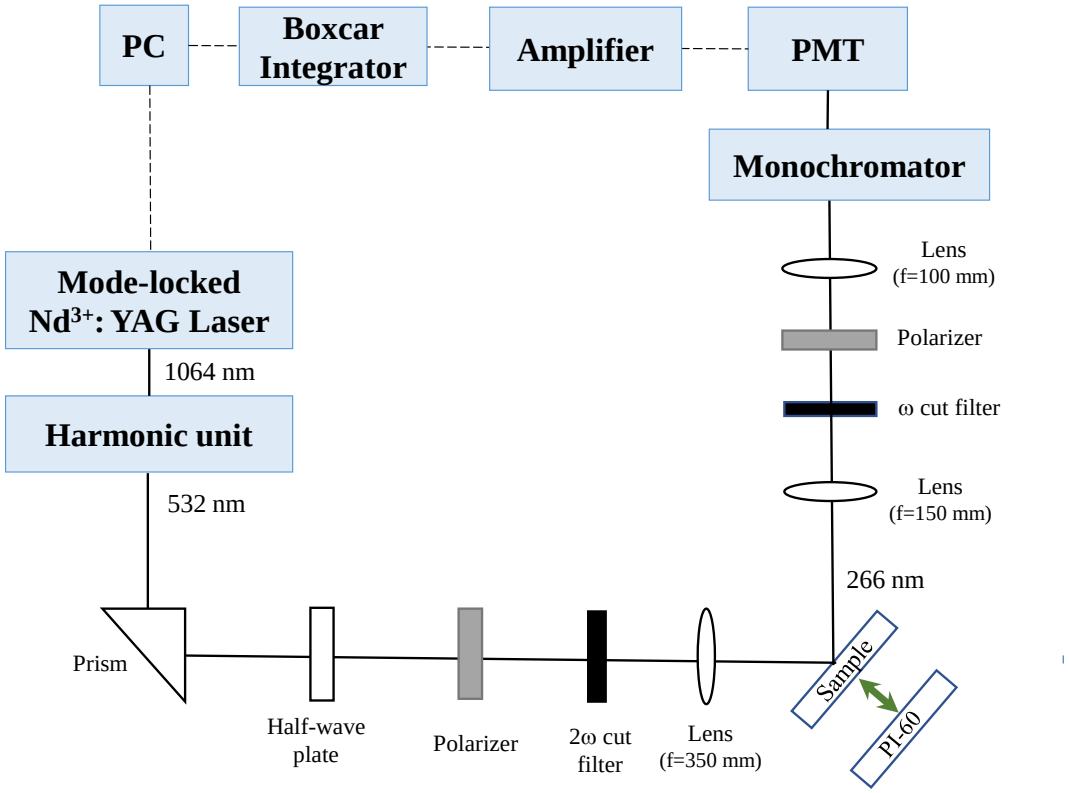

Figure 4.10 SHG optical setup

Table 4.2. Indices of refraction of five unrubbed PI films at different wavelengths

Molar fraction of side-chain diamine in PI containing steroidal side chains [mol%]	Refractive index (n)	
	n (532 nm)	n (266 nm)
0	1.6258	1.7523+0.2733*i*
30	1.5919+0.0002*i*	1.6479+0.2239*i*
60	1.5755	1.6100+0.2103*i*
90	1.5673	1.5506+0.2027*i*
100	1.5602+0.0063*i*	1.6328+0.0975*i*

Table 4.2 shows the refractive indices used for the SHG analysis. The refractive index of five unrubbed PI films was measured using spectroscopic ellipsometry and provided by JSR Corp.

References

[1]EKSPLA, PL2143 Series Laser - Technical description & User's manual, Vilnius (2007).

[2]EKSPLA, Optical parametric generator PG401/DFG - Technical description & User's manual, Vilnius (2007).

[3]EKSPLA, Harmonics Unit - Technical description & User's manual, Vilnius (2007).

CHAPTER 5. INVESTIGATION OF UNRUBBED PI SURFACES AS A FUNCTION OF THE CONTENT OF STEROIDAL STRUCTURE SIDE CHAINS USING OPTICAL SECOND HARMONIC GENERATION

5.1 Introduction

Ullah *et al.* reported that the SHG intensity of rubbed PI-30 film shows anisotropic SHG intensity patterns as a function of the sample rotation angle.[1] They assumed that only the steroidal parts have microscopic optical nonlinearity and then analyzed the experimental data. However, the validity of the assumption has not been checked yet. Therefore, the SHG responses from unrubbed PI film surfaces containing different fractions of steroidal parts were observed to examine whether this assumption was correct.

Unrubbed samples were used in this study because the uncertainty in analyzing the SHG results can be excluded more. Figure 5.1 shows isotropic SHG intensity patterns of the unrubbed PI-30 film.[1] It indicates that a smaller number of non-zero $\chi^{(2)}$ elements are involved in the formation of the SHG pattern than those of rubbed samples. Based on the SHG signals from the surface of unrubbed PI-0, PI-30, PI-60, PI-90, and PI-100 film surfaces, the contribution of main chains and side chains to SHG signals can be deduced.

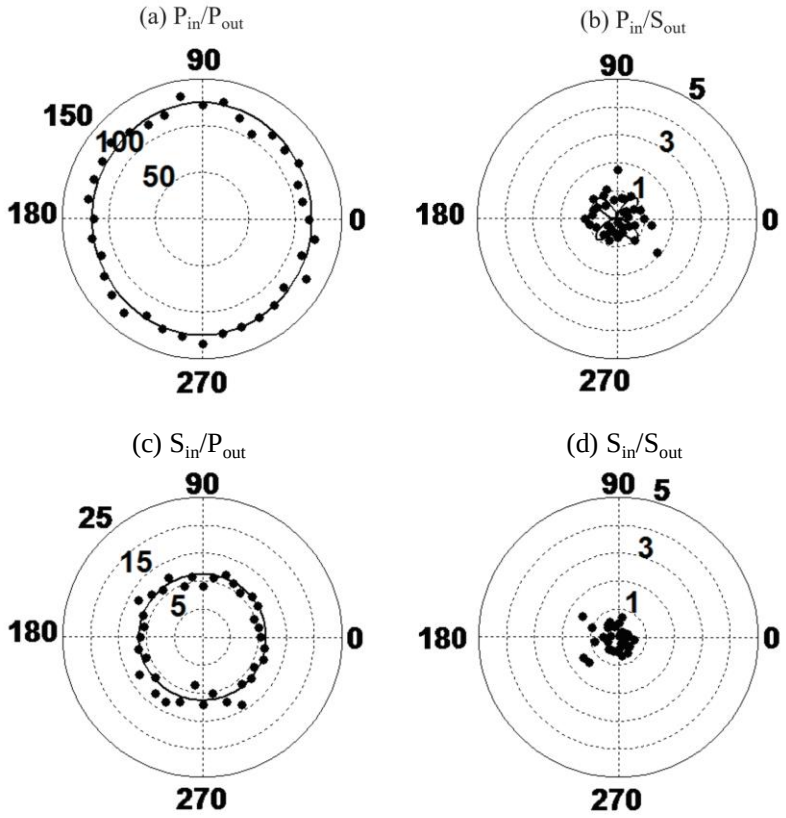

Figure 5.1 SHG intensity from unrubbed PI-30 film as a function of the sample rotation angle for different input/out polarization combinations.[1]

5.2 Results and discussion

The SHG intensity from the unrubbed PI-30 film is isotropic as a function of the sample rotation angle reported by Ullah *et al.*, as shown in Fig. 5.1.[1] S_{out} SHG is below the noise level, as shown in Figs. 5.1(b) and 5.1(d), and it is consistent with symmetry consideration. I, thus, measured SHG intensities of the unrubbed PI films for P_{in}/P_{out} and S_{in}/P_{out} polarization combinations at a fixed azimuthal angle of the samples. The obtained results are shown in Fig. 5.2. Figure 5.2(a) shows the SHG intensity of the unrubbed PI films for the P_{in}/P_{out} polarization combination. The SHG intensity from the PI film without steroidal side chains (PI-0) is not zero. As a result, it suggests that the second-order nonlinear hyperpolarizability of the PI main chain $\beta_M^{(2)}$ is non-zero, i.e.

$$\beta_M^{(2)} \neq 0.$$

In addition, it should be noted that the second-order nonlinear hyperpolarizability of the PI side chain $\beta_{X2}^{(2)}$ was found to contribute significantly to the anisotropy of the SHG intensity for the rubbed PI-30 films.[1]

Figure 5.2(b) shows the SFG intensity of the unrubbed PI films containing different fractions of steroidal side chains for the S_{in}/P_{out} polarization combination. The SHG intensity for the unrubbed PI-0 film is the smallest among the samples. The results of S_{in}/P_{out} SHG intensity normalized by P_{in}/P_{out} SHG intensity of all samples are shown in Fig. 5.2(c). The SHG intensity ratio is the smallest for the unrubbed PI-0 film, around 4%. On the other hand, this ratio is more than 5% for samples containing steroidal side chains. The corresponding ratio of the second-order nonlinear susceptibility elements of the unrubbed PI-0 film, $\chi_{zxx}^{(2)}/\chi_{zzz}^{(2)}$(PI-0), should be the smallest among the unrubbed PI films used in this study.

The reason for the smallest values of I_{SP}(PI-0)/I_{PP}(PI-0) and $\chi_{zxx}^{(2)}(\mathrm{PI}-0)/\chi_{zzz}^{(2)}$(PI-0) can be explained as the following. First, it can be assumed that

$$\beta_M^{(2)} \approx \beta_{X2}^{(2)} \qquad (5.1).$$

Because the imaginary parts of the refractive indices of the PI films are not significant, as shown in Table 4.2 in Chapter 4. Hence, according to Miller, it can be expected that the imaginary parts of the second-order nonlinear hyperpolarizabilities $\beta_M^{(2)}$ and $\beta_{X2}^{(2)}$ are not considerable, either.[2] Additionally, from Fig. 5.2(a), I can say very roughly that

$$I_{PP}\,(\text{PI-0}) \approx I_{PP}\,(\text{PI-100})$$

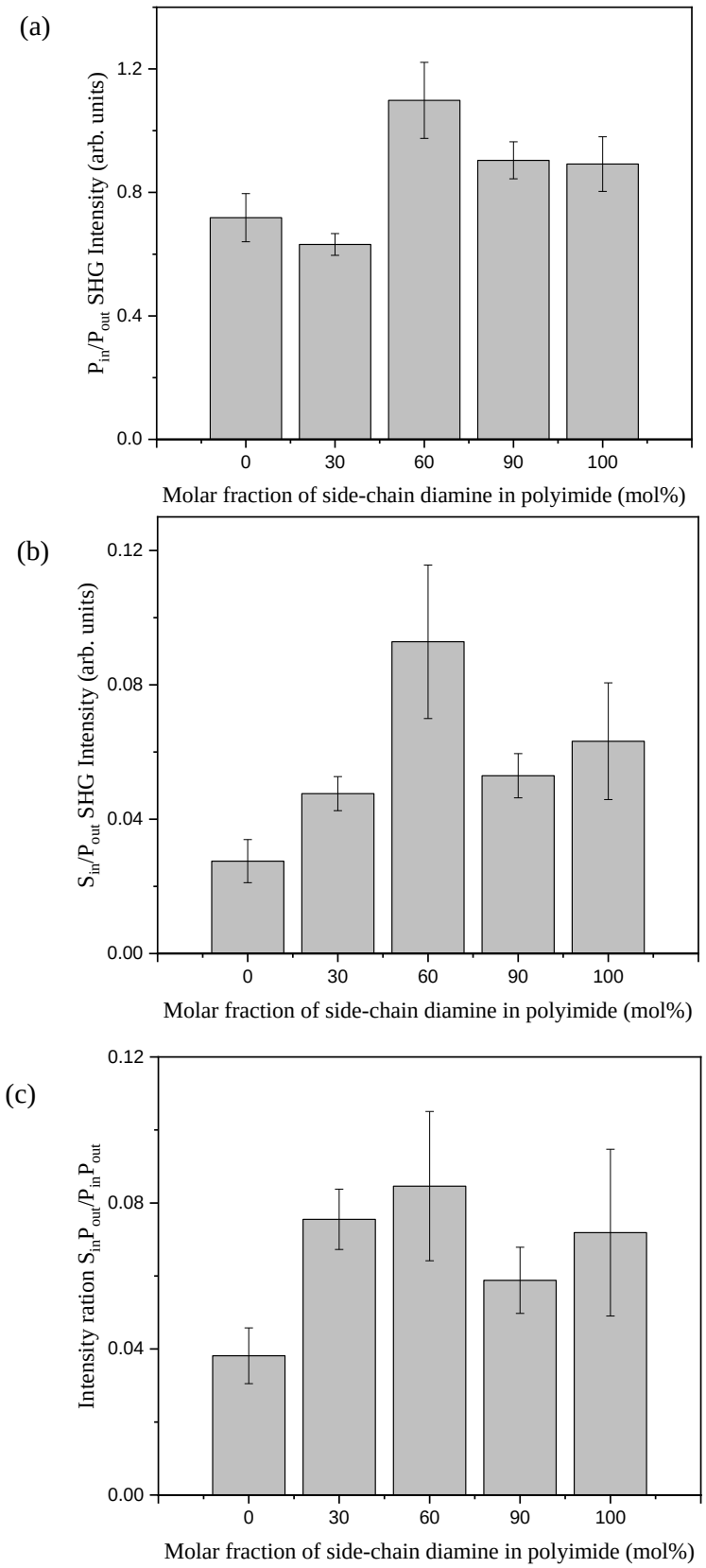

Figure 5.2 Dependence of SHG intensity of unrubbed PI containing steroidal side chain films on the molar fraction of steroidal structure diamine for (a) P_{in}/P_{out} polarization combination, (b) S_{in}/P_{out} polarization combination, and (c) $(S_{in}/P_{out})/(P_{in}/P_{out})$.

This relation suggests that the absolute values of $\beta_M^{(2)}$ and $\beta_{X2}^{(2)}$ should be similar. Due to the negative interference between the nonlinear susceptibilities of $\beta_M^{(2)}$ and $\beta_{X2}^{(2)}$ of the two components since $\beta_M^{(2)}$ and $\beta_{X2}^{(2)}$ have different signs, the SHG intensity of the unrubbed PI films with molar fractions of steroidal structure diamine near 50% should be nearly zero. However, the SHG signal is far from zero in the experimental result of the unrubbed PI-60 film, as shown in Fig. 5.2. It indicates that $\beta_M^{(2)}$ and $\beta_{X2}^{(2)}$ have the same sign. As a result the relation (5.1) can be assumed.

From Eqs. (2.35), (2.36), and (5.1), I can deduce a relation straightforwardly,

$$\frac{\chi_{zxx}^{(2)}}{\chi_{zzz}^{(2)}} = \frac{1}{2}\frac{N_M\langle cos\theta_M - cos^3\theta_M\rangle + N_{X2}\langle cos\theta_{X2} - cos^3\theta_{X2}\rangle}{N_M\langle cos^3\theta_M\rangle + N_{X2}\langle cos^3\theta_{X2}\rangle} \quad (5.2).$$

Because of $0^0 \leq \theta_M, \theta_{X2} \leq 90^0$ the value of Eq. (5.2) takes a real positive value. Hence, the real part of $\chi_{zxx}^{(2)}/\chi_{zzz}^{(2)}$ has a real positive value.

Based on the SHG experimental result, the Fresnel factors and the ratio $\chi_{zxx}^{(2)}/\chi_{zzz}^{(2)}$ of each sample were calculated using the Fortran software reported already.[3] The result is shown in Table 5.1. The refractive indices of the PI films used in calculating the Fresnel factors were measured by a spectroscopic ellipsometer and are shown in Chapter 4. As the previous discussion, it is assumed here that $\chi_{zxx}^{(2)}/\chi_{zzz}^{(2)}$ has real positive value.

Table 5.1. $\chi_{zxx}^{(2)}/\chi_{zzz}^{(2)}$ of unrubbed PI films containing different fractions of steroidal side chains.

Molar fraction of steroidal structure diamine in PI [mol%]	$\chi_{zxx}^{(2)}/\chi_{zzz}^{(2)}$
0	0.0487 ± 0.0062
30	0.0804 ± 0.0071
60	0.0829 ± 0.0145
90	0.0665 ± 0.0065
100	0.0775 ± 0.0168

From Eq. (5.2), putting N_{X2}=0, I have,

$$\chi_{zxx}^{(2)}/\chi_{zzz}^{(2)} = \frac{1}{2}\langle cos\theta_M - cos^3\theta_M\rangle/\langle cos^3\theta_M\rangle \quad (5.3).$$

Because the effective molecules are standing almost upright, it can be roughly assumed here that the statistical average of $\langle cos^3\theta\rangle$ related to the orientation angle θ of effective molecules is approximately unity. Since all the molecules are standing strictly upright or $cos\theta = 0$, the statistical average of $\langle cos\theta - cos^3\theta\rangle$ should be zero. However, the

experimental result shows that the $\chi^{(2)}_{zxx}/\chi^{(2)}_{zzz}$ is not equal to zero but the smallest among the unrubbed PI samples. It indicates that $\langle cos\theta_M - cos^3\theta_M \rangle$ of the PI main chain is non-zero but not significant for the unrubbed PI-0 films. The result suggests that each nonlinear polarization induced in the PI main chains stands almost upright on the PI film surface.

More discussion on the ratio $\chi^{(2)}_{zxx}/\chi^{(2)}_{zzz}$ for the unrubbed PI film containing a larger than 30% fraction of steroidal side chains using Eqs. (2.35), (2.36) in Chapter II is not accessible due to unknown ratios of $\beta^{(2)}_{X2ccc}/\beta^{(2)}_{Mccc}$. However, it can be emphasized that the angles θ_{X2} of the microscopic nonlinear polarization are larger than θ_M in order to explain the ratios $\chi^{(2)}_{zxx}/\chi^{(2)}_{zzz}$ for the unrubbed PI film containing a larger than 30% fraction of steroidal side chains. The microscopic nonlinear polarization of the PI side chains less randomly oriented when increasing the fraction of steroidal side chains might be a reason causing the ratio $\chi^{(2)}_{zxx}/\chi^{(2)}_{zzz}$ of the PI-90 film is smaller than that of the PI-60 film. Therefore, there is not enough space for the random orientation of the PI side chains of the unrubbed PI-90 film in the surrounding neighborhood. Unfortunately, the ratio $S_{in}P_{out}/P_{in}P_{out}$ of the unrubbed PI-100 film has a relatively large error, as shown in Fig. 5.2(c). Hence, it may not give any physical information about this PI-100 film.

5.3 Conclusion

The SHG signals of unrubbed PI films containing different fractions of steroidal side chains were studied systematically. After analyzing the SHG experimental data, it can be concluded that both the PI side chains and the PI main chains contribute to the SHG intensity. Furthermore, the SHG intensity in Sin/Pout polarization combination normalized by that of Pin/Pout polarization combination is the smallest for the unrubbed PI film without steroidal side chains. This result suggests that the nonlinear polarization stands in a more perpendicular direction for the unrubbed PI film without steroidal side chains than for the unrubbed PI films with steroidal side chains.

References

[1] M.S. Ullah, S. Asai, Y. Inomata, K.T.T. Hien, G. Mizutani, Y. Murakami, and T. Okada, E-Journal Surf. Sci. Nanotechnol. **15**, 7 (2017).

[2] R.C. Miller, Appl. Phys. Lett. **5**, 17 (1964).

[3] M. Omote, H. Kitaoka, E. Kobayashi, O. Suzuki, K. Aratake, H. Sano, G. Mizutani, W. Wolf, and R. Podloucky, J. Phys. Condens. Matter **17**, (2005).

CHAPTER 6. INVESTIGATING THE PROPER EXPERIMENTAL CONDITIONS FOR SFG MEASUREMENTS AT POLYIMIDE SURFACES

6.1 SFG intensity of the rubbed PI-30 as a function of the visible beam energy

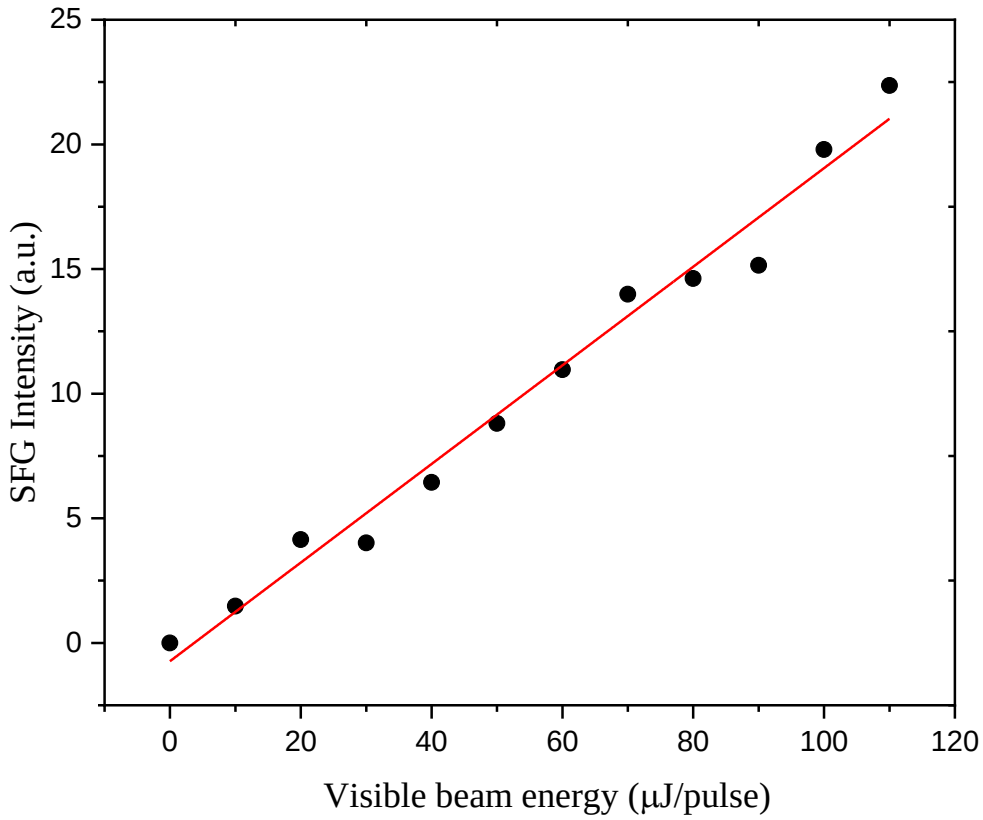

Figure 6.1 SFG intensity of rubbed PI-30 film as a function of the visible beam energy for a PPP polarization combination at 2965 cm^{-1} IR wavenumber.

According to Eq. (2.23) in Chapter 2, SFG intensity is proportional to the visible beam energy. It means that SFG intensity increases as the visible beam energy increases. However, the sample can be damaged if the visible beam energy is too strong. Hence, the selection of the appropriate visible beam energy is extremely important.

In order to find the most appropriate visible beam energy for SFG measurements of the PI films, I investigated the dependence of SFG intensity as a function of the visible beam energy for a PPP polarization combination at 2965 cm^{-1} IR wavenumber as shown in Fig. 6.1. The result is consistent with Eq. (2.23). I chose the visible beam energy as 80 μJ/pulse in this study for two reasons. First, the SFG intensity is not saturated. Second, the PI sample is not broken after measurement.

6.2 Proof that the SFG signal is from the PI-30/air interface

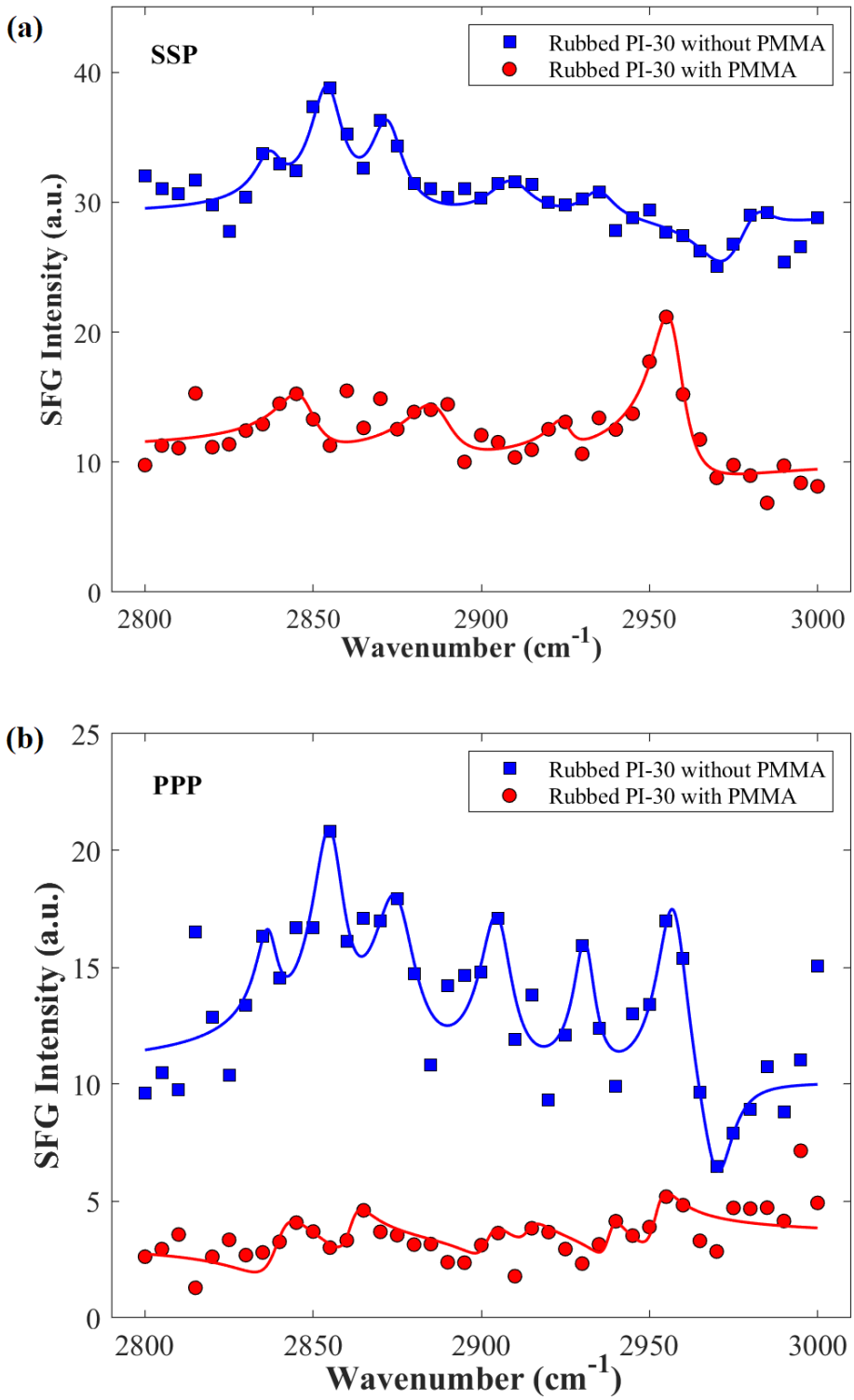

Figure 6.2. SFG spectra of rubbed PI-30 films with and without a PMMA overlayer of 5nm thickness at an azimuthal angle of $\gamma = 0^o$ for (a) SSP, (b) PPP polarization combinations. The solid lines are the fitting curves obtained using Eq. (2.32) in Chapter 2.

In order to prove that all the SFG spectra observed in this study originated mainly from the PI surface, and that the contribution to the SFG from the PI/glass substrate interface and from the bulk PI was not significant, I recorded the SFG spectra of rubbed PI-30 films with and without a poly (methyl methacrylate) (PMMA) overlayer of 5 nm thickness, at an azimuthal angle of $\gamma = 0^o$, for PPP and SSP polarization combinations. The observed spectra are shown in Fig. 6.2. For the PPP polarization combination, the SFG intensity decreased dramatically after the sample was covered with the thin PMMA layer. For the SSP polarization combination, the peaks in the spectra changed drastically after PMMA deposition. Namely, the peak at 2860 cm^{-1} disappeared, and a new peak at 2955 cm^{-1} appeared in the spectrum of the sample with the PMMA layer. It is known that the strong peak at 2955 cm^{-1} is a typical peak of PMMA for the SSP polarization combination.[1,2] It comes from the symmetric stretch of the ester methyl group of PMMA.

Tables 6.1 and 6.2 show the Fresnel factors for the glass/polymer interface for the rubbed polyimide with and without the PMMA layer on top. Indeed, the Fresnel factors for the glass/polymer interface are changed by PMMA deposition. The modulus of the combined Fresnel factors for the two glass/polymer interfaces for the SSP polarization combination was calculated, as shown in Table 6.3. The modulus of the combined Fresnel factors for the glass/polyimide interface for the film without PMMA was much smaller than that of the film with PMMA. If I assume that the signal from the glass/polyimide interface contributes considerably to the measured SFG signal in the upper spectrum of Fig. 6.2(a), the SFG intensity of the rubbed PI film with PMMA (in the lower spectrum) should be much larger than that of the one without PMMA (in the upper spectrum). This was not the observed result in Fig. 6.2(a), at least for the peak at ~2860 cm^{-1}. This peak has disappeared in the lower spectrum in Fig. 6.2(a). Thus, the assumption that "*the signal from the glass/polyimide interface contributes considerably to the measured SFG signal*" is wrong. Hence, the SFG signal originates mainly from the polyimide surface for the peak at ~2860 cm^{-1}. In addition, the lower SFG spectrum in Fig. 6.2(a) is very similar to that of a PMMA film.[1,2] This fact suggests that the glass/polyimide interface contribution is negligible in the lower spectrum of Fig. 6.2(a) in the whole spectral range. Considering the Fresnel factors, as shown in Table 6.3, I can then say that the glass/polyimide interface contribution is negligible in the whole spectral range in the upper spectrum in Fig. 6.2(a).

Table 6.1. Fresnel factors for the incident and output radiations at the free polymer/air interface and the buried glass/polyimide interface for the rubbed polyimide without a PMMA layer.

Fresnel factor	Polyimide/air interface	Glass/polyimide interface
L_{xxIR}	0.921 + 0.010i	0.744+0.092i
L_{xxSFG}	1.248 + 0.005i	-0.282+0.409i
L_{xxVis}	1.473 + 0.006i	0.313+0.165i
L_{yyIR}	0.719+ 0.017i	0.716 + 0.092i
L_{yySFG}	0.328 + 0.014i	-0.221 + 0.309i
L_{yyVis}	0.222 + 0.020i	0.218 + 0.127i
L_{zzIR}	0.706 - 0.007i	0.752 + 0.093i
L_{zzSFG}	0.474 - 0.003i	-0.286 + 0.414i
L_{zzVis}	0.335 - 0.004i	0.316 + 0.167i

Table 6.2. Fresnel factors for the incident and output radiations at the free polymer/air interface, the buried polyimide/PMMA, and glass/polyimide interfaces for the rubbed polyimide with a PMMA layer.

Fresnel factor	PMMA/air interface	Polyimide/PMMA interface	Glass/polyimide interface
L_{xxIR}	0.897 - 0.0004i	0.713 + 0.005i	0.984 + 0.251i
L_{xxSFG}	1.262 - 0.002i	0.455 + 0.061i	-0.580 + 0.839i
L_{xxVis}	1.480 – 0.001i	0.327 + 0.006i	-0.342 + 0.959i
L_{yyIR}	0.679 – 0.001i	0.679 + 0.004i	0.983 + 0.252i
L_{yySFG}	0.370 – 0.005i	0.367 + 0.047i	-0.574 + 0.836i
L_{yyVis}	0.244 – 0.003i	0.244 + 0.003i	-0.337 + 0.952i
L_{zzIR}	0.759 + 0.0003i	0.722 + 0.005i	1.461 + 0.373i
L_{zzSFG}	0.497 + 0.001i	0.461 + 0.062i	-0.880 + 1.272i
L_{zzVis}	0.353 + 0.0007i	0.331 + 0.006i	-0.515 + 1.444i

Table 6.3. Modulus of the combined Fresnel factors for the glass/polyimide interface for the rubbed polyimide films *without and with a PMMA layer* for the SSP polarization combination.

Modulus of the combined Fresnel factors	Glass/polyimide interface	
	Rubbed polyimide films without a PMMA layer	Rubbed polyimide films with a PMMA layer
$\left\|L_{yySFG}L_{yyVis}L_{xxIR}\right\|$	0.072	1.04
$\left\|L_{yySFG}L_{yyVis}L_{zzIR}\right\|$	0.073	1.54

6.3 Investigating the uniformity of rubbed PI-30 films

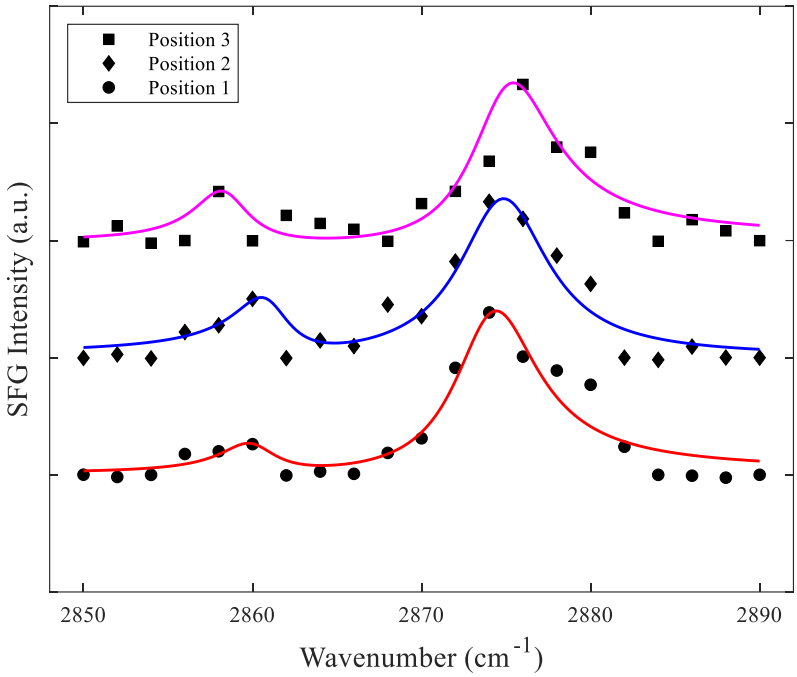

Figure 6.3 SFG spectra of rubbed PI-30 film at several positions at $\gamma = 0^o$ azimuthal angle for a PPP polarization combination. The solid lines are the fitting curves obtained using Eq. (2.32) in Chapter 2.

In order to check the uniformity of the sample, I recorded SFG spectra of the rubbed PI-30 film at several positions. The results are shown in Fig. 6.3 with the fitting parameters given in Table 6.4. Each SFG signal in this study was averaged from 600 laser shots, and each SFG spectrum was recorded at least twice. The SFG spectra show little variation as a function of the position. Namely, two peaks at ~2860 and ~2875 cm^{-1} were observed with the similar amplitudes in the SFG spectra at different positions. These results indicate that the rubbed PI-30 sample is essentially uniform.

Table 6.4 Fitting parameters of the SFG spectra of rubbed PI-30 film at several positions

Parameter	Peak 1			Peak 2		
	Position 1	Position 2	Position 3	Position 1	Position 2	Position 3
ω_q (cm^{-1})	2860	2861	2858	2874	2875	2875
A_q (a. u.)	0.74 ± 0.07	1.05 ± 0.13	1.35 ± 0.27	2.32 ± 0.23	2.30 ± 0.28	2.52 ± 0.50
Γ_q (cm^{-1})	2	2	2	3	3.2	3

6.4 Effect of ambient conditions on the SFG spectra of PI-30 film surfaces

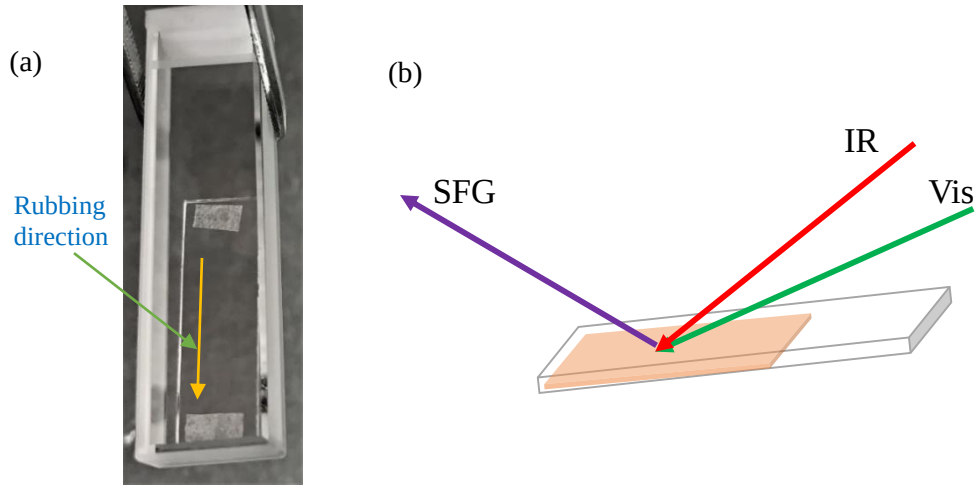

Figure 6.4 (a) Rubbed PI-30 sample in a quartz cell filled with N_2 gas, (b) Experimental geometry.

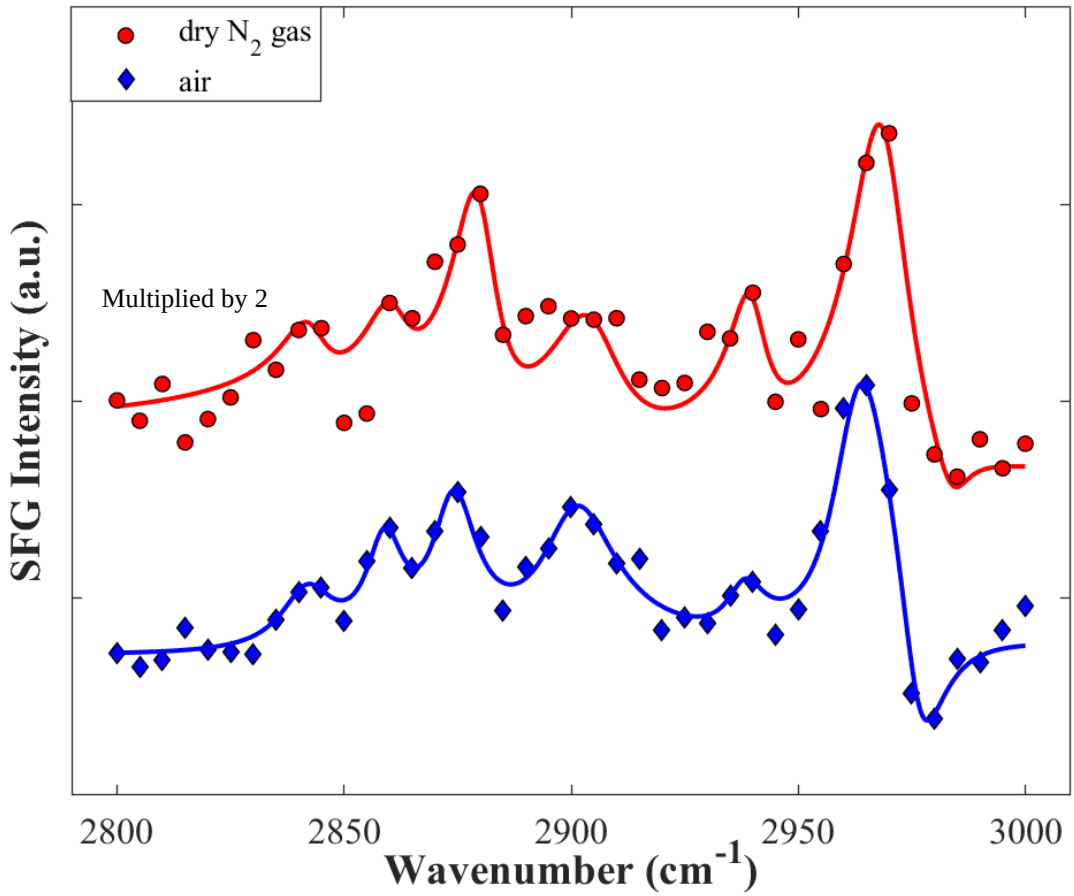

Figure 6.5 SFG spectra of the rubbed PI-30 films in air, and in dry N_2 gas at $\gamma = 0^o$ azimuthal angle for a PPP polarization combination. The solid lines are the fitting curves obtained using Eq. (2.32) in Chapter 2.

Table 6.5 Fitting parameters of the SFG spectra of rubbed PI-30 films in air and in N_2 gas

Parameter	In air	In N_2 gas
A_{NR} (a. u.)	1.91	1.41
ϕ (rad)	-1.38	-2.18
A_1 (a. u.)	0.35	0.23
A_2 (a. u.)	0.54	0.27
A_3 (a. u.)	0.73	0.74
A_4 (a. u.)	0.72	0.48
A_5 (a. u.)	0.27	0.47
A_6 (a. u.)	1.33	1.22
A_7 (a. u.)	-1.16	-0.25
Γ_1 (cm^{-1})	7	6
Γ_2 (cm^{-1})	5	6
Γ_3 (cm^{-1})	6	6
Γ_4 (cm^{-1})	10	10
Γ_5 (cm^{-1})	5	5
Γ_6 (cm^{-1})	8	8
Γ_7 (cm^{-1})	6	5
ω_1 (cm^{-1})	2842	2843
ω_2 (cm^{-1})	2859	2861
ω_3 (cm^{-1})	2874	2880
ω_4 (cm^{-1})	2901	2905
ω_5 (cm^{-1})	2938	2940
ω_6 (cm^{-1})	2963	2969
ω_7 (cm^{-1})	2976	2984

A rubbed PI-30 sample was kept in a quartz cell filled with N_2 gas to avoid the effect of ambient environment as shown in Fig. 6.4(a). Figure 6.4(b) illustrates the SFG experimental geometry for the cell sample. This quartz cell is an IR spectrophotometer cell with 45mm height, 5 mm path length, 10 mm path width and two polished windows (*S10-IR-5 GL Sciences*). In order to investigate the effect of ambient environment such as moisture and oxygen on the orientation of molecules at the rubbed PI-30 surface, I measured SFG spectra of fresh rubbed PI-30 films in air and in N_2 gas in the same experimental conditions. The experimental room temperature and relative humidity were ~22°C and ~30%, respectively.

Figure 6.5 shows the observed SFG spectra. The solid lines in the figure were obtained by fitting using Eq. (2.32) in Chapter 2. The fitting parameters are listed in Table 6.5. The SFG intensity of the rubbed PI-30 film in the quartz cell decreased drastically compared to that of the rubbed PI-30 film in air due to the reflection at the quartz cell surfaces. However, the peak positions and line shapes of these SFG spectra, especially those of three peaks in CH symmetric stretching range (2830-2885 cm^{-1}), are quite similar. It suggests that the ambient environment does not significantly affect the molecular orientation and conformation at the PI surface. Hence, I decided to measure SFG spectra of the rubbed PI-30 film in air.

6.5 Investigating the quality of PI-30 films in use and storage

Polymeric materials can be degraded under the effect of various factors such as temperature (thermal degradation), air (oxidative degradation), moisture (hydrolytic degradation), microorganisms (biodegradation), light (photo degradation), high-energy radiation (UV/γ degradation), chemical agents (corrosion), and mechanical stress.[3,4] In this process, a change in the chemical and/or physical structure of the polymer chain is commonly observed. It is noted that the susceptibility of a polymer to degradation depends on its structure. For example, epoxies and chains containing aromatic functional groups are particularly susceptible to UV degradation, hydrocarbon-based polymers are normally susceptible to thermal degradation, and hydrophilic polymers are more susceptible to hydrolytic degradation than hydrophobic polymers.[4,5]

Although the PI films used in this study were kept in plastic boxes and stored in a dry box to reduce the effect of moisture in the air, they might be degraded for long-term storage. In addition, the structures of these samples can also be changed after irradiating by the strong IR and visible beams for a long time in SFG measurements. In order to check the quality of the PI samples in use and storage, I measured SFG spectra of the rubbed PI-30 films stored at different times (after 4 days, 12 days, 4 months, and 9 months preparation) for a PPP polarization combination at $\gamma = 0^o$ azimuthal angle as shown in Fig. 6.6. The considerable variation of the SFG spectra of the rubbed PI-30 as a function of the storage time was observed. It suggests that the orientation of molecules at the rubbed PI-30 surfaces was changed.

There is no significant difference between the SFG spectrum of the rubbed PI-30 film after 4 days preparation and that of the rubbed PI-30 film after 12 days preparation. On the other hand, the SFG spectrum of the rubbed PI-30 film after 4 months preparation changed obviously. Namely, the peak at 2855 cm^{-1} disappeared, the peak at 2875 cm^{-1} is weaker and the peak at 2840 cm^{-1} is broader compared to the SFG spectrum of the sample after 4 days preparation. The drastic variation of the SFG spectrum was also observed in the sample after 9 months preparation. These results indicate that the orientation of molecules of the PI side chain was changed after 4 months preparation. Hence, in order to get the best result of the orientation and conformation of the molecules at the PI-30 surface the fresh samples or at least the samples fabricated within 3 months should be used.

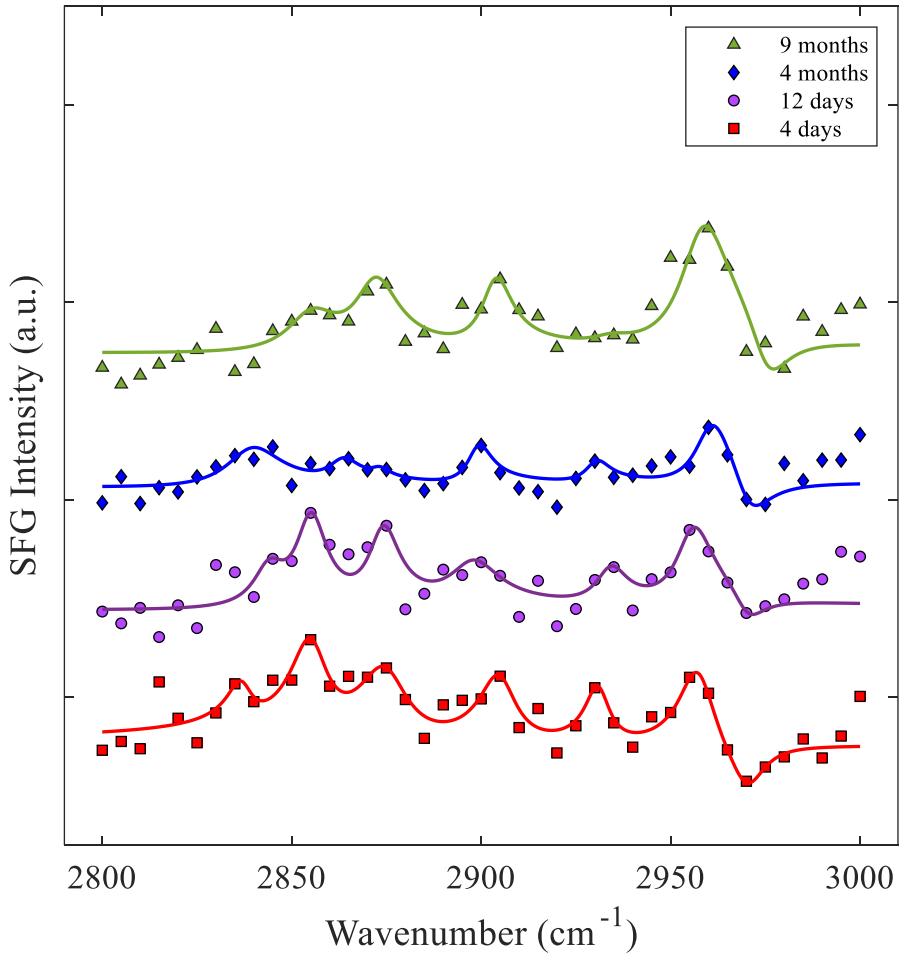

Figure 6.6 SFG spectra of rubbed PI-30 films after 4 days, 12 days, 4 months, and 9 months preparation at $\gamma = 0^o$ azimuthal angle for a PPP polarization combination. The solid lines are the fitting curves obtained using Eq. (2.32) in Chapter 2.

References

[1] J. Wang, C. Chen, S. M. Buck, and Z. Chen, J. Phys. Chem. B **105**, 12118 (2001).

[2] T. Miyamae and H. Nozoye, in *Surf. Sci.* (North-Holland, 2003), pp. 1045–1050.

[3] M. Brebu, Polymers (Basel). **12**, (2020).

[4] A.D. Padsalgikar, in *Plast. Med. Devices Cardiovasc. Appl.*, edited by A.D. Padsalgikar (William Andrew Publishing, 2017), pp. 83–102.

[5] J.G. Speight, in *Handb. Ind. Hydrocarb. Process. (*Second Edition, Gulf Professional Publishing, Boston, 2020), pp. 597–649.

CHAPTER 7. STUDY OF THE MOLECULAR ORIENTATION OF STEROIDAL STRUCTURE SIDE CHAINS AT POLYIMDE SURFACES USING SFG VIBRATIONAL SPECTROSCOPY

7.1 Vibrational mode assignments of rubbed PI-30 film

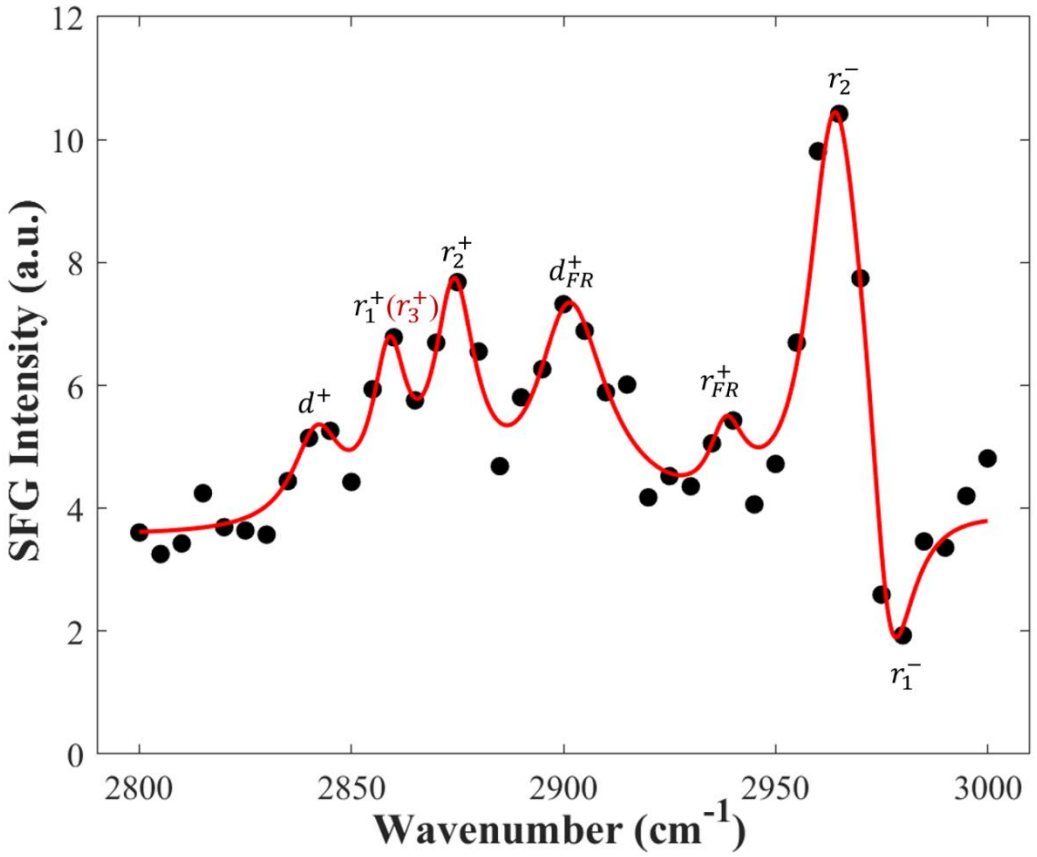

Figure 7.1. SFG spectrum of rubbed PI-30 film for a PPP polarization combination at $\gamma = 0^o$. The red solid line is the fitting curve obtained using Eq. (2.32) in Chapter 2.

Figure 7.1 shows a typical SFG spectrum of the rubbed PI-30 film for the CH-stretching region, from 2800 to 3000 cm^{-1} at an azimuthal angle of $\gamma = 0^o$, and for a PPP polarization combination. The red solid line in this figure was obtained by fitting the data points to Eq. (2.23) in Chapter 2. The fitting parameters are listed in Table 7.1. As mentioned in Chapter 3, the steroidal structure, and the alkyl chain of the PI-30 film in this study constitute the main parts of the molecule cholestanol. Kett *et al.*[1] investigated the SFG spectrum of a cholestanol monolayer film and assigned its vibrational modes. I mainly followed their assignments for the vibrational modes in the PI-30 spectrum in Fig. 7.1 (see Table 7.2).[1–4]

The P-polarized light field has x and z components on the surface. Hence, in the PPP polarization configuration eight non-zero $\chi_{ijk}^{(2)}$ elements, i.e., $\chi_{xxx}^{(2)}$, $\chi_{xxz}^{(2)}$, $\chi_{xzz}^{(2)}$, $\chi_{xzx}^{(2)}$, $\chi_{zxx}^{(2)}$, $\chi_{zzx}^{(2)}$, $\chi_{zxz}^{(2)}$ and $\chi_{zzz}^{(2)}$ contribute to the SFG response. These elements involve vibrational

transition moments directed normal to the surface.[5,6] As a result, the PPP-SFG spectrum of CH resonances is generally sensitive to the polar orientation of CH groups at the surface.

Table 7.1. Fitting parameters of the PPP SFG spectrum of the rubbed PI-30 film at $\gamma = 0^o$.

ω_q (cm^{-1})	A_q (a.u.)	Γ_q (cm^{-1})
2842	0.35	7
2859	0.54	5
2874	0.73	6
2901	0.72	10
2938	0.27	5
2963	1.33	8
2976	-1.16	6

As shown in Table 7.2, the frequencies of the symmetric and anti-symmetric stretching modes of the CH_3 isopropyl group (r_2^+, r_2^-) are different from those of the two methyl groups of the steroidal structure and the adjacent methyl group (r_1^+, r_1^-).[1] The CH_3 isopropyl group contributes two positive peaks at 2874 cm^{-1} (r_2^+) and 2963 cm^{-1} (r_2^-) to the SFG spectrum indicating that the methyl groups are pointing away from the PI surface, in line with the discussion of Kett *et al.*[1] In contrast, r_1^+ and r_1^- modes were observed as positive and negative peaks, respectively. As shown in Table 7.1, the amplitudes of r_1^+ and r_1^- modes have opposite signs. A similar phenomenon is observed for a cholestanol monolayer film by Kett *et al.*[1] They reported that the r^+ and r^- resonances are out of phase in a PPP SFG spectrum because of the CH_3 groups in the film in two different orientation.[7] We would expect the same situation here for the CH_3 groups on the steroidal structure of the PI side chain and the adjacent CH_3 group. The methyl groups on the steroidal structure are pointing toward the surface, and the methyl group next to it is pointing away from the surface. The r_1^+ mode is observed as a positive peak because the symmetric stretching mode of the methyl group adjacent to the steroidal structure is strong enough to cancel out the negative signals from the methyl groups on the steroidal structure. However, the anti-symmetric stretching mode of this methyl group is not strong enough to cancel out the negative signals from the two methyl groups on the steroidal structure, and the r_1^- mode is observed as a negative peak. Here I adopt the interpretation of Kett *et al.* to explain this phenomenon in the SFG spectrum of a PI-30 film.

McGall *et al.*[8] discussed film thickness interference effects in the SFG spectra of polymer films. They reported that interference can occur between SFG sources at the rear and front

interfaces of films and can cause a phase difference between different CH_3 stretching modes. However, such interference is excluded for my sample because the SFG response in this study was shown to originate mainly from the rubbed PI-30 film surface as discussed in Chapter 6.

Table 7.2. Vibrational assignments of the rubbed PI-30 film in the C-H stretching region. (Subscript 1 denotes the CH_3 groups on the steroidal structure and the CH_3 group adjacent to it; subscript 2 denotes the isopropyl group).

Vibrational mode	Wavenumber (cm^{-1})	Description
d^+	2842	CH_2 symmetric stretch
$r_1^+(r_3^+)$	2859	Symmetric stretch of the CH_3 groups on the steroidal structure and the adjacent CH_3 group
r_2^+	2874	CH_3 symmetric stretch of the isopropyl group
d_{FR}^+	2901	Fermi resonance of CH_2 symmetric stretch
r_{FR}^+	2938	Fermi resonance of CH_3 symmetric stretch
r_2^-	2963	CH_3 anti-symmetric stretch of the isopropyl group
r_1^-	2976	Anti-symmetric stretch of the CH_3 groups on the steroidal structure and the adjacent CH_3 group

7.2 Polarization dependence of SFG spectroscopy

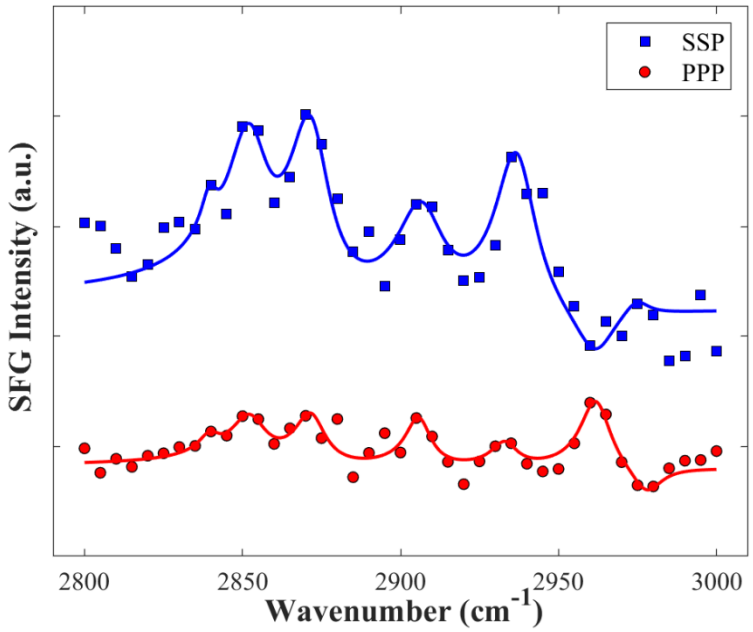

Figure 7.2. SFG spectra of rubbed PI-30 film at $\gamma = 0^o$, for SSP and PPP polarization combinations. The solid lines are the fitting curves obtained using Eq. (2.32) in Chapter 2.

Figure 7.2 presents SFG spectra of rubbed PI-30 film for the PPP and SSP polarization combinations. The symmetric stretching modes of methylene and methyl groups (d^+, r_1^+, and r_2^+) have the strongest intensity for SSP while all the anti-symmetric stretching modes (r_1^-, and r_2^-) have the strongest intensity for PPP. These results are consistent with the general polarization selection rules of CH stretching modes.[6]

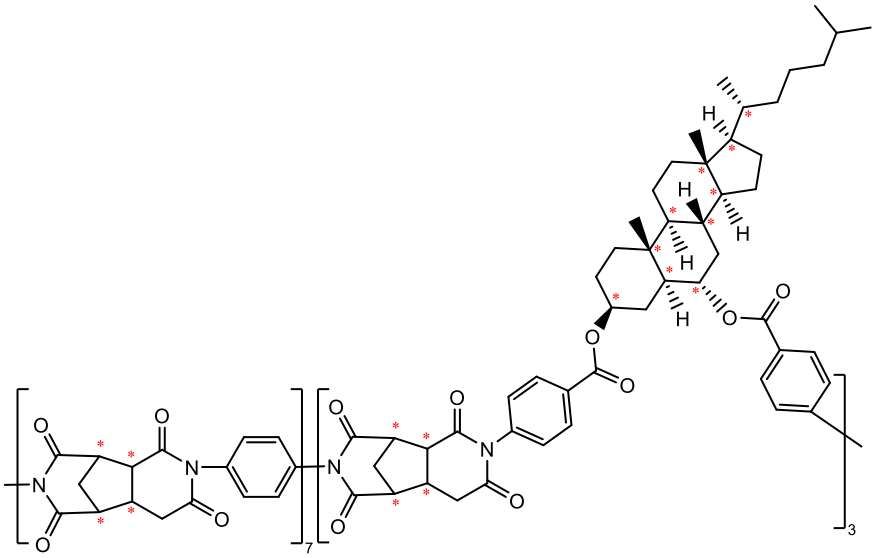

Figure 7.3. Chemical structure of PI with units possessing steroidal side chains of a fraction of 30% (PI-30). The red star indicates a chiral carbon.

It should be noted that the PI used in this study has chiral carbons, as shown in Fig. 7.3. Hence, I recorded SFG spectra of rubbed and unrubbed PI-30 films for PSP and SPP polarization combinations to probe chiral SFG signals of this PI in the CH stretching region, as shown in Fig. 7.4. Comparing SFG spectra between the unrubbed and unrubbed PI-30 films, the SFG intensity and the line shapes were changed after the sample was rubbed in both PSP and SPP polarization combinations. Namely, the peak at 2860 cm^{-1} is weaker and narrower after rubbing for SPP polarization combination. The results suggest that chiral SFG signals obtained mainly originate from the PI surface. Because if these signals mainly originate from the bulk, the line shapes of SFG spectra of the unrubbed and rubbed PI-30 films should be the same.

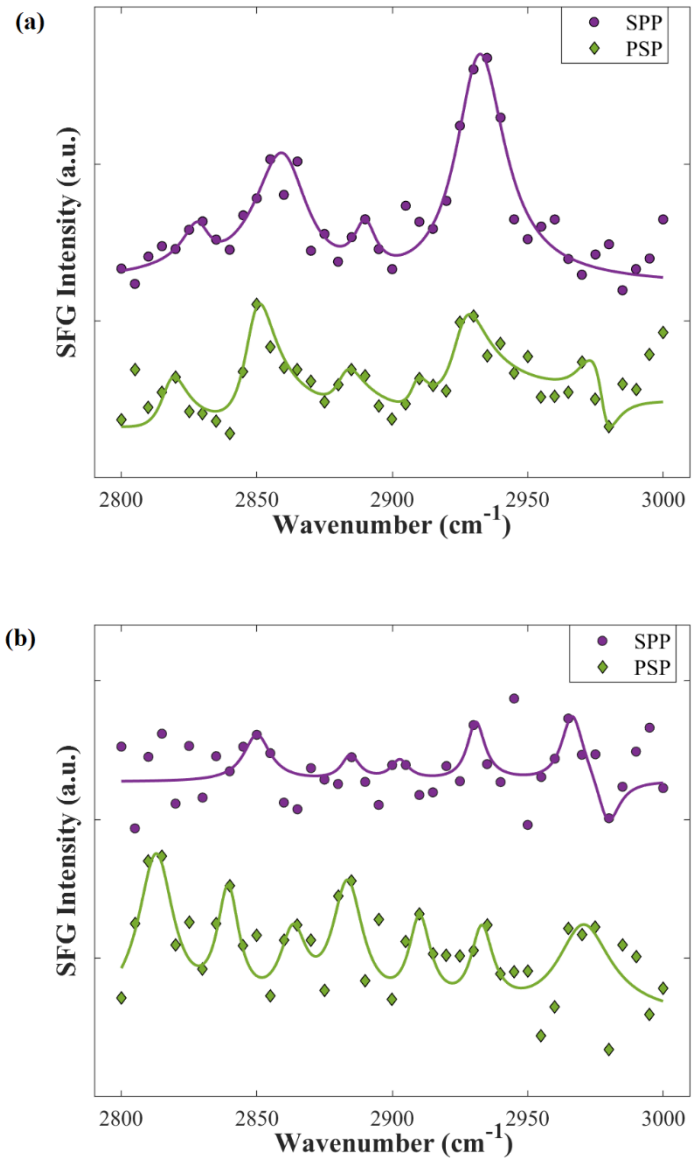

Figure 7.4. SFG spectra of (a) unrubbed PI-30 film, (b) rubbed PI-30 film at $\gamma = 0^o$ for PSP and SPP polarization combinations. The solid lines are the fitting curves obtained using Eq. (2.32) in Chapter 2.

7.3 Azimuthal angle dependence of SFG spectroscopy

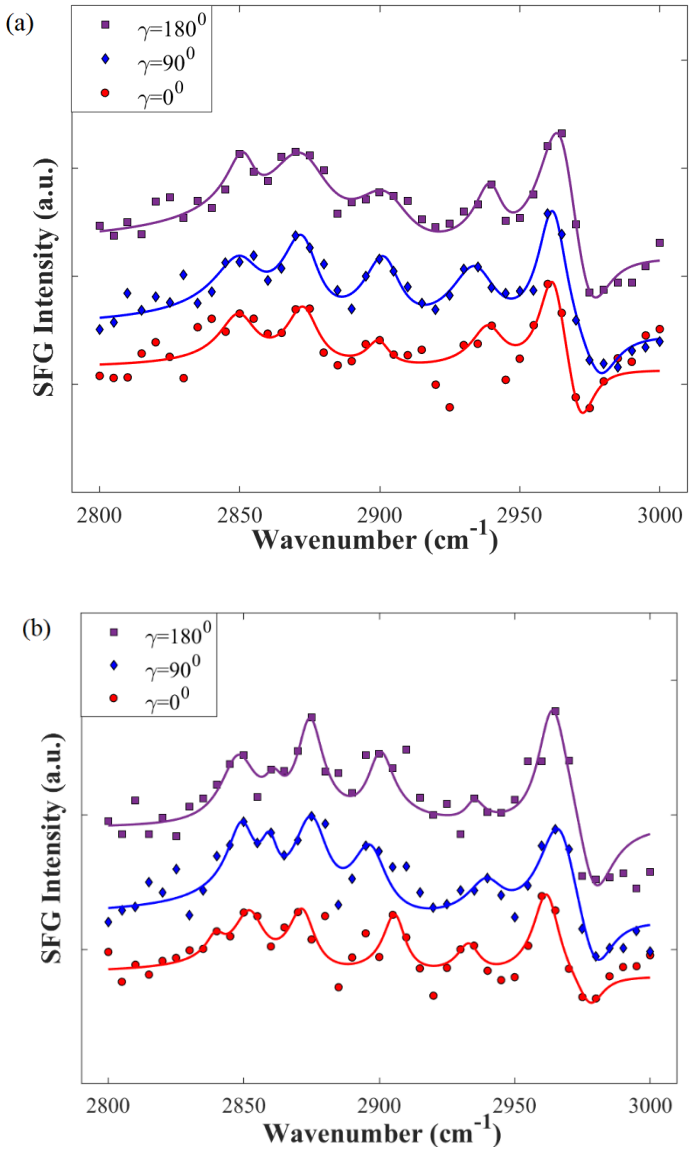

Figure 7.5 SFG spectra of (a) unrubbed PI-30 film, (b) rubbed PI-30 film for a PPP polarization combination at γ=0^o, 90^o, and 180^o azimuthal angles. The solid lines are the fitting curves obtained using Eq. (2.32) in Chapter 2.

To consider the effect of the rubbing process on the molecular orientation of the PI side chains, I measured SFG spectra at different azimuthal angles γ before and after rubbing. Figure 7.4 shows SFG spectra of unrubbed and rubbed PI-30 films for a PPP polarization combination, at γ=0°, 90°, and 180° azimuthal angles. γ=0° means that the beam propagation direction is in the rubbing direction. The solid lines in Fig. 7.5 were obtained by fitting using Eq. (2.32) in Chapter 2. The fitting parameters are listed in Tables 7.3 and 7.4. As expected, the spectral shapes of *unrubbed* PI-30 film in Fig. 7.5(a) do not show significant variation as a function of the azimuthal angle. Figure 7.5(b) for *rubbed* PI-30 film does not appear to show a clear

azimuthal angle dependence, either. So far as I measure the spectra of rubbed PI-30 film in this condition the difference is not easy to see.

Table 7.3 Fitting parameters of the SFG spectra of unrubbed PI-30 film for a PPP polarization combination, at γ=0^o, 90^o, and 180^{o}azimuthal angles

Parameter	γ=0^o	γ=90^o	γ=180^o
A_{NR} (a. u.)	3.38	2.81	2.91
ϕ (rad)	-1.74	-1.94	-2.0
A_1 (a. u.)	0.58	0.70	0.63
A_2 (a. u.)	0.70	1.07	1.10
A_3 (a. u.)	0.32	0.92	0.70
A_4 (a. u.)	0.50	0.87	0.75
A_5 (a. u.)	1.30	1.77	2.23
A_6 (a. u.)	-0.98	-0.90	-1.50
Γ_1 (cm^{-1})	8	10	6
Γ_2 (cm^{-1})	7	8	14
Γ_3 (cm^{-1})	5	8	12
Γ_4 (cm^{-1})	7	10	6
Γ_5 (cm^{-1})	6	6.5	9
Γ_6 (cm^{-1})	6	8	9
ω_1 (cm^{-1})	2850	2851	2852
ω_2 (cm^{-1})	2873	2873	2873
ω_3 (cm^{-1})	2900	2902	2903
ω_4 (cm^{-1})	2939	2935	2940
ω_5 (cm^{-1})	2962	2962	2965
ω_6 (cm^{-1})	2972	2979	2975

Table 7.4 Fitting parameters of the SFG spectra of rubbed PI-30 film for a PPP polarization combination, at γ=0^o, 90^o, and 180^{o}azimuthal angles

Parameter	γ=0^o	γ=90^o	γ=180^o
A_{NR} (a. u.)	2.84	2.69	3.02
ϕ (rad)	-1.79	-1.87	-1.47
A_1 (a. u.)	0.24	0.75	0.71
A_2 (a. u.)	0.62	0.50	0.28
A_3 (a. u.)	0.69	1.0	1.0
A_4 (a. u.)	0.68	0.8	0.7
A_5 (a. u.)	0.35	0.42	0.22
A_6 (a. u.)	1.0	1.35	1.32
A_7 (a. u.)	-0.46	-0.95	-1.2
Γ_1 (cm^{-1})	4	6	8
Γ_2 (cm^{-1})	7	4	4
Γ_3 (cm^{-1})	6	8	6
Γ_4 (cm^{-1})	5	8	6
Γ_5 (cm^{-1})	5	8	4
Γ_6 (cm^{-1})	6	9	7
Γ_7 (cm^{-1})	6	8	8
ω_1 (cm^{-1})	2840	2850	2848
ω_2 (cm^{-1})	2853	2860	2861
ω_3 (cm^{-1})	2872	2876	2874
ω_4 (cm^{-1})	2906	2897	2900
ω_5 (cm^{-1})	2933	2940	2935
ω_6 (cm^{-1})	2962	2967	2963
ω_7 (cm^{-1})	2978	2980	2979

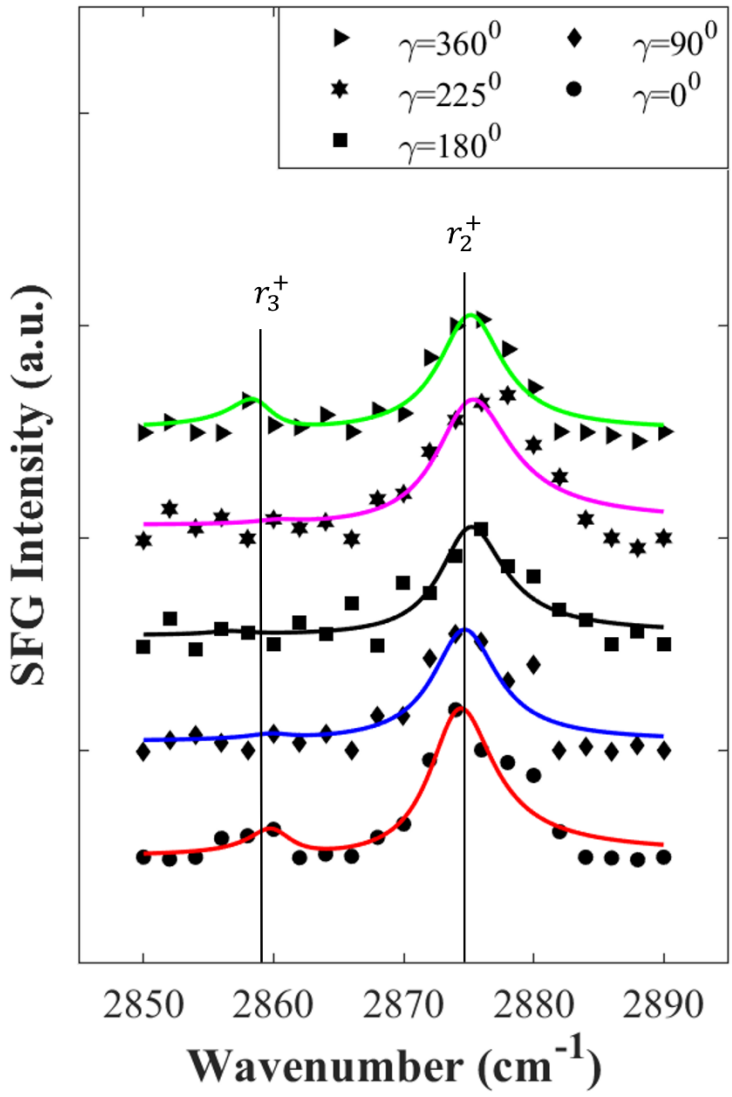

Figure 7.6 SFG spectra of rubbed PI-30 film for a PPP polarization combination at γ=0^o, 90^o, 180^o, 225^o, and 360^o azimuthal angles in the 2850-2890 cm^{-1} region. The solid lines are the fitting curves obtained using Eq. (2.32) in Chapter 2.

For a detailed analysis of rubbed PI-30 film, I focus on the CH_3 symmetric stretching modes in the 2850-2890 cm^{-1} region for the following reasons: (i) The molecular hyperpolarizability tensor elements for these modes are well-known;[2,4,6] (ii) the main polyimide chain in the PI-30 film does not have CH_3 groups and so all CH_3 signals likely come from the side chains; and (iii) symmetric stretching modes are normally less sensitive to intermolecular interactions.[2]

I observed SFG spectra for rubbed PI-30 film at azimuthal-angle intervals of 45^o with a PPP polarization combination to further investigate the effect of the rubbing process on the orientation of the methyl groups. The results are presented in Fig. 7.6. As previously discussed, the symmetric stretching mode of the methyl group adjacent to the steroidal structure

overwhelms the negative signals from the methyl groups on the steroidal structure, so the main contribution to the positive peak at ~2860 cm^{-1} is assumed to be from the methyl group adjacent to the steroidal structure. The "r_1^+mode", therefore, is renamed "r_3^+mode". The subscript 3 denotes the CH_3 group adjacent to the steroidal structure. The best-fit parameters for the CH_3 symmetric stretching modes (r_3^+ and r_2^+) are summarized in Table 7.5. I note here that the values of ω_1 inside parentheses are tentative values because these values cannot be precisely determined when the amplitude of the r_3^+ mode is too small. The r_3^+ mode appears to show a slight anisotropy in the SFG spectra, i.e., the intensity of this mode appears to be stronger in the rubbing direction at γ =0° and 360° and weaker at γ =180°. The results suggest that the methyl group adjacent to the steroidal structure is aligned in the rubbing direction. However, the rubbing process does not affect the r_2^+ peaks of the CH_3 isopropyl group significantly. As shown in Table 7.5, the amplitudes, and positions of the r_2^+ mode are generally similar to each other at different azimuthal angles to within the bounds of statistical error.

Table 7.5. Fitting results for CH_3 symmetric stretching modes of rubbed PI-30 film.

γ(deg)	Symmetric stretch of CH_3 group adjacent to the steroidal structure (r_3^+)		Symmetric stretch of CH_3 isopropyl group (r_2^+)	
	ω_1 (cm^{-1})	A_1 (a.u.)	ω_2 (cm^{-1})	A_2 (a.u.)
0	2860	0.74 ± 0.074	2874	2.32 ± 0.232
45	2859	0.54 ± 0.162	2875	1.38 ± 0.414
90	(2860)	0.13 ± 0.023	2875	1.72 ± 0.310
135	(2859)	0.15 ± 0.008	2874	2.30 ± 0.127
180	(2857)	0.10 ± 0.020	2875	1.68 ± 0.336
225	(2860)	0.08 ± 0.015	2875	1.75 ± 0.333
270	2862	0.30 ± 0.057	2875	2.06 ± 0.391
315	2860	0.85 ± 0.298	2874	2.00 ± 0.700
360	2859	0.80 ± 0.096	2875	2.04 ± 0.245

In order to analyze the dependence of the peak intensity of the CH_3 symmetric stretching mode r_3^+ from the methyl group adjacent to the steroidal-structure on the azimuthal angle, I show $\left|\chi^{(2)}_{PPP}(\gamma)\right|^2$ values in Fig. 7. obtained using the relationship:[2]

$$\left|\chi^{(2)}_{PPP,r_3^+}\right|^2 \equiv |A_1|^2. \qquad (7.1)$$

The vertical axis in Fig. 7.7 is normalized to unity at γ=0°. Using these measured values, I can obtain an approximate orientational distribution function $f(\theta,\psi,\varphi)$ for the methyl group adjacent to the steroidal structure using Eqs. (2.24), and (2.) in Chapter 2. The measured and calculated $\left|\chi^{(2)}_{PPP}(\gamma)\right|^2$ dependencies are shown in Fig. 7.7. As mentioned in Chapter 2, the value

of $r = \frac{\beta_{aac}}{\beta_{ccc}}$, and the IR refractive index are not well-known, but I found that the curve shape in Fig. 7.7 is not sensitive to the values of these parameters when r is between 1.7 and 4.0 and the refractive index is between 1.4 and 1.8. On the other hand, the curve shape is sensitive to the value of the average tilt angle θ_0. As shown in Fig. 7.7, the $\theta_0 = 40^o$ curve describes the best data. The uncertainty of θ_0 was estimated by carrying out the model calculations for a range of θ_0. I found that the best estimation of the angle θ_0 is $\theta_0 = 40° \pm 10°$.

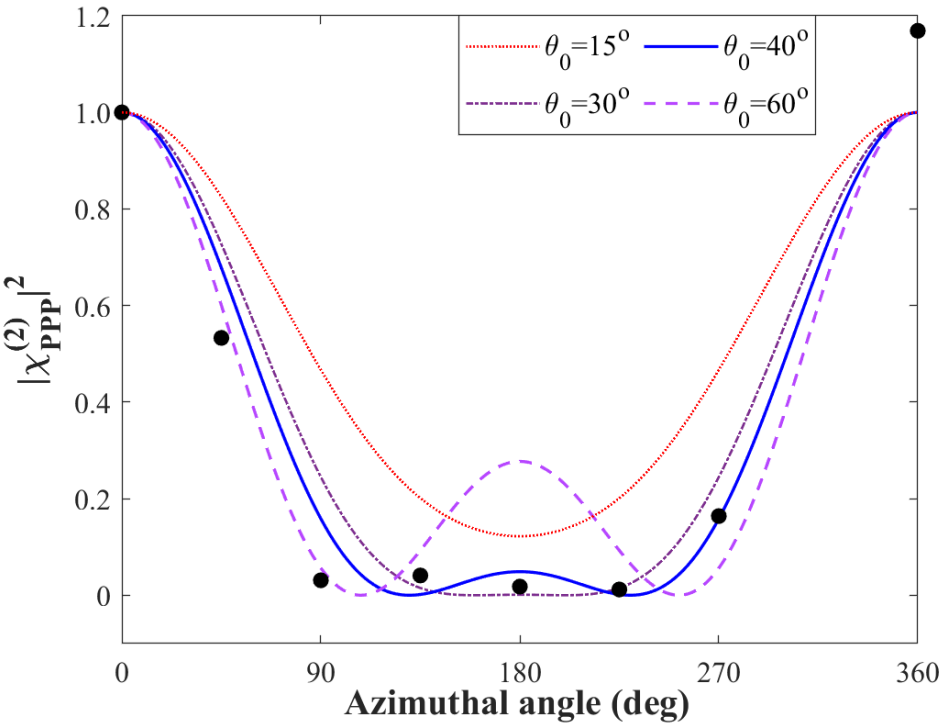

Figure 7.7 Experimental (dots) and calculated (curves) azimuthal angle dependence of SFG intensity of the CH_3 symmetric stretching mode from the CH_3 group adjacent to the steroidal structure. Orientational parameters used in model calculation: $\sigma_\theta = 15°$, $\sigma_\psi = 10°$.

The effect of σ_θ and σ_ψ on the curve shape were also investigated, as shown in Fig. 7.8. Both of them affect the width of the curve. By carrying out the model calculations for $\theta_0 = 40°$, $\sigma_\psi = 10°$ and a range of σ_θ, I can estimate the best fit of σ_θ. As shown in Fig. 7.8(a), the $\sigma_\theta = 15° \pm 10°$ curve describes the best data. Similarly, I can estimate the best fit of σ_ψ by carrying out the model calculations for $\theta_0 = 40°$, $\sigma_\theta = 15°$ and a range of σ_ψ. The curve shape does not show any significant variation between $\sigma_\psi = 2°$ and $10°$ as shown in Fig. 7.8(b). At these values, curves also describe the best data. Additionally, the variation of the curve shapes below $\sigma_\psi = 20°$ is not too much but it becomes big above $\sigma_\psi = 30°$. Consequently, the best estimation of σ_ψ is $\sigma_\psi \leq 20°$.

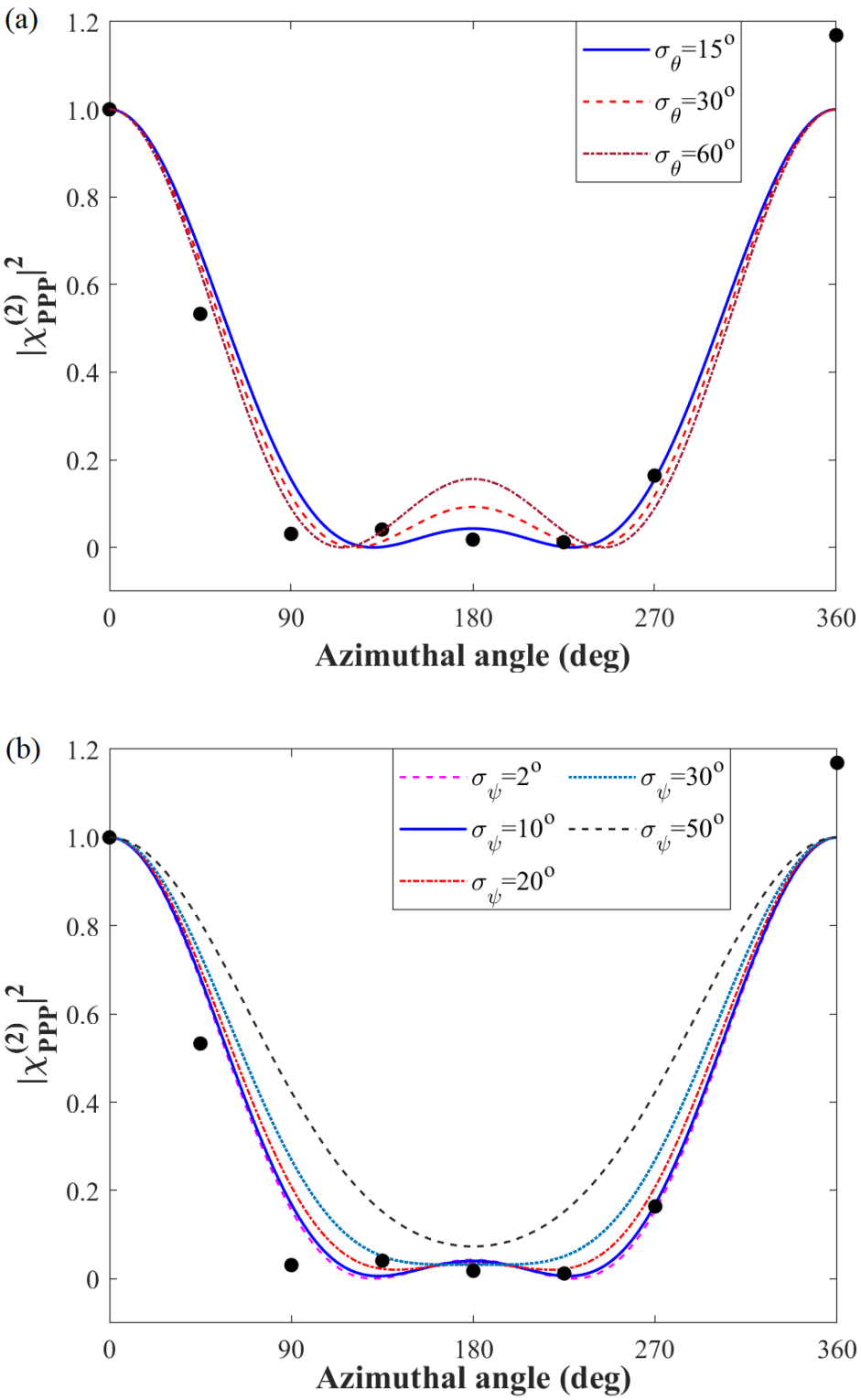

Figure 7.8 Intensity of the CH_3 symmetric stretching mode from the CH_3 group adjacent to the steroidal structure as a function of the azimuthal angle. Dots are the experimental data and curves are the calculation. Orientational parameters used in model calculation: (a) $\theta_0 = 40°$, $\sigma_\psi = 10°$; and (b) $\theta_0 = 40°$, $\sigma_\theta = 15°$.

The value of the angle θ_0 indicates that the methyl group adjacent to the steroidal structure is aligned with the rubbing direction on the surface, with an average 40° upward tilt, as illustrated in Fig. 7.9, the tilt angle distribution width σ_θ and the azimuthal distribution width σ_ψ are not very broad. The terminal CH_3 groups are randomly oriented because the length of the alkyl chain in the PI-30 film is short. Similar results have been observed in PIs with short alkyl side chains (1-7 carbon atoms).[3] It is known that the length of an alkyl side chain is a crucial parameter in determining the molecular organization and order of the terminal CH_3 group at surfaces or interfaces.[2] More specifically, long alkyl chains with more than 10 carbon atoms have better molecular organization and order at surfaces than shorter alkyl chains.

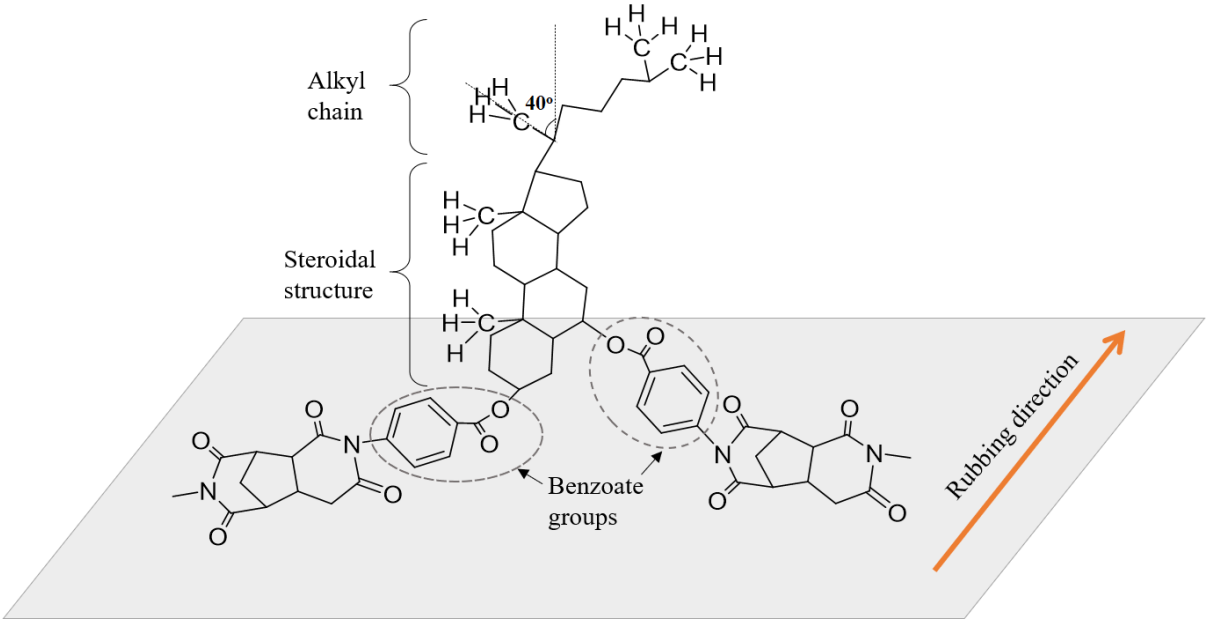

Figure 7.9. Schematic representation of the conformation of the steroidal side chain.

7.4 Correlation between the PI surface molecular orientation and the alignment of LC molecules on the PI surface

It is known that the molecular interaction between the alignment layer and LC molecules is the most important factor in LC alignment.[9,10] Therefore, the ultimate goal of my study was to establish which structural factor of rubbed PI films with steroidal side chains is most strongly correlated with LC alignment. Practically, LC molecules become aligned in the rubbing direction when they are placed on rubbed PI-30 films.[11] To establish which structural factor has the strongest correlation, the possible candidate structures were considered:

(1) The phenyl rings
(2) The steroidal structure and the adjacent CH_3 group
(3) The isopropyl group and the neighboring methylene group in the PI side chain

First, I discuss factor (1), namely the orientation and conformation of phenyl rings. Ullah *et al.* reported that the SHG intensity of rubbed PI-30 film shows anisotropic SHG intensity

patterns as a function of the sample rotation angle as presented in Fig. 7.10.[12] It is known that SHG is sensitive to the anisotropy of the orientation of phenyl rings.[13] This result suggests that the phenyl rings in the PI-30 film are aligned after rubbing. Hence, the correlation between factor (1) and LC alignment is possible.

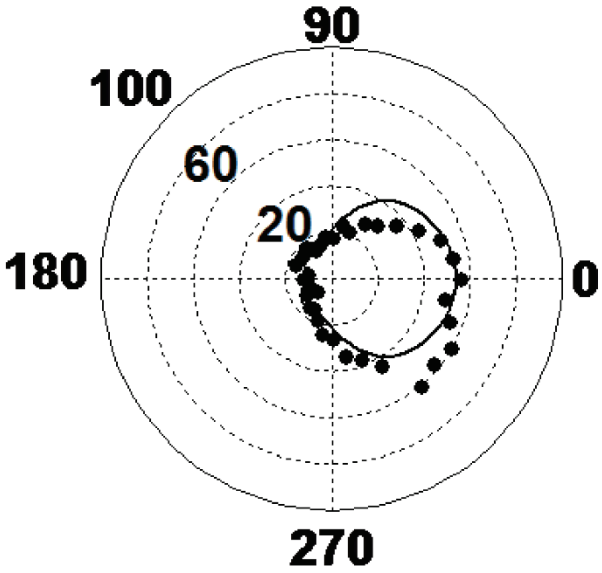

Figure 7.10. SHG intensity pattern of rubbed PI-30 film as a function of sample rotation angle in a Pin/Pout polarization combination. "0 degrees" means that the beam propagation direction is in the rubbing direction.[12]

Next, I discuss factor (2), namely the orientation and conformation of the steroidal structure and the CH_3 group adjacent to it. In my case, the SFG response of the CH_2 and CH_3 groups of the steroidal structure is weak because the steroidal structure has a roughly flat shape; and so, little can be said about the orientation of the steroidal structure using these CH_2 and CH_3 groups. However, Fig. 7.6 shows that the CH_3 group adjacent to the steroidal structure is oriented. This means that not only the CH_3 group adjacent to the steroidal structure, but also the steroidal structure, are oriented because the orientation of the CH_3 group restricts the structural boundary condition of the steroidal part. Thus, a correlation between the steroidal structure, the CH_3 group adjacent to the steroidal structure, and LC alignment, is possible.

Finally, I look at factor (3), namely the orientation and conformation of the isopropyl group and the neighboring methylene group in the PI side chain. In the SFG spectra of the rubbed PI-30 films in Fig. 7.6, the intensity of the symmetric stretching mode of the terminal CH_3 groups does not change as a function of the azimuthal angle, and hence the terminal CH_3 groups are not aligned in the rubbing direction. As discussed earlier, when the length of an alkyl chain in the PI-30 film is short, the terminal CH_3 groups do not become significantly oriented by rubbing. Thus, the result in Fig. 7.6 is unsurprising. The observation that the isopropyl group is not aligned, and LC alignment occurs on the PI surface means that LC alignment is not

correlated with orientation of the isopropyl group. Consequently, the correlation between factor (3) and LC alignment is denied.

So far, factors (1) and (2), namely the orientation of the phenyl rings and the steroidal structure and the adjacent CH_3 group, are possibly correlated with LC alignment. Unfortunately, I have no further evidence to determine which of these two factors is the most likely cause of LC alignment. However, the results of my study clearly show no correlation between the isopropyl group and the neighboring methylene group in the PI side chain [factor (3)] and LC alignment. To the best of my knowledge, there has not yet been an analysis of the orientation of an isopropyl group on a rubbed PI surface, like the one in this study.

7.5 Comparison with other research results

The results achieved in this study are consistent with the results in previous research that the correlation between LC molecules and the alignment layer depends on the alignment material used.[2,14–18] In general, microgrooves are created on the PI surface in the rubbing direction. Hence, LC alignment on the rubbed PI film surfaces is determined by the interactions between LC molecules with (1) the oriented molecules of the PI main chains, (2) the oriented molecules of the PI side chains and (3) the microgrooves.[16] However, it is known that LC alignment is dominated by the molecular interaction between the PI film and LC molecules rather than by interaction with the microgrooves.[9,10]

Chemical structure of the PI side chains of the PI used in this study and LC molecules are similar. It suggests that the orientation direction of the rubbed PI side chains may efficiently be transmitted to LC molecules. Typically, an LC molecule is composed of an aromatic mesogen and an aliphatic tail. The aromatic mesogens might interact with the phenyl rings of the PIs through π-π interactions and the aliphatic tails might interact with the aliphatic chain components of the PIs through van der Waals interactions.[16] For example, Wang *et al.*[15] reported that it is much easier to form intermolecular interaction with the biphenyl groups of PI side chain than with other units on the surface due to the similarity of their chemical structure and conformation for the biphenyl groups of LC molecules.

Practically, the length of an alkyl side chain is directly related to the alignment of LC molecules for PIs containing alkyl side chains. Lee *et al*. reported that LC molecules on the rubbed PI film surfaces of *C8*-PMDA-PDA PI were aligned *parallel* to the rubbing direction whereas the LC molecules on the rubbed PI film surfaces of *C4*-PMDA-PDA PI, *C6*-PMDA-PDA PI, and *C7*-PMDA-PDA PI were aligned *perpendicular* to the rubbing direction.[16] It can be explained by intermolecular interaction between LC molecules and PI side chains. Similar results were observed by Liu *et al.*, they investigated a series of diamines with a side chain containing rigid biphenyl unit and nonpolar alkoxy side end group [4-alkoxy-biphenol-3',5'-diaminobenzoate] (Cm-BBDA, m = 4, 6, 12) to study the effect of the length of alkoxy side end group on LC alignment.[14] Liu *et al.* found that the *planar alignment* was obtained for PI

with side chain containing alkoxy side end group of *4 carbon atoms* and the *vertical alignment* was observed for alkoxy side end groups of *6 or 12 carbon atoms*.

References

[1] P.J.N. Kett, M.T.L. Casford, and P.B. Davies, J. Phys. Chem. B **117**, 6455 (2013).

[2] H.D. Jayathilake, M.H. Zhu, C. Rosenblatt, A.N. Bordenyuk, C. Weeraman, and A. V. Benderskii, J. Chem. Phys. **125**, (2006).

[3] M. Oh-e, A.I. Lvovsky, X. Wei, and Y.R. Shen, J. Chem. Phys. **113**, 8827 (2000).

[4] X. Zhuang, P.B. Miranda, D. Kim, and Y.R. Shen, Phys. Rev. B - Condens. Matter Mater. Phys. **59**, 12632 (1999).

[5] A.G. Lambert, P.B. Davies, and D.J. Neivandt, Appl. Spectrosc. Rev. **40**, 103 (2005).

[6] H.F. Wang, W. Gan, R. Lu, Y. Rao, and B.H. Wu, Int. Rev. Phys. Chem. **24**, 191 (2005).

[7] P.J.N. Kett, M.T.L. Casford, and P.B. Davies, Mol. Phys. **111**, 175 (2013).

[8] S.J. McGall, P.B. Davies, and D.J. Neivandt, J. Phys. Chem. B **108**, 16030 (2004).

[9] J.M. Geary, J.W. Goodby, A.R. Kmetz, and J.S. Patel, J. Appl. Phys. **62**, 4100 (1987).

[10] S.G. Hahm, Y.G. Ko, Y. Rho, B. Ahn, and M. Ree, Curr. Opin. Chem. Eng. **2**, 71 (2013).

[11] M. Nishikawa, J. Photopolym. Sci. Technol. **24**, 317 (2011).

[12] M.S. Ullah, S. Asai, Y. Inomata, K.T.T. Hien, G. Mizutani, Y. Murakami, and T. Okada, E-Journal Surf. Sci. Nanotechnol. **15**, 7 (2017).

[13] S.C. Hong, M. Oh-E, X. Zhuang, Q. Shen, J.J. Ge, B.W. Harris, and S.Z.D. Cheng, Phys. Rev. E - Stat. Nonlinear, Soft Matter Phys. **63**, 517061 (2001).

[14] Z. Liu, F. Yu, Q. Zhang, Y. Zeng, and Y. Wang, Eur. Polym. J. **44**, 2718 (2008).

[15] X. Wang, P. Zhang, Y. Chen, L. Luo, Y. Pang, and X. Liu, Macromolecules **44**, 9731 (2011).

[16] S. W. Lee, S. J. Lee, S. G. Hahm, T. J. Lee, B. Lee, B. Chae, S. B. Kim, J. C. Jung, W. C. Zin, B. H. Sohn, and M. Ree, Macromolecules **38**, 4331 (2005).

[17] Y.J. Lee, J.G. Choi, I.K. Song, J.M. Oh, and M.H. Yi, Polymer (Guildf). **47**, 1555 (2006).

[18] T. Sakai, K. Ishikawa, H. Takezoe, N. Matsuie, Y. Yamamoto, H. Ishii, Y. Ouchi, H. Oji, and K. Seki, J. Phys. Chem. B **105**, 9191 (2001).

CHAPTER 8. GENERAL CONCLUSION

The contribution of main chains and side chains of unrubbed PI films with steroidal side chains to SHG signal was studied by changing the fraction of steroidal side chains. In P_{in}/P_{out} polarization combination, the SHG intensity does not depend strongly on the fraction of steroidal side chains. It indicates that both the PI main chains and PI side chains at the PI surface contribute similarly to the SHG intensity. The SHG intensity of samples in S_{in}/P_{out} normalized by that in P_{in}/P_{out} is the smallest for the unrubbed PI film without steroidal side chains. This result suggests that the microscopic nonlinear dipoles stand almost upright at the surface of the unrubbed PI without steroidal side chains film. In contrast, their orientational spread is wider in the unrubbed PI with steroidal side chains film.

SFG vibrational spectroscopy has been utilized to analyze the molecular orientation and conformation of the steroidal structure and the alkyl chain at the rubbed polyimide films with units possessing steroidal side chains of a fraction of 30% (PI-30). To the best of my knowledge, this is the first time the orientation of these parts at the rubbed PI surface like the one in this study has been analyzed.

I have proved that all the SFG spectra in this study mainly originate from the PI surface and the SFG contribution from the PI/glass substrate interface and the bulk PI are not significant by measuring the SFG spectra of rubbed PI-30 films with and without PMMA overlayer. The SFG intensity decreased dramatically after the sample was covered with the very thin PMMA layer for the PPP polarization combination. Additionally, the peaks in the spectra changed drastically by the PMMA deposition for the SSP polarization combination.

To obtain the best SFG signal of the PI film surfaces, SFG measurement was optimized by investigating the visible beam energy and the uniformity of the PI sample. I found that 80 μJ/pulse is the most appropriate visible beam energy for SFG measurements of the PI films. In addition, the SFG spectra of the PI-30 sample at different positions show little variation. It indicates that the sample is essentially uniform.

I have evaluated the effect of the ambient environment, such as moisture and air, on the orientation of molecules at the fresh rubbed PI-30 surface by comparing the SFG spectra of the sample in air and dry N_2 gas. Due to the reflection at the surfaces of the quartz cell, the SFG intensity of the rubbed PI-30 film in dry N_2 gas was much weaker than that of the rubbed PI-30 film in air. However, the peak positions and line shapes of these SFG spectra are pretty similar. Therefore, it suggests that the ambient environment does not significantly affect the molecular orientation of the PI-30 film surface. The result thus allows me to carry out SFG measurements of the PI-30 film in air.

I measured SFG spectra of the rubbed PI-30 films stored at different times to check the quality of the PI samples in use and storage. A significant variation of the SFG spectrum was observed in the sample after four months of preparation. It suggests that the orientation of

molecules at the PI side chain was changed. As a result, I should use the fresh samples or at least the samples fabricated within three months to investigate the orientation and conformation of the molecules at the PI-30 surface.

To investigate the effect of the rubbing process on the orientation of the CH_3 groups, I have observed SFG spectra of the rubbed PI-30 at azimuthal-angle intervals of 45^o with a PPP polarization combination. After analyzing these SFG spectra, I can conclude that the isopropyl group is pointing toward the air side from the PI surface. However, their average orientation is not affected by rubbing because the length of the alkyl chain in this PI is short. This result contrasts the many past examples with the CH_3 end group of alkyl chains affecting the LC alignment. A slight anisotropy of the symmetric stretching mode of the CH_3 group adjacent to the steroidal structure is observed after rubbing in the SFG spectra, and its average tilt angle is estimated to be $\theta_0 = 40^o \pm 10^o$ in the rubbing direction.

In practice, LC molecules are aligned when they are put on the rubbed PI-30 films. There are three possible structural factors of the rubbed PI films containing steroidal side chains correlated with LC alignment: (1) the phenyl rings, (2) the steroidal structure and the adjacent CH_3 group, and (3) the isopropyl group and the neighboring methylene group in the PI side chain. Among them, factor (3) can be excluded because it does not show any anisotropy after rubbing. Consequently, factors (1) and (2) are possibly correlated with LC alignment. Unfortunately, I cannot determine which of them is the main factor causing LC alignment so far, and further study is necessary.

APPENDICIES

Appendix A – Academic Conferences and Publications

Conferences

1. **Nguyen Thi Trinh**, Khuat Thi Thu Hien, Goro Mizutani, Yoshitaka Murakami and Takashi Okada, "Nonlinear optical spectroscopic study of a rubbed polyimide film with steroidal structure side chains", *JAIST Japan-India Symposium on Advanced Science*, 2019, Ishikawa, Japan.
2. **N. T. Trinh**, K. T. T. Hien, G. Mizutani, Y. Murakami and T. Okada, "Surface characterization of a rubbed polyimide film containing steroidal structure side chains by using sum frequency generation", *The Physical Society of Japan 2019 Autumn Meeting*, Gifu, Japan.
3. **Nguyen Thi Trinh**, Khuat Thi Thu Hien, Goro Mizutani, Yoshitaka Murakami and Takashi Okada, "Nonlinear vibrational spectroscopy of steroidal structure side chains of polyimide surface", 12th *International Symposium on Atomic Level Characterizations for New Materials and Devices*, 2019, Kyoto, Japan.
4. **N. T. Trinh**, Yu Sheng, K. T. T. Hien, G. Mizutani, Y. Murakami and T. Okada, "Investigation of unrubbed surfaces of polyimide containing steroidal structure side chains using optical second harmonic generation", *The Physical Society of Japan 2020 Annual (75th) Meeting*, Nagoya, Japan.
5. **N. T. Trinh**, K. T. T. Hien, G. Mizutani, Y. Murakami and T. Okada, "Sum Frequency Generation Vibrational Spectroscopy of Polyimide Containing Steroidal Structure Side Chains", *The Physical Society of Japan 2021 Annual (76th) Meeting*, Japan.

Publications

1. **Nguyen Thi Trinh**, Yu Sheng, Shinya Asakura, Khuat Thi Thu Hien, Goro Mizutani, Yoshitaka Murakami and Takashi Okada, "Optical second harmonic generation analysis of unrubbed polyimide surfaces as a function of the content of steroidal structure side chains", *e-J. Surf. Sci. Nanotechnol*. **18**, 175-179 (2020).
2. **Trinh Thi Nguyen**, Hien Thi Thu Khuat, Shinya Asakura, Goro Mizutani, Yoshitaka Murakami and Takashi Okada, "Study of the molecular orientation of steroidal side chains at polyimide surfaces using sum frequency generation vibrational spectroscopy", *J. Chem. Phys.* **155**, 084702 (2021).

Appendix B – Abstract of Minor Research Project

Molecular Orientation of Polyimide Containing Steroidal Structure Thin Films Studied by p-Polarized Multiple-Angle Incidence Resolution Spectrometry

Supervisor: Assoc. Prof. Yuki Nagao

Polyimide containing steroidal structure side chains spin-coated on a non-alkali glass substrate was used in this work. Due to the low refractive index of the glass substrate, the validation of this substrate for p-polarized multiple-angle incidence resolution spectrometry (pMAIRS) measurement has been checked. The results indicate that the pMAIRS technique cannot be applied to the analysis of the polyimide deposited on the glass substrate. To overcome this experimental limitation, the sample deposited on a Si substrate should be used. In addition, based on the Fourier-transform infrared spectra of the sample, I found that the mechanical rubbing process does not significantly affect the molecular orientation in the bulk of the PI film. However, the reorientation of molecules on the PI surface was observed by sum frequency generation vibrational spectroscopy.

Appendix C – Transformation coefficients $U_{ijk,lmn}$ for PPP polarization combination

As mentioned in Chapter II, I assume that the CH_3 group has C_{3v} symmetry, and each CH_3 group can freely rotate around the c-axis. Using Table II in Hirose *et al.*'s paper(*), I can deduce transformation coefficients $U_{ijk,lmn}$ easily. There are eight elements of the second-order nonlinear susceptibility $\chi^{(2)}_{ijk}$ contribute to the SFG signal for the PPP polarization combination: $\chi^{(2)}_{xxx}$, $\chi^{(2)}_{xxz}$, $\chi^{(2)}_{xzz}$, $\chi^{(2)}_{xzx}$, $\chi^{(2)}_{zxx}$, $\chi^{(2)}_{zzx}$, $\chi^{(2)}_{zxz}$, and $\chi^{(2)}_{zzz}$.

1. $U_{xxx,lmn}$

$$U_{xxx,aac} = -\frac{\sin\theta}{8}(\cos\psi - \cos 3\psi) - \frac{\sin\theta + \sin 3\theta}{32}(3\cos\psi + \cos 3\psi)$$

$$U_{xxx,bbc} = -\frac{\sin\theta}{8}(\cos\psi - \cos 3\psi) - \frac{\sin\theta + \sin 3\theta}{32}(3\cos\psi + \cos 3\psi)$$

$$U_{xxx,ccc} = -\frac{3\sin\theta - \sin 3\theta}{16}(3\cos\psi + \cos 3\psi)$$

2. $U_{xxz,lmn}$

$$U_{xxz,aac} = \frac{\cos\theta}{2} - \frac{\cos\theta - \cos 3\theta}{16}(1 + \cos 2\psi)$$

$$U_{xxz,bbc} = \frac{\cos\theta}{2} - \frac{\cos\theta - \cos 3\theta}{16}(1 + \cos 2\psi)$$

$$U_{xxz,ccc} = \frac{\cos\theta - \cos 3\theta}{8}(1 + \cos 2\psi)$$

3. $U_{xzz,lmn}$

$$U_{xzz,aac} = \frac{\sin\theta + \sin 3\theta}{8}\cos\psi$$

$$U_{xzz,bbc} = \frac{\sin\theta + \sin 3\theta}{8}\cos\psi$$

$$U_{xzz,ccc} = -\frac{\sin\theta + \sin 3\theta}{4}\cos\psi$$

4. $U_{xzx,lmn}$

$$U_{xzx,aac} = -\frac{\cos\theta - \cos 3\theta}{16}(1 + \cos 2\psi)$$

$$U_{xzx,bbc} = -\frac{\cos\theta - \cos 3\theta}{16}(1 + \cos 2\psi)$$

$$U_{xzx,ccc} = \frac{\cos\theta - \cos 3\theta}{8}(1 + \cos 2\psi)$$

5. $U_{zxx,lmn}$

$$U_{zxx,aac} = -\frac{\cos\theta - \cos 3\theta}{16}(1 + \cos 2\psi)$$

$$U_{zxx,bbc} = -\frac{\cos\theta - \cos 3\theta}{16}(1 + \cos 2\psi)$$

$$U_{zxx,ccc} = \frac{\cos\theta - \cos 3\theta}{8}(1 + \cos 2\psi)$$

6. $\boldsymbol{U_{zzx,lmn}}$

$$U_{zzx,aac} = -\frac{3\sin\theta - \sin 3\theta}{8}\cos\psi$$

$$U_{zzx,bbc} = -\frac{3\sin\theta - \sin 3\theta}{8}\cos\psi$$

$$U_{zzx,ccc} = -\frac{\sin\theta + \sin 3\theta}{4}\cos\psi$$

7. $\boldsymbol{U_{zxz,lmn}}$

$$U_{zxz,aac} = \frac{\sin\theta + \sin 3\theta}{8}\cos\psi$$

$$U_{zxz,bbc} = \frac{\sin\theta + \sin 3\theta}{8}\cos\psi$$

$$U_{zxz,ccc} = -\frac{\sin\theta + \sin 3\theta}{4}\cos\psi$$

8. $\boldsymbol{U_{zzz,lmn}}$

$$U_{zzz,aac} = \frac{\cos\theta - \cos 3\theta}{8}$$

$$U_{zzz,bbc} = \frac{\cos\theta - \cos 3\theta}{16}$$

$$U_{zzz,ccc} = \frac{3\cos\theta + \cos 3\theta}{4}$$

(*) C. Hirose, N. Akamatsu, and K. Domen, Appl. Spectrosc. **46**, 1051 (1992).

Appendix D – Model to calculate effective second order nonlinear susceptibility for azimuthal angle dependence of CH_3 symmetric stretch mode of C_{3v} symmetry

(This model was adopted from the model of Jayathilake et al. as mentioned in Chapter 2)

```
%Load data
xx = 0:pi/4:2*pi;
%load experimental data after normalization
yy=[1.000
0.533
0.031
0.041
0.018
0.012
0.164
1.319
1.169];
% Molecular hyperpolarizability: nonzero tensor elements
% symmetry group (CH3 symmetric stretching mode of C3v symmetry)
betaac=3.4;
betbbc=3.4;
betccc=1;
%-------------------------------------------------------------------------
%experimental geometry and refractive indices of materials
%incidient angle of visible light [rad]
xvis=80*pi/180;
%incidient angle of IR light [rad]
xir=45*pi/180;
%reflected angle of SFG light [rad]
xsfg=73*pi/180;
%-------------------------------------------------------------------------
%Local field correction was done assuming four layer
n1sfg=1; % refractive index medium 1 (air) for SFG
n2sfg=1.606; % refractive index medium 2 (polyimide) for SFG
n3sfg=1.465; %refractive index medium 3 (glass) for SFG
n1vis=1; % refractive index medium 1 (air) for visble light
n2vis=1.590; % refractive index medium 2 (polyimide) for visble light
n3vis=1.461; %refractive index medium 3 (glass) for visble light
n1ir=1; % refractive index medium 1 (air) for IR light
n2ir=1.546; % refractive index medium 2 (polyimide) for IR light
n3ir=1.436; %refractive index medium 3 (glass) for IR light
% refracted angle of sfg, vis, IR [rad] between medium 1 (air) and 2
(polyimide)
a12sfg=asin(n1sfg*sin(xsfg)/n2sfg);
a12vis=asin(n1vis*sin(xvis)/n2vis);
a12ir=asin(n1ir*sin(xir)/n2ir);
```

```
% refracted angle of sfg, vis, IR [rad] between medium 2 (polyimde) and 3
(glass)
a23sfg=asin(n2sfg*sin(a12sfg)/n3sfg);
a23vis=asin(n2vis*sin(a12vis)/n3vis);
a23ir=asin(n2ir*sin(a12ir)/n3ir);
% refrative index for surface between air and polyimde n4
n4sfg=sqrt(n2sfg^2*(n2sfg^2+5)/(4*n2sfg^2+2));
n4vis=sqrt(n2vis^2*(n2vis^2+5)/(4*n2vis^2+2));
n4ir=sqrt(n2ir^2*(n2ir^2+5)/(4*n2ir^2+2));
%-------------------------------------------------------------------------
h=80; % film thickness (nm)
%-------------------------------------------------------------------------
%Calculating Fresnel factors for SFG
lamdasfg=532*(10^7/2860)/(532+(10^7/2860));
bsfg=(2*pi/lamdasfg)*n2sfg*h*cos(a12sfg);
%reflection Fresnel factor for p polarized light at air/polyimide interface
r12psfg=(n2sfg*cos(xsfg)-
n1sfg*cos(a12sfg))/(n2sfg*cos(xsfg)+n1sfg*cos(a12sfg));
%reflection Fresnel factor for p polarized light at polyimide/glass
interface
r23psfg=(n3sfg*cos(a12sfg)-
n2sfg*cos(a23sfg))/(n3sfg*cos(a12sfg)+n2sfg*cos(a23sfg));
%reflection Fresnel factor for s polarized light at air/polyimide interface
r12ssfg=(n1sfg*cos(xsfg)-
n2sfg*cos(a12sfg))/(n1sfg*cos(xsfg)+n2sfg*cos(a12sfg));
%reflection Fresnel factor for s polarized light at polyimide/glass
interface
r23ssfg=(n2sfg*cos(a12sfg)-
n3sfg*cos(a23sfg))/(n2sfg*cos(a12sfg)+n3sfg*cos(a23sfg));
%the complex Fresnel factors
Lxsfg=1-(r12psfg+r23psfg*exp(2i*bsfg))/(1+r12psfg*r23psfg*exp(2i*bsfg));
Lysfg=1+(r12ssfg+r23ssfg*exp(2i*bsfg))/(1+r12ssfg*r23ssfg*exp(2i*bsfg));
Lzsfg=(1+(r12psfg+r23psfg*exp(2i*bsfg))/(1+r12psfg*r23psfg*exp(2i*bsfg)))*(
n1sfg/n4sfg)^2;
%-------------------------------------------------------------------------
%Calculating Fresnel factors for visible light
lamdavis=532;%nm
bvis=(2*pi/lamdavis)*n2vis*h*cos(a12vis);
%reflection Fresnel factor for p polarized light at air/polyimide interface
r12pvis=(n2vis*cos(xvis)-
n1vis*cos(a12vis))/(n2vis*cos(xvis)+n1vis*cos(a12vis));
%reflection Fresnel factor for p polarized light at polyimide/glass
interface
r23pvis=(n3vis*cos(a12vis)-
n2vis*cos(a23vis))/(n3vis*cos(a12vis)+n2vis*cos(a23vis));
%reflection Fresnel factor for s polarized light at air/polyimide interface
```

```
r12svis=(n1vis*cos(xvis)-
n2vis*cos(a12vis))/(n1vis*cos(xvis)+n2vis*cos(a12vis));
%reflection Fresnel factor for s polarized light at polyimide/glass
interface
r23svis=(n2vis*cos(a12vis)-
n3vis*cos(a23vis))/(n2vis*cos(a12vis)+n3vis*cos(a23vis));
%the complex Fresnel factors
Lxvis=1-(r12pvis+r23pvis*exp(2i*bvis))/(1+r12pvis*r23pvis*exp(2i*bvis));
Lyvis=1+(r12svis+r23svis*exp(2i*bvis))/(1+r12svis*r23svis*exp(2i*bvis));
Lzvis=(1+(r12pvis+r23pvis*exp(2i*bvis))/(1+r12pvis*r23pvis*exp(2i*bvis)))*(
n1vis/n4vis)^2;
%-------------------------------------------------------------------------
%Calculating Fresnel factors for IR
lamdair=10^7/2860;%nm
bir=(2*pi/lamdair)*n2ir*h*cos(a12ir);
%reflection Fresnel factor for p polarized light at air/polyimide interface
r12pir=(n2ir*cos(xir)-n1ir*cos(a12ir))/(n2ir*cos(xir)+n1ir*cos(a12ir));
%reflection Fresnel factor for p polarized light at polyimide/glass
interface
r23pir=(n3ir*cos(a12ir)-n2ir*cos(a23ir))/(n3ir*cos(a12ir)+n2ir*cos(a23ir));
%reflection Fresnel factor for s polarized light at air/polyimide interface
r12sir=(n1ir*cos(xir)-n2ir*cos(a12ir))/(n1ir*cos(xir)+n2ir*cos(a12ir));
%reflection Fresnel factor for s polarized light at polyimide/glass
interface
r23sir=(n2ir*cos(a12ir)-n3ir*cos(a23ir))/(n2ir*cos(a12ir)+n3ir*cos(a23ir));
%the complex Fresnel factors
Lxir=1-(r12pir+r23pir*exp(2i*bir))/(1+r12pir*r23pir*exp(2i*bir));
Lyir=1+(r12sir+r23sir*exp(2i*bir))/(1+r12sir*r23sir*exp(2i*bir));
Lzir=(1+(r12pir+r23pir*exp(2i*bir))/(1+r12pir*r23pir*exp(2i*bir)))*(n1ir/n4ir)^2;
%-------------------------------------------------------------------------
% Molecular orientation
%theta=angle between surface normal and c3 axis of the molecules [rad]
% Numerical integration over Gaussian theta distribution f(theta). Step
size 1 degree
Ntheta=180;
dtheta=pi/Ntheta;
%Gaussian distribution with centered at theta00 and rms deltheta
% Average tilt angle theta00 from normal theta00=0 means hydrogens of CH3
point up in the air
theta00=30; % tilt angle in degrees
deltheta=15*pi/180; %Gaussian width
theta0=pi-theta00*pi/180;
A=1/(sqrt(2*pi)*deltheta);
%PPP polarization
% Calculate azimuthal angle dependence
Nki=180;
step=2*pi/Nki;
```

```
for k=1:Nki+1
    ki=(k-1)*step;
    sum=0.0;
    for j=1:Ntheta
        theta=-pi/2+theta0+(j-1)*dtheta;
 %r+ mode (C3v)conversion of surface fixed coordinates into molecular coordinates
(using the table from Hirose paper)
  Uzxxaac(k)=(-1)*((cos(theta)-cos(3*theta))/16)*(1+cos(2*ki));
  Uzxxbbc(k)=(-1)*((cos(theta)-cos(3*theta))/16)*(1+cos(2*ki));
  Uzxxccc(k)=((cos(theta)-cos(3*theta))/8)*(1+cos(2*ki));

  Uxxzaac(k)=(cos(theta)/2)-((cos(theta)-cos(3*theta))/16)*(1+cos(2*ki));
  Uxxzbbc(k)=(cos(theta)/2)-((cos(theta)-cos(3*theta))/16)*(1+cos(2*ki));
  Uxxzccc(k)=((cos(theta)-cos(3*theta))/8)*(1+cos(2*ki));

  Uxzxaac(k)=(-1)*((cos(theta)-cos(3*theta))/16)*(1+cos(2*ki));
  Uxzxbbc(k)=(-1)*((cos(theta)-cos(3*theta))/16)*(1+cos(2*ki));
  Uxzxccc(k)=((cos(theta)-cos(3*theta))/8)*(1+cos(2*ki));

  Uzzzaac(k)=(cos(theta)-cos(3*theta))/8;
  Uzzzbbc(k)=(cos(theta)-cos(3*theta))/16;
  Uzzzccc(k)=(3*cos(theta)+cos(3*theta))/4;

  Uxxxaac(k)=(-1)*(sin(theta))/8*(cos(ki)-cos(3*ki))-((sin(theta)...
  +sin(3*theta))/32)*(3*cos(ki)+cos(3*ki));
  Uxxxbbc(k)=(-1)*(sin(theta))/8*(cos(ki)-cos(3*ki))-((sin(theta)...
      +sin(3*theta))/32)*(3*cos(ki)+cos(3*ki));
  Uxxxccc(k)=(-1)*((3*sin(theta)-sin(3*theta))/16)*(3*cos(ki)+cos(3*ki));

  Uxzzaac(k)=((sin(theta)+sin(3*theta))/8)*cos(ki);
  Uxzzbbc(k)=((sin(theta)+sin(3*theta))/8)*cos(ki);
  Uxzzccc(k)=(-1)*((sin(theta)+sin(3*theta))/4)*cos(ki);

  Uzzxaac(k)=(-1)*((3*sin(theta)-sin(3*theta))/8)*cos(ki);
  Uzzxbbc(k)=(-1)*((3*sin(theta)-sin(3*theta))/8)*cos(ki);
  Uzzxccc(k)=(-1)*((sin(theta)+sin(3*theta))/4)*cos(ki);

  Uzxzaac(k)=((sin(theta)+sin(3*theta))/8)*cos(ki);
  Uzxzbbc(k)=((sin(theta)+sin(3*theta))/8)*cos(ki);
  Uzxzccc(k)=(-1)*((sin(theta)+sin(3*theta))/4)*cos(ki);

  Xzxx=Uzxxaac(k)*betaac+Uzxxbbc(k)*betbbc+Uzxxccc(k)*betccc;
  Xxxz=Uxxzaac(k)*betaac+Uxxzbbc(k)*betbbc+Uxxzccc(k)*betccc;
  Xxzx=Uxzxaac(k)*betaac+Uxzxbbc(k)*betbbc+Uxzxccc(k)*betccc;
  Xzzz=Uzzzaac(k)*betaac+Uzzzbbc(k)*betbbc+Uzzzccc(k)*betccc;
  Xxxx=Uxxxaac(k)*betaac+Uxxxbbc(k)*betbbc+Uxxxccc(k)*betccc;
  Xxzz=Uxzzaac(k)*betaac+Uxzzbbc(k)*betbbc+Uxzzccc(k)*betccc;
```

```
  Xzzx=Uzzxaac(k)*betaac+Uzzxbbc(k)*betbbc+Uzzxccc(k)*betccc;
  Xzxz=Uzxzaac(k)*betaac+Uzxzbbc(k)*betbbc+Uzxzccc(k)*betccc;

  % Effective second order nonlinear susceptibility for PPP polarization
  f=A*exp(-(theta-theta0)^2/(2*(deltheta^2)));
  X=((-1)*(Lxsfg)*(Lxvis)*(Lzir)*cos(xsfg)*cos(xvis)*sin(xir)*f*Xxxz-
Lxsfg)...
      *(Lzvis)*(Lxir)*cos(xsfg)*sin(xvis)*cos(xir)*f*Xxzx-
(Lxsfg)*(Lzvis)...
      *(Lzir)*cos(xsfg)*sin(xvis)*sin(xir)*f*Xxzz+(Lzsfg)*(Lzvis)*(Lxir)...

*sin(xsfg)*sin(xvis)*cos(xir)*f*Xzzx+(Lzsfg)*(Lxvis)*(Lzir)*sin(xsfg)...

*cos(xvis)*sin(xir)*f*Xzxz+(Lzsfg)*(Lxvis)*(Lxir)*sin(xsfg)*cos(xvis)...

*cos(xir)*f*Xzxx+(Lzsfg)*(Lzvis)*(Lzir)*sin(xsfg)*sin(xvis)*sin(xir)*f*Xzzz
;
  sum=sum+X*dtheta*step;%sum1=sum
    end
    CHI(k)=ki;
    INT1(k)=(abs(sum))^2;
end
% Averaging over Gaussian azimuthal distribution
deltadeg=10; % Azimuthal Gaussian distribution width in degrees
delta=deltadeg*pi/180;
A1=1/(sqrt(2*pi)*delta);
for m=1:Nki+1
    sum2=0;
    for n=1:Nki
        y=(n-1)*step;
        if ((CHI(m)-y)<-pi)
            g=A1*exp(-(CHI(m)-y+2*pi)^2/(2*(delta^2)));
        elseif ((CHI(m)-y)>-pi) && ((CHI(m)-y)<pi)
             g=A1*exp(-(CHI(m)-y)^2/(2*(delta^2)));
        else
             g=A1*exp(-(CHI(m)-y-2*pi)^2/(2*(delta^2)));
        end
        sum2=sum2+INT1(n)*g*step;
    end
    INT2(m)=sum2;
end
INT1max=max(INT1);
INT11=INT1/INT1(1);

INT2max=max(INT2);
INT21=INT2/INT2(1);
```

```
MAX1=max(INT11);
MAX2=max(INT21);
MAX=max(MAX1,MAX2);
 plot(xx,yy,'ok','MarkerFaceColor','k','MarkerSize',6);
 hold on
 plot(CHI,INT11,'r','Linewidth',1.25);
plot(CHI,INT21,'b','Linewidth',1.25);
% hold off
axis ([0 2*pi -0.1 1.2]);
xtixr = get(gca, 'XTick');
xtixlbl = regexp(sprintf('%.1f°\n',xtixr*180/pi), '\n', 'split');
set(gca, 'XTick', xtixr, 'XTickLabel',xtixlbl);
xlabel('Azimuthal angle \Psi (deg)', 'FontSize',13,'FontName','Times New
Roman');
ylabel('|\chi^{(2)}_{PPP}|^{2}','FontSize',13,'FontName','Times New
Roman');
```

Appendix E – MATLAB program for extracting data from Curve Fitting Tool

```
%clc;
clear;

% Load sfit file from Curve Fitting Tool
load('xxx.sfit', '-mat')

% Loop all tabs
for i = 1: length(savedSession.AllFitdevsAndConfigs)
    % Data regarding tab i=1,2,3,…
    tabObject = savedSession.AllFitdevsAndConfigs{1};

    % Tab name
    tabName = tabObject.Fitdev.FitName;

    % Set of coefficients, e.g. gamma1, omega1, ...
    coefficientsObject = tabObject.Fitdev.Fit;

    % Get (x, y) (original data)
    [xOrigin, yOrigin] = tabObject.Fitdev.FittingData.getValues;

    % Symbolic function
    func = str2sym(tabObject.Fitdev.FitTypeString);

    % Load variable names
    variableNames = [];
    variableNamesAsString = coeffnames(coefficientsObject);
    for k = 1 : length(coeffnames(coefficientsObject))
        variableNames = [variableNames
str2sym(variableNamesAsString{k})];
    end

    % Substitute values to variables
    funcWithSubsParams = subs(func, variableNames,
coeffvalues(coefficientsObject));

    % Get smooth curve
      x = 2800:0.2:3000;  % The variable name must be 'x', the range of
x depends on the IR wavenumber range in SFG measurement
    y = eval(subs(funcWithSubsParams));
end
```

Appendix F – Design of the new sample holder